JOINT TRANSPORTATION
RESEARCH PROGRAM
INDIANA DEPARTMENT OF TRANSPORTATION
AND PURDUE UNIVERSITY

CPT-Based Geotechnical Design Manual, Volume 3: CPT-Based Design of Foundations—Example Problems

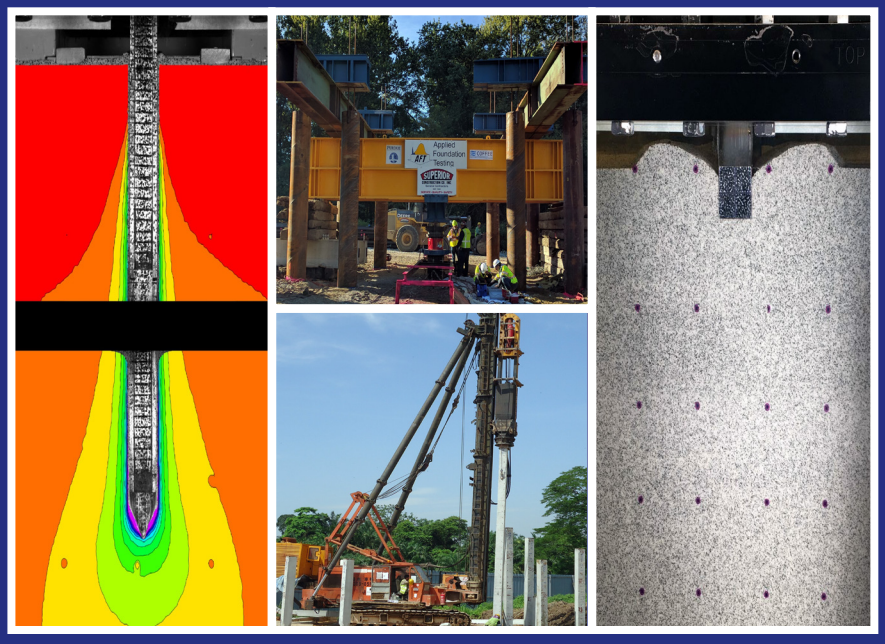

Venkata A. Sakleshpur, Monica Prezzi,
Rodrigo Salgado, Mir Zaheer

SPR-4108 • Report Number: FHWA/IN/JTRP-2021/24 • DOI: 10.5703/1288284317348

RECOMMENDED CITATION

Sakleshpur, V. A., Prezzi, M., Salgado, R., & Zaheer, M. (2021). *CPT-based geotechnical design manual, Volume 3: CPT-based design of foundations—Example problems* (Joint Transportation Research Program Publication No. FHWA/IN/JTRP-2021/24). West Lafayette, IN: Purdue University. https://doi.org/10.5703/1288284317348

AUTHORS

Venkata A. Sakleshpur
Graduate Research Assistant
Lyles School of Civil Engineering
Purdue University

Rodrigo Salgado, PhD
Charles Pankow Professor of Civil Engineering
Lyles School of Civil Engineering
Purdue University

Monica Prezzi, PhD
Professor of Civil Engineering
Lyles School of Civil Engineering
Purdue University
(765) 494-5034
mprezzi@ecn.purdue.edu
Corresponding Author

Mir Zaheer, PE
Geotechnical Design Engineer
Indiana Department of Transportation

JOINT TRANSPORTATION RESEARCH PROGRAM

The Joint Transportation Research Program serves as a vehicle for INDOT collaboration with higher education institutions and industry in Indiana to facilitate innovation that results in continuous improvement in the planning, design, construction, operation, management and economic efficiency of the Indiana transportation infrastructure. https://engineering.purdue.edu/JTRP/index_html

Published reports of the Joint Transportation Research Program are available at http://docs.lib.purdue.edu/jtrp/.

NOTICE

ACKNOWLEDGEMENTS

This research was funded with the support provided by the Indiana Department of Transportation (INDOT) through the Joint Transportation Research Program (JTRP) at Purdue University. The authors would like to thank the agency for the support. The authors are very grateful for the support received from the project administrator, Peter Becker, the business owner, Athar Khan, and the study advisory committee, composed of Samy Noureldin and Jose Ortiz, throughout the duration of the project and for their valuable comments and suggestions. The authors are very grateful to Barry Partridge and Darcy Bullock for their valuable support throughout the project. Special thanks are due to Alebachew Tilahun, Jonathan Paauwe, and Nayyar Zia Siddiki for sharing the soil investigation data for sites in Indiana, and to Kamran Ghani, Min Sang Lee, and Victoria Leffel for their comments. The authors would also like to thank Daniel Alzamora and Derrick Dasenbrock from the Federal Highway Administration (FHWA) for their detailed comments and suggestions.

TECHNICAL REPORT DOCUMENTATION PAGE

1. Report No. FHWA/IN/JTRP-2021/24	**2. Government Accession No.**	**3. Recipient's Catalog No.**
4. Title and Subtitle CPT-Based Geotechnical Design Manual, Volume 3: CPT-Based Design of Foundations—Example Problems		**5. Report Date** June 2021 **6. Performing Organization Code**
7. Author(s) Venkata A. Sakleshpur, Monica Prezzi, Rodrigo Salgado, and Mir Zaheer		**8. Performing Organization Report No.** FHWA/IN/JTRP-2021/24
9. Performing Organization Name and Address Joint Transportation Research Program Hall for Discovery and Learning Research (DLR), Suite 204 207 S. Martin Jischke Drive West Lafayette, IN 47907		**10. Work Unit No.** **11. Contract or Grant No.** SPR-4108
12. Sponsoring Agency Name and Address Indiana Department of Transportation (SPR) State Office Building 100 North Senate Avenue Indianapolis, IN 46204		**13. Type of Report and Period Covered** Final Report **14. Sponsoring Agency Code**
15. Supplementary Notes Conducted in cooperation with the U.S. Department of Transportation, Federal Highway Administration.		

16. Abstract

This manual provides guidance on how to use the cone penetration test (CPT) for site investigation and foundation design. The manual has been organized into three volumes. Volume 1 covers the execution of CPT-based site investigations and presents a comprehensive literature review of CPT-based soil behavior type (SBT) charts and estimation of soil variables from CPT results. Volume 2 covers the methods and equations needed for CPT data interpretation and foundation design in different soil types, while Volume 3 includes several example problems (based on instrumented case histories) with detailed, step-by-step calculations to demonstrate the application of the design methods. The methods included in the manual are current, reliable, and demonstrably the best available for Indiana geology based on extensive CPT research carried out during the past two decades. The design of shallow and pile foundations in the manual is based on the load and resistance factor design (LRFD) framework. The manual also indicates areas of low reliability and limited knowledge, which can be used as indicators for future research.

17. Key Words cone penetration test, soil behavior type, shallow foundation, pile foundation, load and resistance factor design	**18. Distribution Statement** No restrictions. This document is available through the National Technical Information Service, Springfield, VA 22161.

19. Security Classif. (of this report) Unclassified	**20. Security Classif. (of this page)** Unclassified	**21. No. of Pages** 70	**22. Price**

EXECUTIVE SUMMARY

Introduction

This manual provides guidance on how to use the cone penetration test (CPT) for site investigation and foundation design. The manual has been organized into three volumes.

Volume I covers the execution of CPT-based site investigations, a comprehensive literature review of CPT-based soil behavior type (SBT) charts, and several correlations for estimation of a soil variable of interest from CPT results. The volume has been organized into two chapters. Chapter 1 details the components of a CPT system, types of CPT equipment, testing procedures and precautions, maintenance of CPT equipment, and planning and execution of a CPT-based site investigation. Chapter 2 presents a compilation of correlations for the estimation of a soil variable of interest from CPT data, and also presents a comprehensive review of the chronological development of the SBT classification systems that have advanced during the past 55 years of CPT history.

Volume II covers the methods and equations needed for CPT data interpretation and foundation design in different soil types. The volume has been organized into four chapters. Chapter 1 provides an introduction to the manual. Chapter 2 presents an overview of Indiana geology, the typical CPT and soil profiles found in Indiana, and the influence of these profiles on CPT-based site variability assessment. Chapter 3 details the methods for the estimation of limit bearing capacity and settlement of shallow foundations from CPT data. Chapter 4 describes the methods for estimation of limit unit shaft resistance and ultimate unit base resistance of displacement, non-displacement, and partial displacement piles and pile groups from CPT data. The design of both shallow and pile foundations is based on the load and resistance factor design (LRFD) framework.

Volume III contains several example problems (based on case histories) with detailed, step-by-step calculations to demonstrate the application of the CPT-based foundation design methods covered in Volume II. The volume has been organized into three chapters. Chapter 1 includes example problems for the estimation of optimal spacing between CPT soundings performed in line and distributed in two dimensions using CPT data obtained from the Sagamore Parkway Bridge construction site in Lafayette, Indiana. Chapter 2 contains example problems for the estimation of limit bearing capacity and settlement of shallow foundations using CPT data reported in literature for sites in the US, UK, and Australia. Chapter 3 includes example problems for the estimation of limit unit shaft resistance and ultimate unit base resistance of displacement, non-displacement, and partial displacement piles using CPT data obtained from three sites in Indiana. The predicted foundation load capacities and settlements were found to be in agreement with the measured load test data reported for these sites.

Findings

Not applicable.

Implementation

The *CPT-Based Geotechnical Design Manual* can be used to train new employees and to facilitate interaction between INDOT engineers, industry, and consultants. Specific implementation items for each volume are listed below.

Volume I

A spreadsheet for the estimation of fundamental soil variables from CPT results was developed. INDOT engineers can use the spreadsheet on a routine basis to interpret CPT data, generate an SBT profile, and obtain the depth profile of a soil property of interest.

Volumes II and III

Spreadsheets for the estimation of optimal spacing between CPT soundings and CPT-based design of shallow and pile foundations were developed. INDOT engineers can use the spreadsheets on a routine basis for the design of transportation infrastructure projects in Indiana.

A relationship between cone resistance q_c, corrected SPT blow count N_{60}, and mean particle size D_{50} was developed using data reported by Robertson et al. (1983) and data obtained from 15 sites in Indiana. The relationship can be used to obtain an estimate of q_c for use in a CPT-based foundation design method when only SPT blow counts are available for a site.

A relationship between critical-state friction angle ϕ_c, mean particle size D_{50}, coefficient of uniformity C_U, and particle roundness R was developed using test data reported for 23 clean silica sands in the literature. In the absence of direct shear or triaxial compression test results, the relationship can be used to obtain an estimate of ϕ_c for poorly-graded, clean silica sands with D_{50}, C_U, and R values ranging from 0.15–2.68 mm (0.006–0.105 in.), 1.2–3.1, and 0.3–0.8, respectively.

CONTENTS

LIST OF TABLES

LIST OF FIGURES

1. OPTIMAL SPACING BETWEEN CPT SOUNDINGS

1.1 Optimal Spacing Between CPT Soundings Performed in Line

Figure 1.1 shows the layout of two CPT soundings, CPT-1 and CPT-2, performed at a bridge construction site located on the east bank of the Wabash River at its intersection with Sagamore Parkway in Lafayette, Tippecanoe County, Indiana. The spacing s_{xy} between CPT-1 and CPT-2 is 14.20 m (46.59 ft). Figure 1.2 shows the cone resistance profiles obtained from soundings CPT-1 and CPT-2 performed up to depths of 15.80 m (51.84 ft) and 17.35 m (56.92 ft), respectively. The soil profile at the site consists primarily of layers of poorly-graded sand and gravel mixtures. The following steps show how to estimate the optimal spacing $(s_{yz})_{opt}$ of the next sounding CPT-3 that needs to be performed at the site. Consider that sounding CPT-3 will be performed in line with soundings CPT-1 and CPT-2, as shown in Figure 1.1.

Step 1: Set the analysis (segment) length L as the minimum of the sounding depths of CPT-1 and CPT-2.

Depth of sounding CPT-1 = 51.84 ft, and depth of sounding CPT-2 = 56.92 ft.

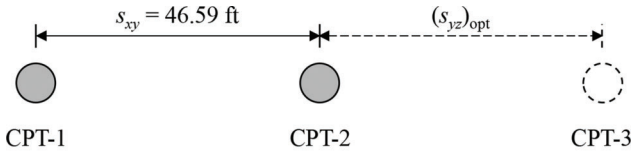

Figure 1.1 Layout of CPT soundings for example problem 1.1.

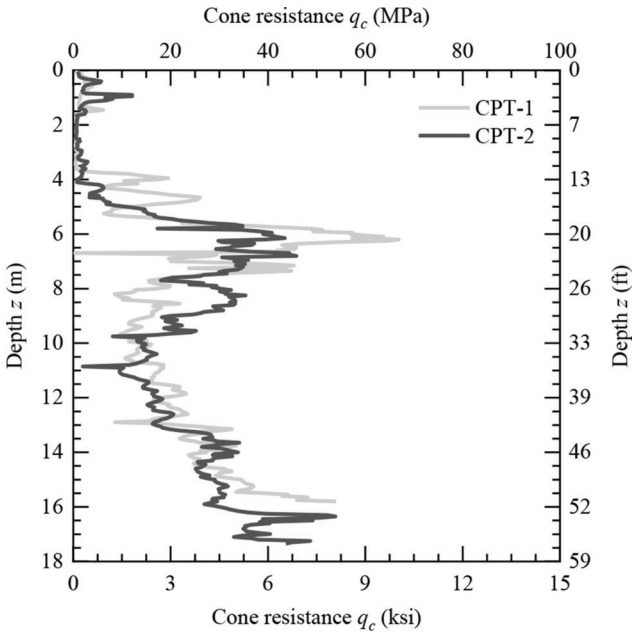

Figure 1.2 Cone resistance profiles of soundings CPT-1 and CPT-2 at the Sagamore Parkway Bridge construction site.

Segment length L = min[51.84 ft ; 56.92 ft] = 51.84 ft.

Step 2: Determine the number N of cone resistance data points contained within the segment length L.

Number N of cone resistance data points within the segment length = 316

Step 3: Calculate the mean cone resistances $\bar{x}$ and $\bar{y}$ of soundings CPT-1 and CPT-2, respectively, for the segment length considered.

Mean cone resistance $\bar{x}$ of sounding CPT-1 within the segment length = 2.63 ksi.

Mean cone resistance $\bar{y}$ of sounding CPT-2 within the segment length = 2.53 ksi.

Step 4: Calculate the standard deviations σ_x and σ_y of the q_c values of soundings CPT-1 and CPT-2, respectively (using Eqs. 2.8 and 2.9 from Volume II).

$$\sigma_x = \sqrt{\frac{1}{N-1}\sum_{i=1}^{N}(x_i-\bar{x})^2} = \sqrt{\frac{1}{316-1}\times 1{,}363.08} = 2.08 \text{ ksi}$$

$$\sigma_y = \sqrt{\frac{1}{N-1}\sum_{i=1}^{N}(y_i-\bar{y})^2} = \sqrt{\frac{1}{316-1}\times 1{,}006.22} = 1.79 \text{ ksi}$$

Step 5: Estimate the cross-covariance C_{xy} and the cross-correlation coefficient ρ_{xy} between soundings CPT-1 and CPT-2 (using Eqs. 2.10 and 2.11 from Volume II).

$$C_{xy} = \frac{1}{N}\sum_{i=0}^{N-1}(x_i-\bar{x})(y_i-\bar{y}) = \frac{1}{316}\times 899.28 = 2.85 \text{ ksi}^2$$

$$\rho_{xy} = \frac{C_{xy}}{\sigma_x\sigma_y} = \frac{2.85}{2.08\times 1.79} = 0.77$$

Step 6: Calculate the average q_c difference $|\Delta q_{c,avg}|$ between soundings CPT-1 and CPT-2 (using Eq. 2.12 from Volume II).

$$|\Delta q_{c,avg}| = \frac{\sum_{i=1}^{N}|x_i-y_i|}{N} = \frac{295.74}{316} = 0.94 \text{ ksi}$$

Step 7: Estimate the maximum credible difference $|\Delta q_{c,avg}|_{max}$ between q_c trends for the segment length considered (using Eq. 2.13 from Volume II).

$$\frac{|\Delta q_{c,avg}|_{max}}{p_A} = 23.86\left(\frac{L}{L_R}\right)^{0.46} - 4.30$$

$$= 23.86\left(\frac{51.84}{3.28}\right)^{0.46} - 4.30 = 80.64$$

$$|\Delta q_{c,avg}|_{max} = 80.64 p_A = 80.64\times 0.0145 = 1.17 \text{ ksi}$$

Step 8: Calculate the values of functions f_0, f_1, and f_2 (using Eqs. 2.14, 2.15, and 2.16 from Volume II).

$$f_0 = \min\left[\frac{|\Delta q_{c,avg}|}{|\Delta q_{c,avg}|_{\max}}; 1\right] = \min\left[\frac{0.94}{1.17}; 1\right] = 0.80$$

$$f_1 = \frac{\rho_{xy}+1}{2} = \frac{0.77+1}{2} = 0.88$$

$$f_2 = 1 - \exp\left(-0.25\frac{s_{xy}}{L_R}\right) = 1 - \exp\left(-0.25 \times \frac{46.59}{3.28}\right) = 0.97$$

Step 9: Estimate the horizontal variability index (HVI) for soundings CPT-1 and CPT-2 (using Eq. 2.17 from Volume II).

$$\text{HVI} = 1 - f_2[0.8(1-f_0) + 0.2f_1]$$
$$= 1 - 0.97[0.8(1-0.80) + 0.2(0.88)] = 0.67$$

Step 10: Compute the optimal spacing $(s_{yz})_{\text{opt}}$ of the next sounding CPT-3 (using Eq. 2.18 from Volume II).

$$(s_{yz})_{\text{opt}} = (1.5 - \text{HVI})s_{xy} = (1.5 - 0.67) \times 46.59 = 38.67 \text{ ft}$$

Table 1.1 summarizes the results obtained from Microsoft Excel for the CPT-1 and CPT-2 sounding pair.

1.2 Optimal Spacing Between CPT Soundings Distributed in Two Dimensions

Figure 1.3 shows the layout of three CPT soundings, CPT-1, CPT-2, and CPT-3, performed at the Sagamore Parkway bridge construction site. The spacing between CPT-1 and CPT-2 is 14.20 m (46.59 ft) and that between CPT-2 and CPT-3 is 9.82 m (32.22 ft).

TABLE 1.1
Calculation table for CPT-1 and CPT-2 sounding pair

i	z_i (ft)	x_i (ksi)	y_i (ksi)	$x_i - \bar{x}$ (ksi)	$y_i - \bar{y}$ (ksi)	$(x_i - \bar{x})(y_i - \bar{y})$ (ksi^2)	$\lvert x_i - y_i \rvert$ (ksi)
1	0.16	0.06	0.13	-2.57	-2.40	6.18	0.07
2	0.33	0.19	0.15	-2.44	-2.38	5.81	0.03
3	0.49	0.26	0.17	-2.37	-2.37	5.61	0.09
4	0.66	0.26	0.17	-2.37	-2.37	5.62	0.09
5	0.82	0.33	0.21	-2.30	-2.33	5.34	0.13
6	0.98	0.39	0.32	-2.24	-2.21	4.96	0.07
7	1.15	0.40	0.58	-2.23	-1.96	4.37	0.18
8	1.31	0.35	0.83	-2.28	-1.70	3.89	0.48
9	1.48	0.32	0.80	-2.31	-1.73	4.00	0.48
10	1.64	0.38	0.53	-2.25	-2.01	4.52	0.15
11	1.80	0.59	0.38	-2.04	-2.15	4.39	0.21
12	1.97	0.53	0.32	-2.10	-2.21	4.65	0.20
13	2.13	0.45	0.30	-2.18	-2.23	4.87	0.15
14	2.30	0.43	0.30	-2.20	-2.23	4.89	0.13
15	2.46	0.36	0.27	-2.27	-2.27	5.15	0.09
16	2.62	0.29	0.28	-2.34	-2.25	5.27	0.01
17	2.79	0.25	0.36	-2.38	-2.17	5.16	0.11
Results are Truncated to Fit to One Page							
300	49.21	5.01	4.22	2.38	1.69	4.02	0.79
301	49.38	5.03	4.22	2.40	1.68	4.05	0.82
302	49.54	5.10	4.27	2.47	1.74	4.29	0.82
303	49.70	5.15	4.39	2.53	1.85	4.68	0.77
304	49.87	5.34	4.55	2.71	2.02	5.48	0.79
305	50.03	5.37	4.60	2.74	2.07	5.67	0.77
306	50.20	5.30	4.43	2.67	1.89	5.07	0.88
307	50.36	5.21	4.33	2.58	1.79	4.62	0.88
308	50.52	4.98	4.36	2.35	1.82	4.29	0.63
309	50.69	4.85	4.35	2.22	1.82	4.04	0.50
310	50.85	5.75	4.40	3.12	1.86	5.81	1.35
311	51.02	6.39	4.53	3.76	1.99	7.49	1.87
312	51.18	6.22	4.47	3.59	1.94	6.97	1.75
313	51.35	6.99	4.49	4.36	1.96	8.52	2.50
314	51.51	6.81	4.16	4.18	1.63	6.81	2.65
315	51.67	6.66	4.14	4.03	1.60	6.45	2.52
316	51.84	7.83	4.28	5.20	1.75	9.11	3.55

Note: z_i = depth from the ground surface to data point i, x_i and y_i = q_c values of the i^{th} data point obtained from soundings CPT-1 and CPT-2, respectively, and $\bar{x}$ and $\bar{y}$ = mean values of q_c for soundings CPT-1 and CPT-2, respectively, within the segment length considered.

Figure 1.4 shows the cone resistance profiles obtained from soundings CPT-1, CPT-2, and CPT-3 performed up to depths of 15.80 m (51.84 ft), 17.35 m (56.92 ft), and 32.65 m (107.12 ft), respectively. Due to the high gravel content of the soil layers at the site, a drill-and-push scheme was adopted for sounding CPT-3 to obtain the complete cone resistance profile. This scheme consisted of pushing the cone through a hollow stem auger that was used to drill through the hard layers. The assumed q_c distribution in Figure 1.4 corresponds to those depths where drilling was in operation. The following steps show how to estimate the optimal spacing $(s_{yz})_{\text{opt}}$ of the next sounding CPT-4 that needs to be performed at the site.

As the CPT soundings are not performed in line but are distributed in two dimensions, the HVI values need to be calculated for all pairs of soundings available at the site. The number of pairs of CPT soundings available at the site are (using Eq. 2.19 from Volume II):

$$ {}^{n}C_r = \frac{n!}{(n-r)!r!} \Rightarrow {}^{3}C_2 = \frac{3!}{(3-2)!2!} = \frac{3!}{1!2!} = \frac{3\times 2\times 1}{1\times 2\times 1} = 3$$

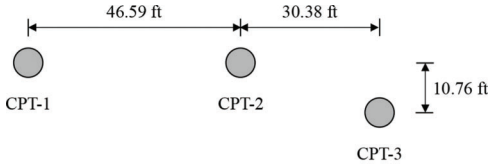

Figure 1.3 Layout of CPT soundings for example problem 1.2.

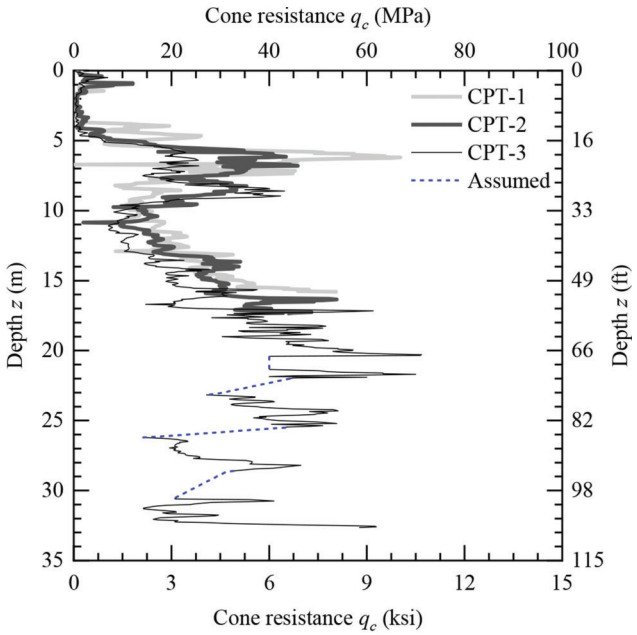

Figure 1.4 Cone resistance profiles for soundings CPT-1, CPT-2, and CPT-3 at Sagamore Parkway Bridge construction site.

The three pairs of CPT soundings are: (1) CPT-1 and CPT-2, (2) CPT-2 and CPT-3, and (3) CPT-3 and CPT-1. From the solution of example problem 1.1, we know that the HVI value for the CPT-1 and CPT-2 pair is 0.67. The HVI values for the CPT-2 and CPT-3 pair and the CPT-3 and CPT-1 pair are calculated below.

Calculation of HVI for CPT-2 and CPT-3 Pair

Step 1: Set the analysis (segment) length L as the minimum of the sounding depths of CPT-2 and CPT-3.

Depth of sounding CPT-2 = 56.92 ft, and depth of sounding CPT-3 = 107.12 ft.

Segment length L = min[56.92 ft; 107.12 ft] = 56.92 ft.

Step 2: Determine the number N of cone resistance data points contained within the segment length L.

Number N of cone resistance data points within the segment length = 347.

Step 3: Calculate the mean cone resistances $\bar{x}$ and $\bar{y}$ of soundings CPT-2 and CPT-3, respectively, for the segment length considered.

Mean cone resistance $\bar{x}$ of sounding CPT-2 within the segment length = 2.80 ksi.

Mean cone resistance $\bar{y}$ of sounding CPT-3 within the segment length = 2.10 ksi.

Step 4: Calculate the standard deviations σ_x and σ_y of the q_c values of soundings CPT-2 and CPT-3, respectively (using Eqs. 2.8 and 2.9 from Volume II).

$$\sigma_x = \sqrt{\frac{1}{N-1}\sum_{i=1}^{N}(x_i-\bar{x})^2} = \sqrt{\frac{1}{347-1}\times 1{,}290.66} = 1.93 \text{ ksi}$$

$$\sigma_y = \sqrt{\frac{1}{N-1}\sum_{i=1}^{N}(y_i-\bar{y})^2} = \sqrt{\frac{1}{347-1}\times 951.17} = 1.66 \text{ ksi}$$

Step 5: Estimate the cross-covariance C_{xy} and the cross-correlation coefficient ρ_{xy} between soundings CPT-2 and CPT-3 (using Eqs. 2.10 and 2.11 from Volume II).

$$C_{xy} = \frac{1}{N}\sum_{i=0}^{N-1}(x_i-\bar{x})(y_i-\bar{y}) = \frac{1}{347}\times 921.72 = 2.66 \text{ ksi}^2$$

$$\rho_{xy} = \frac{C_{xy}}{\sigma_x\sigma_y} = \frac{2.66}{1.93\times 1.66} = 0.83$$

Step 6: Calculate the average q_c difference $|\Delta q_{c,avg}|$ between soundings CPT-2 and CPT-3 (using Eq. 2.12 from Volume II).

$$|\Delta q_{c,avg}| = \frac{\sum_{i=1}^{N}|x_i-y_i|}{N} = \frac{327.53}{347} = 0.94 \text{ ksi}$$

Step 7: Estimate the maximum credible difference $|\Delta q_{c,avg}|_{\max}$ between q_c trends for the segment length considered (using Eq. 2.13 from Volume II).

$$\frac{|\Delta q_{c,avg}|_{\max}}{p_A} = 23.86\left(\frac{L}{L_R}\right)^{0.46} - 4.30$$

$$= 23.86\left(\frac{56.92}{3.28}\right)^{0.46} - 4.30 = 84.37$$

$$|\Delta q_{c,avg}|_{\max} = 84.37 p_A = 84.37 \times 0.0145 = 1.22 \text{ ksi}$$

Step 8: Calculate the values of functions f_0, f_1, and f_2 (using Eqs. 2.14, 2.15, and 2.16 from Volume II).

$$f_0 = \min\left[\frac{|\Delta q_{c,avg}|}{|\Delta q_{c,avg}|_{\max}}; 1\right] = \min\left[\frac{0.94}{1.22}; 1\right] = 0.77$$

$$f_1 = \frac{\rho_{xy} + 1}{2} = \frac{0.83 + 1}{2} = 0.91$$

$$f_2 = 1 - \exp\left(-0.25\frac{s_{xy}}{L_R}\right)$$

$$= 1 - \exp\left(-0.25 \times \frac{32.22}{3.28}\right) = 0.91$$

Step 9: Estimate the horizontal variability index (HVI) for soundings CPT-2 and CPT-3 (using Eq. 2.17 from Volume II).

$$\text{HVI} = 1 - f_2[0.8(1 - f_0) + 0.2 f_1]$$

$$= 1 - 0.91[0.8(1 - 0.77) + 0.2(0.91)] = 0.67$$

Table 1.2 summarizes the Microsoft Excel results for the CPT-2 and CPT-3 sounding pair.

Calculation of HVI for CPT-1 and CPT-3 Pair

Step 1: Set the analysis (segment) length L as the minimum of the sounding depths of CPT-1 and CPT-3.

TABLE 1.2
Calculation table for CPT-2 and CPT-3 sounding pair

i	z_i (ft)	x_i (ksi)	y_i (ksi)	$x_i - \bar{x}$ (ksi)	$y_i - \bar{y}$ (ksi)	$(x_i - \bar{x})(y_i - \bar{y})$ (ksi^2)	$\lvert x_i - y_i \rvert$ (ksi)
1	0.16	0.13	0.06	-2.67	-2.03	5.43	0.07
2	0.33	0.15	0.11	-2.65	-1.98	5.25	0.04
3	0.49	0.17	0.21	-2.63	-1.88	4.96	0.04
4	0.66	0.17	0.29	-2.63	-1.80	4.75	0.12
5	0.82	0.21	0.27	-2.60	-1.83	4.74	0.06
6	0.98	0.32	0.23	-2.48	-1.87	4.63	0.10
7	1.15	0.58	0.16	-2.22	-1.94	4.30	0.42
8	1.31	0.83	0.16	-1.97	-1.93	3.81	0.67
9	1.48	0.80	0.74	-2.00	-1.36	2.72	0.06
10	1.64	0.53	1.01	-2.28	-1.08	2.46	0.49
11	1.80	0.38	0.81	-2.42	-1.29	3.12	0.43
12	1.97	0.32	0.61	-2.48	-1.49	3.69	0.28
13	2.13	0.30	0.44	-2.50	-1.66	4.15	0.13
14	2.30	0.30	0.36	-2.50	-1.74	4.34	0.05
15	2.46	0.27	0.44	-2.53	-1.65	4.19	0.18
16	2.62	0.28	0.36	-2.52	-1.73	4.36	0.08
17	2.79	0.36	0.33	-2.44	-1.77	4.30	0.03
Results are Truncated to Fit to One Page							
331	54.30	5.56	3.11	2.76	1.02	2.80	2.45
332	54.46	5.85	3.16	3.05	1.07	3.25	2.69
333	54.63	5.31	3.21	2.51	1.12	2.80	2.10
334	54.79	5.12	3.26	2.32	1.17	2.71	1.86
335	54.95	5.14	3.31	2.34	1.22	2.85	1.82
336	55.12	5.06	3.36	2.26	1.27	2.87	1.70
337	55.28	5.12	3.42	2.32	1.32	3.06	1.70
338	55.45	5.16	3.47	2.36	1.37	3.24	1.70
339	55.61	5.49	3.52	2.69	1.42	3.82	1.97
340	55.77	5.86	3.57	3.06	1.47	4.51	2.29
341	55.94	5.03	4.97	2.23	2.88	6.41	0.05
342	56.10	4.79	6.96	1.99	4.87	9.67	2.18
343	56.27	5.31	8.89	2.51	6.80	17.05	3.59
344	56.43	5.51	8.33	2.71	6.23	16.87	2.82
345	56.59	7.06	7.57	4.26	5.47	23.28	0.51
346	56.76	6.53	5.64	3.72	3.55	13.20	0.88
347	56.92	6.34	4.76	3.54	2.66	9.41	1.58

Note: z_i = depth from the ground surface to data point i, x_i and $y_i = q_c$ values of the i^{th} data point obtained from soundings CPT-2 and CPT-3, respectively, and $\bar{x}$ and $\bar{y}$ = mean values of q_c for soundings CPT-2 and CPT-3, respectively, within the segment length considered.

Depth of sounding CPT-1 = 51.84 ft, and depth of sounding CPT-3 = 107.12 ft.

Segment length L = min[51.84 ft ; 107.12 ft] = 51.84 ft.

Step 2: Determine the number N of cone resistance data points contained within the segment length L.

Number N of cone resistance data points within the segment length = 316.

Step 3: Calculate the mean cone resistances $\bar{x}$ and $\bar{y}$ of soundings CPT-1 and CPT-3, respectively, for the segment length considered.

Mean cone resistance $\bar{x}$ of sounding CPT-1 within the segment length = 2.63 ksi.

Mean cone resistance $\bar{y}$ of sounding CPT-3 within the segment length = 1.87 ksi.

Step 4: Calculate the standard deviations σ_x and σ_y of the q_c values of soundings CPT-1 and CPT-3, respectively (using Eqs. 2.8 and 2.9 from Volume II).

$$\sigma_x = \sqrt{\frac{1}{N-1}\sum_{i=1}^{N}(x_i-\bar{x})^2} = \sqrt{\frac{1}{316-1}\times 1{,}363.08} = 2.08 \text{ ksi}$$

$$\sigma_y = \sqrt{\frac{1}{N-1}\sum_{i=1}^{N}(y_i-\bar{y})^2} = \sqrt{\frac{1}{316-1}\times 701.55} = 1.49 \text{ ksi}$$

Step 5: Estimate the cross-covariance C_{xy} and the cross-correlation coefficient ρ_{xy} between soundings CPT-1 and CPT-3 (using Eqs. 2.10 and 2.11 from Volume II).

$$C_{xy} = \frac{1}{N}\sum_{i=0}^{N-1}(x_i-\bar{x})(y_i-\bar{y}) = \frac{1}{316}\times 585.82 = 1.85 \text{ ksi}^2$$

$$\rho_{xy} = \frac{C_{xy}}{\sigma_x\sigma_y} = \frac{1.85}{2.08\times 1.49} = 0.60$$

Step 6: Calculate the average q_c difference $|\Delta q_{c,avg}|$ between soundings CPT-1 and CPT-3 (using Eq. 2.12 from Volume II).

$$|\Delta q_{c,avg}| = \frac{\sum_{i=1}^{N}|x_i-y_i|}{N} = \frac{412.22}{316} = 1.30 \text{ ksi}$$

Step 7: Estimate the maximum credible difference $|\Delta q_{c,avg}|_{\max}$ between q_c trends for the segment length considered (using Eq. 2.13 from Volume II).

$$\frac{|\Delta q_{c,avg}|_{\max}}{p_A} = 23.86\left(\frac{L}{L_R}\right)^{0.46} - 4.30$$

$$= 23.86\left(\frac{51.84}{3.28}\right)^{0.46} - 4.30 = 80.64$$

$$|\Delta q_{c,avg}|_{\max} = 80.64 p_A = 80.64\times 0.0145 = 1.17 \text{ ksi}$$

Step 8: Calculate the values of functions f_0, f_1, and f_2 (using Eqs. 2.14, 2.15 and 2.16 from Volume II).

$$f_0 = \min\left[\frac{|\Delta q_{c,avg}|}{|\Delta q_{c,avg}|_{\max}}; 1\right] = \min\left[\frac{1.30}{1.17}; 1\right] = 1.00$$

$$f_1 = \frac{\rho_{xy}+1}{2} = \frac{0.60+1}{2} = 0.80$$

$$f_2 = 1 - \exp\left(-0.25\frac{s_{xy}}{L_R}\right)$$

$$= 1 - \exp\left(-0.25\times\frac{77.72}{3.28}\right) = 1.00$$

Step 9: Estimate the horizontal variability index (HVI) for soundings CPT-1 and CPT-3 (using Eq. 2.17 from Volume II).

$$\text{HVI} = 1 - f_2[0.8(1-f_0)+0.2f_1]$$

$$= 1 - [0.8(1-1)+0.2(0.80)] = 0.84$$

Step 10: Compute the optimal spacing $(s_{yz})_{\text{opt}}$ of the next sounding CPT-4 (using Eq. 2.18 from Volume II).

Average HVI value for the three pairs of CPT soundings = (0.67 + 0.67 + 0.84)/3 = 0.73.

Center-to-center spacing s_{xy} between soundings CPT-2 and CPT-3 = 32.22 ft.

Optimal spacing of the next sounding CPT-4:

$$(s_{yz})_{\text{opt}} = (1.5-\text{HVI})s_{xy} = (1.5-0.73)\times 32.22 = 24.81 \text{ ft}$$

Table 1.3 summarizes the results obtained from Microsoft Excel for the CPT-1 and CPT-3 sounding pair.

TABLE 1.3
Calculation table for CPT-1 and CPT-3 sounding pair

i	z_i (ft)	x_i (ksi)	y_i (ksi)	$x_i - \bar{x}$ (ksi)	$y_i - \bar{y}$ (ksi)	$(x_i - \bar{x})(y_i - \bar{y})$ (ksi^2)	$\lvert x_i - y_i \rvert$ (ksi)
1	0.16	0.06	0.06	-2.57	-1.81	4.65	0.00
2	0.33	0.19	0.11	-2.44	-1.76	4.30	0.08
3	0.49	0.26	0.21	-2.37	-1.66	3.94	0.05
4	0.66	0.26	0.29	-2.37	-1.58	3.75	0.03
5	0.82	0.33	0.27	-2.30	-1.60	3.68	0.06
6	0.98	0.39	0.23	-2.24	-1.65	3.69	0.16
7	1.15	0.40	0.16	-2.23	-1.71	3.83	0.24
8	1.31	0.35	0.16	-2.28	-1.71	3.91	0.19
9	1.48	0.32	0.74	-2.31	-1.14	2.62	0.41
10	1.64	0.38	1.01	-2.25	-0.86	1.93	0.63
11	1.80	0.59	0.81	-2.04	-1.06	2.17	0.22
12	1.97	0.53	0.61	-2.10	-1.27	2.66	0.08
13	2.13	0.45	0.44	-2.18	-1.44	3.13	0.01
14	2.30	0.43	0.36	-2.20	-1.52	3.33	0.08
15	2.46	0.36	0.44	-2.27	-1.43	3.25	0.09
16	2.62	0.29	0.36	-2.34	-1.51	3.53	0.07
17	2.79	0.25	0.33	-2.38	-1.54	3.67	0.08
Results are Truncated to Fit to One Page							
300	49.21	5.01	2.80	2.38	0.92	2.20	2.22
301	49.38	5.03	2.74	2.40	0.86	2.08	2.30
302	49.54	5.10	2.84	2.47	0.96	2.38	2.26
303	49.70	5.15	3.02	2.53	1.15	2.90	2.13
304	49.87	5.34	3.10	2.71	1.23	3.33	2.24
305	50.03	5.37	3.04	2.74	1.17	3.20	2.33
306	50.20	5.30	2.93	2.67	1.06	2.82	2.38
307	50.36	5.21	3.01	2.58	1.14	2.94	2.20
308	50.52	4.98	3.03	2.35	1.16	2.73	1.95
309	50.69	4.85	3.21	2.22	1.34	2.97	1.64
310	50.85	5.75	3.47	3.12	1.60	4.98	2.28
311	51.02	6.39	3.57	3.76	1.70	6.40	2.82
312	51.18	6.22	4.51	3.59	2.64	9.48	1.71
313	51.35	6.99	5.45	4.36	3.58	15.57	1.54
314	51.51	6.81	5.32	4.18	3.45	14.43	1.49
315	51.67	6.66	3.65	4.03	1.77	7.15	3.01
316	51.84	7.83	3.63	5.20	1.75	9.12	4.21

Note: z_i = depth from the ground surface to data point i, x_i and $y_i = q_c$ values of the i^{th} data point obtained from soundings CPT-1 and CPT-3, respectively, and $\bar{x}$ and $\bar{y}$ = mean values of q_c for soundings CPT-1 and CPT-3, respectively, within the segment length considered.

2. SHALLOW FOUNDATIONS

2.1 Square Footings in Clean Sand (Perth, Australia)

2.1.1 Site Description and Soil Profile

Lehane et al. (2008) reported the results of four, instrumented, footing load tests performed at the University of Western Australia (UWA) test site at Shenton Park, Perth, Australia. The soil profile at the site consists of 5–7 m (16–23 ft) of poorly-graded, medium-dense, siliceous dune sand overlying weakly-cemented Tamala limestone. The sand layer is of Holocene age and was formed from the chemical weathering (dissolution) of limestone with subsequent erosion, transportation, and re-deposition by wind. The groundwater table is typically located at a depth of about 5.5 m (18 ft), just above the limestone layer. Table 2.1 summarizes the properties of Shenton Park sand; the sand particles are sub-angular to sub-rounded in shape. Figure 2.1 shows the cone resistance profiles obtained from four CPT soundings performed at the site.

Based on self-boring pressuremeter test (SBPMT) results, Lehane et al. (2008) stated that the coefficient of lateral earth pressure at-rest K_0 decreases from 0.70 at a depth of 1.3 m (4.3 ft) to a relatively constant value of 0.43 below a depth of 2.3 m (7.5 ft). Using this information, we considered a constant K_0 value of 0.70 between 0–1.3 m (0–4.3 ft) depth, a linear decrease in K_0 from 0.70 to 0.43 between 1.3–2.3 m (4.3–7.5 ft) depth, and a constant K_0 value of 0.43 for depths greater than 2.3 m (7.5 ft) (Figure 2.2).

TABLE 2.1
Properties of Shenton Park sand (Lehane et al., 2004; Schneider, 2007)

Property	Units	Value
Particle sizes D_{10}, D_{50}, D_{60}	mm	0.21, 0.42, 0.47
	(mils)	(8.3, 16.5, 18.5)
Coefficient of uniformity C_U	—	2.24
Fines content	%	< 5
Unit weight γ_m[1]	kN/m^3	16.14–16.63
	(pcf)	(102.7–105.8)
Minimum void ratio e_{min}	—	0.45
Maximum void ratio e_{max}	—	0.81
Relative density D_R	%	35–55
Critical-state friction angle ϕ_c[2]	(°)	32

[1]Based on *in situ* sand replacement density tests.
[2]Based on isotropically-consolidated (p' = 100 kPa (14.5 psi)) triaxial compression tests performed on specimens reconstituted to e_0 = 0.60 (D_R = 58.3%).

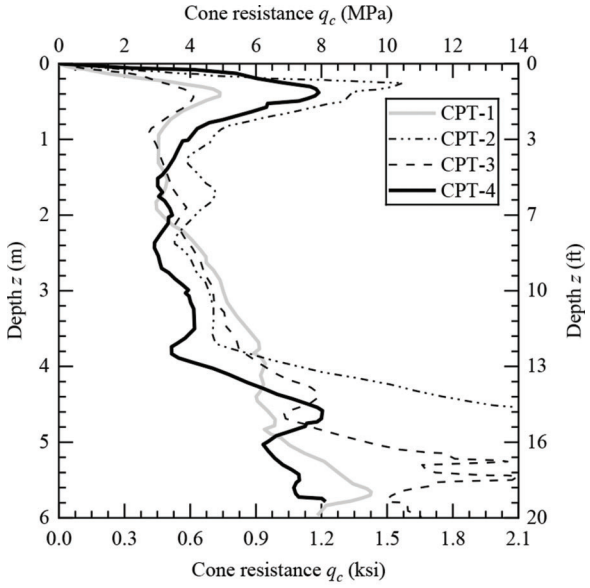

Figure 2.1 Cone resistance profiles obtained from four CPT soundings performed at Shenton Park (digitized from Schneider, 2007).

2.1.2 Footing Dimensions and Loading Details

Table 2.2 summarizes the width, thickness, and embedment depth of four square footings constructed inline at the site. The center-to-center distance between the footings is about 5.5 m (18.0 ft) for footings 1 and 2, 5.2 m (17.1 ft) for footings 2 and 3, and 4.1 m (13.5 ft) for footings 3 and 4. The four CPT soundings, CPT-1 to CPT-4, were performed at a horizontal distance of about 3 m (10 ft) away from the centerline of footings 1–4, respectively. The soundings were performed 9 days after the footings were constructed and 6 days before they were load tested. The footings were loaded up to a maximum value of about 200 kN (45 kips) in

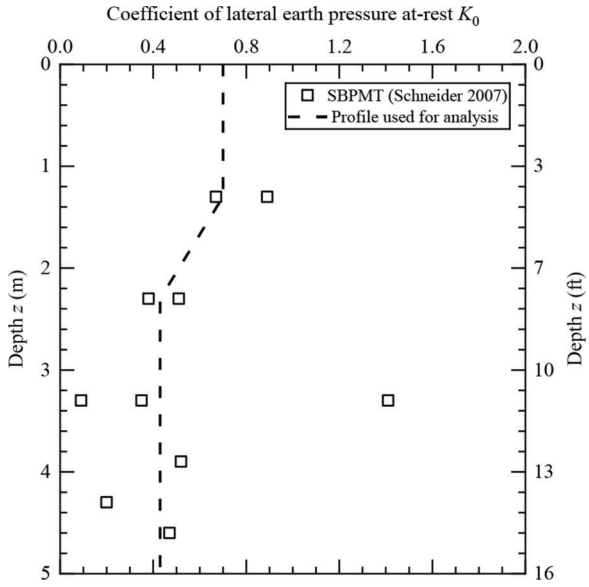

Figure 2.2 Coefficient of lateral earth pressure at-rest K_0 versus depth at Shenton Park.

increments of 15–20 kN (3.4–4.5 kips) using the reaction provided by a 25 tonne CPT truck. Each load increment was maintained for about 10 minutes.

2.1.3 Estimation of Footing Settlement

Figure 2.3 to Figure 2.6 compare the load-settlement curves predicted using both the Lee and Salgado (2002) method and the traditional Schmertmann et al. (1978) method with those obtained from the static load test results reported by Lehane et al. (2008) for footings 1–4, respectively. The measured data points, which correspond to the footing settlements obtained at the end of each load increment, were extracted from the footing load-settlement curves reported by Lehane et al. (2008). For aged, normally consolidated silica sand, the parameter λ (Eq. 3.13 from Volume II) in Lee and Salgado's method was set to a value of 0.53, and the E/q_c ratio in Schmertmann's method was set to a value of 3.5 (Robertson & Campanella, 1989). An average unit weight of 16.4 kN/m^3 (104.3 pcf) (Table 2.1) was used for the sand layer in the analysis. Table 2.3 to Table 2.6 summarize the settlement calculations for footings 1–4, respectively, subjected to an unfactored structural load of 100 kN (22.5 kips). For convenience, the values of cone resistance and elastic modulus reported in the tables have been rounded to the nearest whole number.

The tolerable settlement for shallow foundations in sand has traditionally been assumed to be 25 mm (1 in.). Figure 2.6b shows that, for a settlement of 25 mm (1 in.), the footing load predicted using Lee and Salgado's method is in excellent agreement with that obtained from the static load test, while Schmertmann's method overpredicts the footing load by a factor of 1.4. For a settlement of 25 mm (1 in.), the net unit load

TABLE 2.2
Dimensions of Shenton Park footings (Lehane et al., 2008)

Footing	Width B	Embedment Depth D	Thickness t
1	1.5 m (4.9 ft)	1.0 m (3.3 ft)	1.0 m (3.3 ft)
2	1.0 m (3.3 ft)	1.0 m (3.3 ft)	1.0 m (3.3 ft)
3	1.0 m (3.3 ft)	0.5 m (1.65 ft)	0.5 m (1.65 ft)
4	0.67 m (2.2 ft)	1.0 m (3.3 ft)	1.0 m (3.3 ft)

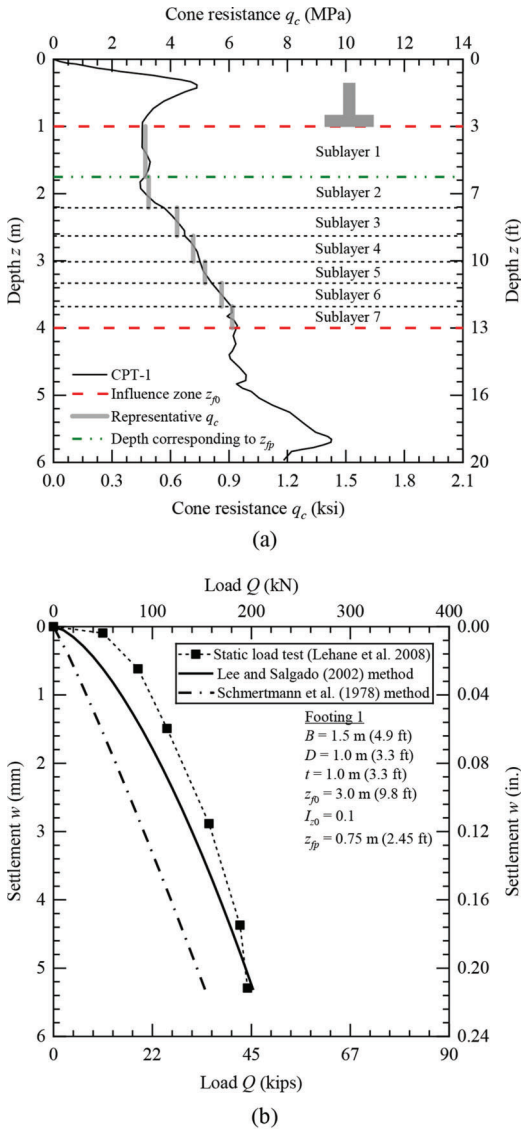

Figure 2.3 Analysis of footing 1 at Shenton Park: (a) discretization of q_c profile into sublayers and (b) comparison between predicted and measured load-settlement curves.

$q_{b,\text{net}}$ (= $q_b - \sigma'_{v0}$) at the base of footing 4 (B = 0.67 m (2.2 ft)) obtained from Lee and Salgado's method is 320 kPa (46 psi) while that obtained from Schmertmann's method is 450 kPa (65 psi); q_b = gross unit load on the footing base, and σ'_{v0} = *in situ* vertical effective stress. Note that the net unit load $q_{b,\text{net}}$ for footings in sand is a function of footing settlement level, footing size, and relative density. Figure 2.7 shows that the difference between the settlements predicted using Lee and Salgado's method and those obtained from the static load tests are mostly within ± 30% for all the footings tested at Shenton Park.

A step-by-step example calculation for footing 4, based on the procedure outlined in Section 3.1 of Chapter 3 of Volume II, is shown as follows.

Step 1: Obtain the site stratigraphy, the groundwater table depth, and the unit weight of the soil in each layer of the profile.

a. The site stratigraphy is described in Section 2.1.1.
b. Depth z_w of groundwater table ≈ 18 ft.
c. The unit weight γ_m of the sand layer is in the range of 102.7–105.8 pcf; an average value of 104.3 pcf was used in the calculations.

Step 2: Set the footing shape, geometry, and embedment depth.

Footing shape = square.

Footing width B = 2.20 ft and footing length L = 2.20 ft.

Footing thickness t = 3.28 ft.

Embedment depth D of the footing = 3.28 ft.

Step 3: Classify the soil layers for footing design.

The soil layer below the footing is clean silica sand with fines content less than 5%.

Step 4: Correct the q_c data for pore pressure.

The pore water pressure correction to the q_c data was ignored because (a) the soil is clean silica sand, and (b) the location of the groundwater table is outside the zone of influence of the footing.

Step 5: Obtain the footing load and maximum tolerable settlement.

a. Unfactored structural load Q on the footing = 22.5 kips (assumed).
b. Maximum tolerable angular distortion $\alpha_{\max}$ = 1/500 (or 0.002).
c. Maximum tolerable settlement of the footing (from Table 3.1 of Volume II):

$$w_{\max} = 15 L_R \alpha_{\max} = 15 \times 39.4 \times 0.002 = 1.2 \text{ in.}$$

Step 6: Calculate the total settlement of the footing.

a. Critical-state friction angle ϕ_c = 32° (Table 2.1).
b. Cross-sectional area A of the footing = $L \times B$ = 2.2 × 2.2 = 4.84 ft^2.
Weight W_{ftg} of the footing = $\gamma_c A t$ = 150 × 4.84 × 3.28 = 2,381.28 lb = 2.38 kips.
Weight W_{fill} of the backfill soil = $\gamma_{\text{fill}} A(D - t)$ = 0 (since $D = t$ = 3.28 ft).

TABLE 2.3
Calculation of $I_{zi}\Delta z_i/E_i$ using Lee and Salgado's method for footing 1 at Shenton Park for Q = 22.5 kips (100 kN)

Sublayer i	z_{top} (ft)	z_{bottom} (ft)	z_{middle} (ft)	Δz_i (ft)	q_{ci} (psi)	σ'_{v0} (psi)	K_0	σ'_{h0} (psi)	D_R (%)	$\frac{E_i}{q_{ci}}$	E_i (psi)	z_f (ft)	I_{zi}	$I_{zi}\Delta z_i/E_i$ (in./psi)
1	3.3	5.7	4.5	2.5	456	3.27	0.68	2.22	42	6.80	3,097	1.2	0.367	0.0035
2	5.7	7.3	6.5	1.5	472	4.71	0.52	2.43	41	6.88	3,249	3.2	0.570	0.0032
3	7.3	8.6	7.9	1.4	613	5.75	0.43	2.47	50	6.06	3,715	4.7	0.446	0.0020
4	8.6	9.9	9.3	1.2	694	6.70	0.43	2.88	51	5.97	4,144	6.0	0.333	0.0012
5	9.9	10.9	10.4	1.0	752	7.53	0.43	3.24	51	5.95	4,470	7.1	0.234	0.0007
6	10.9	12.1	11.5	1.1	834	8.33	0.43	3.58	53	5.83	4,859	8.2	0.140	0.0004
7	12.1	13.1	12.6	1.0	887	9.13	0.43	3.92	53	5.81	5,150	9.3	0.045	0.0001

Note: z_{top}, z_{bottom}, and z_{middle} = depth measured from the ground surface to the top, bottom and middle of the sublayer, respectively; Δz_i = thickness of the sublayer; q_{ci} = representative cone resistance of the sublayer; σ'_{v0} and σ'_{h0} = *in situ* vertical and horizontal effective stresses, respectively, at the middle of the sublayer; K_0 = coefficient of lateral earth pressure at-rest; D_R = relative density; E_i = elastic modulus of the sublayer; z_f = vertical distance from the footing base to the middle of the sublayer; and I_{zi} = strain influence factor for the sublayer.

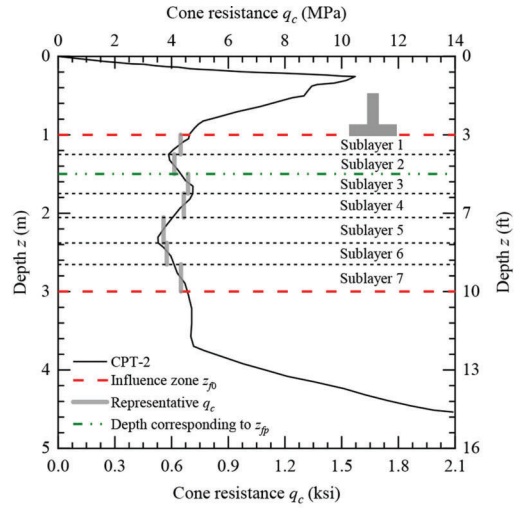

(a)

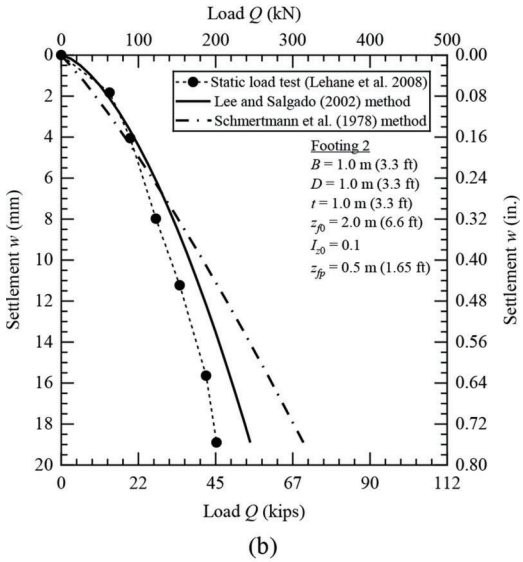

(b)

Figure 2.4 Analysis of footing 2 at Shenton Park: (a) discretization of q_c profile into sublayers and (b) comparison between predicted and measured load-settlement curves.

Gross unit load on the footing base (using Eq. 3.3 from Volume II):

$$q_b = \frac{Q + W_{ftg} + W_{fill}}{A} = \frac{22.5 + 2.38 + 0}{4.84} = 5.14 \text{ ksf (or 35.7 psi)}$$

c. Influence depth measured from the footing base (using Eq. 3.5 from Volume II):

$$\frac{z_{f0}}{B} = 2 + 0.4\left[\min\left(\frac{L}{B}; 6\right) - 1\right] = 2 + 0.4\left[\min\left(\frac{2.2}{2.2}; 6\right) - 1\right] = 2$$

$$\Rightarrow z_{f0} = 2B = 2 \times 2.2 = 4.4 \text{ ft}$$

d. Depth measured from the footing base at which the strain influence factor peaks (using Eq. 3.6 from Volume II):

$$\frac{z_{fp}}{B} = 0.5 + 0.1\left[\min\left(\frac{L}{B}; 6\right) - 1\right] = 0.5 + 0.1\left[\min\left(\frac{2.2}{2.2}; 6\right) - 1\right] = 0.5$$

$$\Rightarrow z_{fp} = 0.5B = 0.5 \times 2.2 = 1.1 \text{ ft}$$

e. Based on the cone resistance profile, the sand layer below the footing was divided into two sublayers (Figure 2.6a), and representative (average) q_c values were assigned to each sublayer. The green dashed double dot line in Figure 2.6a indicates the depth z_{fp} below the footing base at which the strain influence factor peaks. It is useful to have a subdivision at the depth z_{fp} because the slope of the strain influence factor diagram (Figure 3.1 of Volume II) changes at this depth.

f. The following calculations are for sublayer i = 1 with results listed in Table 2.6.
Depth z_{top} measured from the ground surface to the top of the sublayer = 3.28 ft.
Depth z_{bottom} measured from the ground surface to the bottom of the sublayer = 4.38 ft.
Depth measured from the ground surface to the middle of the sublayer:

$$z_{middle} = \frac{z_{top} + z_{bottom}}{2} = \frac{3.28 + 4.38}{2} = 3.83 \text{ ft}$$

Thickness Δz of the sublayer = $z_{bottom} - z_{top}$ = 4.38 – 3.28 = 1.1 ft (or 13.2 in.).

TABLE 2.4
Calculation of $I_{zi}\Delta z_i/E_i$ using Lee and Salgado's method for footing 2 at Shenton Park for Q = 22.5 kips (100 kN)

Sublayer i	z_{top} (ft)	z_{bottom} (ft)	z_{middle} (ft)	Δz_i (ft)	q_{ci} (psi)	σ'_{v0} (psi)	K_0	σ'_{h0} (psi)	D_R (%)	$\frac{E_i}{q_{ci}}$	E_i (psi)	z_f (ft)	I_{zi}	$I_{zi}\Delta z_i/E_i$ (in./psi)
1	3.3	4.1	3.7	0.8	627	2.67	0.70	1.87	56	3.68	2,305	0.4	0.252	0.0011
2	4.1	4.9	4.5	0.8	595	3.27	0.68	2.22	51	3.92	2,331	1.2	0.557	0.0024
3	4.9	5.7	5.3	0.8	665	3.86	0.61	2.36	53	3.80	2,522	2.0	0.650	0.0025
4	5.7	6.7	6.2	1.0	643	4.52	0.54	2.43	52	3.88	2,494	3.0	0.519	0.0025
5	6.7	7.8	7.3	1.1	540	5.27	0.45	2.38	46	4.19	2,259	4.0	0.370	0.0021
6	7.8	8.7	8.3	0.9	556	5.98	0.43	2.57	45	4.22	2,349	5.0	0.228	0.0011
7	8.7	9.8	9.3	1.1	628	6.72	0.43	2.89	47	4.12	2,588	6.0	0.082	0.0004

Note: z_{top}, z_{bottom}, and z_{middle} = depth measured from the ground surface to the top, bottom and middle of the sublayer, respectively; Δz_i = thickness of the sublayer; q_{ci} = representative cone resistance of the sublayer; σ'_{v0} and σ'_{h0} = *in situ* vertical and horizontal effective stresses, respectively, at the middle of the sublayer; K_0 = coefficient of lateral earth pressure at-rest; D_R = relative density; E_i = elastic modulus of the sublayer; z_f = vertical distance from the footing base to the middle of the sublayer; and I_{zi} = strain influence factor for the sublayer.

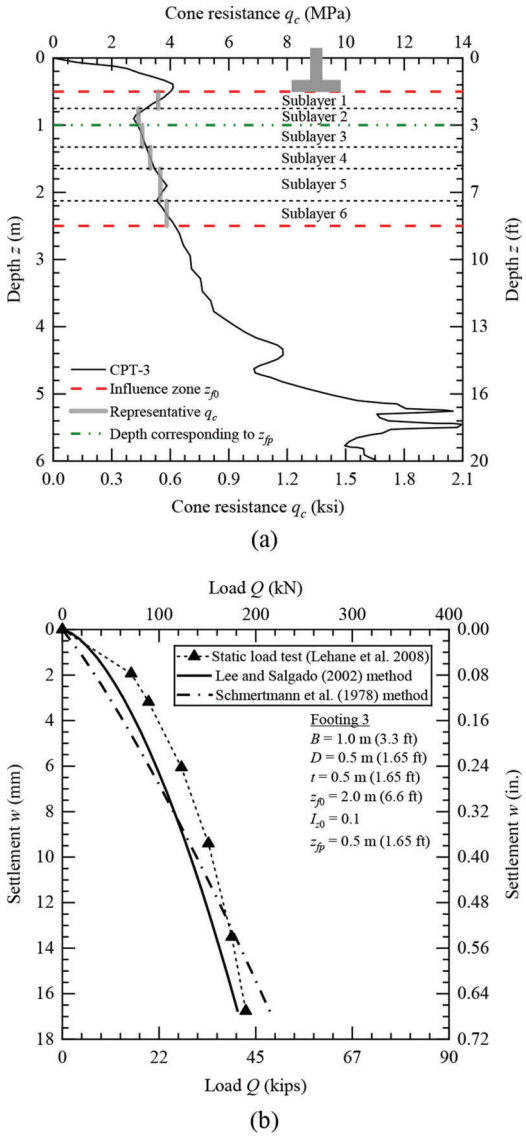

Figure 2.5 Analysis of footing 3 at Shenton Park: (a) discretization of q_c profile into sublayers and (b) comparison between predicted and measured load-settlement curves.

Vertical distance from the footing base to the middle of the sublayer:

$$z_f = z_{middle} - D = 3.83 - 3.28 = 0.55 \text{ ft}$$

Strain influence factor at the footing base level (using Eq. 3.8 from Volume II):

$$I_{z0} = \min\left[0.1 + 0.0111\left(\frac{L}{B} - 1\right); 0.2\right]$$
$$= \min\left[0.1 + 0.0111\left(\frac{2.2}{2.2} - 1\right); 0.2\right] = 0.1$$

In situ vertical effective stress at the footing base level:

$$\sigma'_{v0}\big|_{z_f = 0} = \gamma_m D = 104.3 \times 3.28 = 342.1 \text{ psf (or 2.38 psi)}$$

In situ vertical effective stress at the depth corresponding to z_{fp}:

$$\sigma'_{v0}\big|_{z_f = z_{fp}} = \gamma_m (D + z_{fp})$$
$$= 104.3 \times (3.28 + 1.1) = 456.8 \text{ psf (or 3.17 psi)}$$

Peak strain influence factor (using Eq. 3.9 from Volume II):

$$I_{zp} = 0.5 + 0.1\sqrt{\frac{q_b - \sigma'_{v0}\big|_{z_f = 0}}{\sigma'_{v0}\big|_{z_f = z_{fp}}}}$$

$$= 0.5 + 0.1\sqrt{\frac{35.7 - 2.38}{3.17}} = 0.824$$

Strain influence factor I_z for the sublayer (using Eq. 3.7 from Volume II):

$$I_z = I_{z0} + \frac{z_f}{z_{fp}}(I_{zp} - I_{z0}) = 0.1 + \frac{0.55}{1.1}(0.824 - 0.1) = 0.462$$

g. Coefficient of lateral earth pressure at-rest K_0 of the sublayer = 0.70 (Figure 2.2).
h. *In situ* horizontal effective stress at the middle of the sublayer:

TABLE 2.5
Calculation of $I_{zi}\Delta z_i/E_i$ using Lee and Salgado's method for footing 3 at Shenton Park for Q = 22.5 kips (100 kN)

Sublayer i	z_{top} (ft)	z_{bottom} (ft)	z_{middle} (ft)	Δz_i (ft)	q_{ci} (psi)	σ'_{v0} (psi)	K_0	σ'_{h0} (psi)	D_R (%)	$\frac{E_i}{q_{ci}}$	E_i (psi)	z_f (ft)	I_{zi}	$I_{zi}\Delta z_i/E_i$ (in./psi)
1	1.6	2.5	2.1	0.8	520	1.49	0.70	1.04	61	3.15	1,638	0.4	0.263	0.0016
2	2.5	3.3	2.9	0.8	423	2.08	0.70	1.46	48	3.67	1,554	1.2	0.589	0.0037
3	3.3	4.3	3.8	1.1	441	2.76	0.70	1.93	44	3.92	1,727	2.2	0.670	0.0050
4	4.3	5.4	4.9	1.1	482	3.53	0.65	2.29	43	3.96	1,906	3.2	0.508	0.0034
5	5.4	7.0	6.2	1.6	531	4.49	0.54	2.43	45	3.83	2,037	4.6	0.307	0.0028
6	7.0	8.2	7.6	1.2	563	5.50	0.43	2.36	48	3.70	2,079	6.0	0.093	0.0007

Note: z_{top}, z_{bottom}, and z_{middle} = depth measured from the ground surface to the top, bottom and middle of the sublayer, respectively, Δz_i = thickness of the sublayer, q_{ci} = representative cone resistance of the sublayer, σ'_{v0} and σ'_{h0} = *in situ* vertical and horizontal effective stresses, respectively, at the middle of the sublayer, K_0 = coefficient of lateral earth pressure at-rest, D_R = relative density, E_i = elastic modulus of the sublayer, z_f = vertical distance from the footing base to the middle of the sublayer, and I_{zi} = strain influence factor for the sublayer.

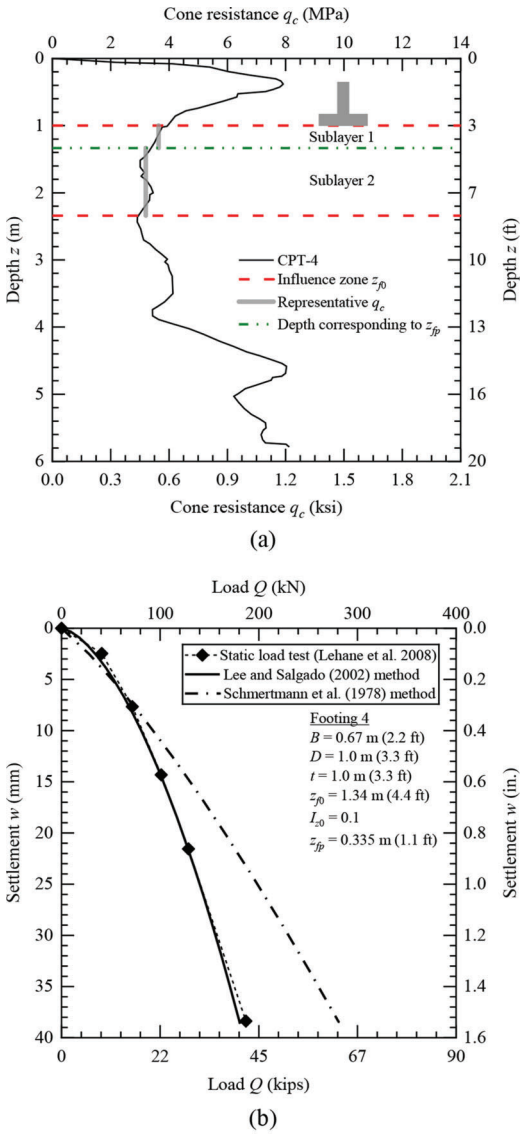

Figure 2.6 Analysis of footing 4 at Shenton Park: (a) discretization of q_c profile into sublayers and (b) comparison between predicted and measured load-settlement curves.

$$\sigma'_{h0} = K_0\sigma'_{v0} = K_0(\gamma_m z_{middle}) = 0.70 \times 104.3 \times 3.83$$
$$= 279.61 \text{ psf (or } 1.94 \text{ psi)}$$

Representative cone resistance q_c of the sublayer = 528.5 psi (or 0.53 ksi).
Relative density of the sublayer (using Eq. 3.10 from Volume II):

$$D_R(\%) = \frac{\ln\left(\frac{q_c}{p_A}\right) - 0.4947 - 0.1041\phi_c - 0.841\ln\left(\frac{\sigma'_{h0}}{p_A}\right)}{0.0264 - 0.0002\phi_c - 0.0047\ln\left(\frac{\sigma'_{h0}}{p_A}\right)}$$
$$= \frac{\ln\left(\frac{528.5}{14.5}\right) - 0.4947 - 0.1041(32) - 0.841\ln\left(\frac{1.94}{14.5}\right)}{0.0264 - 0.0002(32) - 0.0047\ln\left(\frac{1.94}{14.5}\right)}$$
$$= 49.6\% (\approx 50\%)$$

i. Initial guess value for footing settlement $w = w_{max}$ = 1.2 in. (Trial 1). Elastic modulus of the sublayer (using Eq. 3.12 from Volume II):

$$\frac{E}{q_c} = \lambda\left(\frac{w}{L_R}\right)^{-0.285}\left(\frac{B}{L_R}\right)^{0.4}\left(\frac{D_R}{100}\right)^{-0.65}$$
$$= 0.53\left(\frac{1.2}{39.4}\right)^{-0.285}\left(\frac{2.2}{3.28}\right)^{0.4}\left(\frac{49.6}{100}\right)^{-0.65} = 1.927$$

$$\Rightarrow E = 1.927q_c = 1.927 \times 528.5 = 1{,}018 \text{ psi}$$

Recall that the previous calculations were performed for sublayer 1. Repeating substeps f to i for sublayer 2, we obtain Δz = 39.6 in., I_z = 0.412, D_R = 40.3%, and E = 1,024 psi.

j. Depth factor (using Eq. 3.15 from Volume II):

$$C_1 = 1 - 0.5\left(\frac{\sigma'_{v0}|_{z_f=0}}{q_b - \sigma'_{v0}|_{z_f=0}}\right)$$
$$= 1 - 0.5\left(\frac{2.38}{35.7 - 2.38}\right) = 0.964$$

The time factor C_2 is taken as 1.0 because the footing is part of a load test program and not part of a superstructure that is designed to function for several years.

TABLE 2.6
Calculation of $I_{zi}\Delta z_i/E_i$ using Lee and Salgado's method for footing 4 at Shenton Park for Q = 22.5 kips (100 kN)

Sublayer i	z_{top} (ft)	z_{bottom} (ft)	z_{middle} (ft)	Δz_i (ft)	q_{ci} (psi)	σ'_{v0} (psi)	K_0	σ'_{h0} (psi)	D_R (%)	$\frac{E_i}{q_{ci}}$	E_i (psi)	z_f (ft)	I_{zi}	$I_{zi}\Delta z_i/E_i$ (in./psi)
1	3.3	4.4	3.8	1.1	529	2.77	0.70	1.94	50	2.38	1,259	0.5	0.462	0.0048
2	4.4	7.7	6.0	3.3	465	4.37	0.55	2.42	40	2.73	1,266	2.7	0.412	0.0129

Note: z_{top}, z_{bottom}, and z_{middle} = depth measured from the ground surface to the top, bottom and middle of the sublayer, respectively; Δz_i = thickness of the sublayer; q_{ci} = representative cone resistance of the sublayer, σ'_{v0} and σ'_{h0} = *in situ* vertical and horizontal effective stresses, respectively, at the middle of the sublayer; K_0 = coefficient of lateral earth pressure at-rest; D_R = relative density; E_i = elastic modulus of the sublayer; z_f = vertical distance from the footing base to the middle of the sublayer; and I_{zi} = strain influence factor for the sublayer.

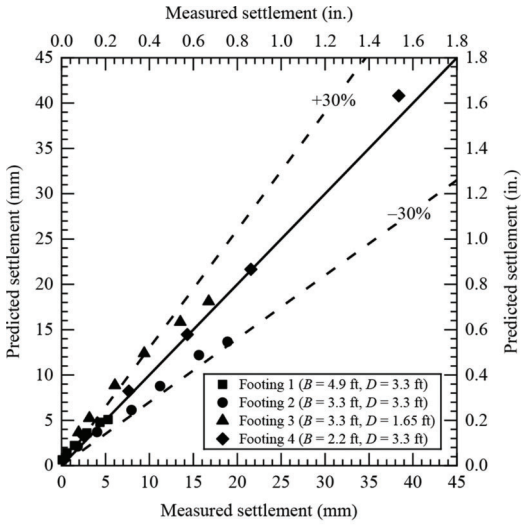

Figure 2.7 Comparison between predicted and measured settlements of footings 1–4 at Shenton Park.

TABLE 2.7
Iterative calculation of total settlement of footing 4 at Shenton Park for Q = 22.5 kips

Trial	Initial Guess Value for Settlement w_{guess} (in.)	Elastic Modulus E (psi)		Calculated Settlement $w_{calculated}$ (in.)
		Sublayer 1	Sublayer 2	
1	1.20	1,018	1,024	0.70
2	0.70	1,185	1,192	0.61
3	0.61	1,238	1,245	0.58
4	0.58	1,253	1,260	0.57
5	0.57	1,259	1,266	0.57

Note: Values of elastic modulus have been rounded to the nearest whole number.

Total settlement of the footing (using Eq. 3.14 from Volume II):

$$w = C_1 C_2 \left(q_b - \sigma'_{v0}\big|_{z_f=0}\right) \sum_{i=1}^{n} \left(\frac{I_{zi}\Delta z_i}{E_i}\right) = 0.964 \times$$

$$1 \times (35.7 - 2.38) \times \left[\frac{0.462(13.2)}{1{,}018} + \frac{0.412(39.6)}{1{,}024}\right]$$

$$= 0.70 \text{ in.}$$

k. Since the calculated value of w (= 0.70 in.) is not equal to the initial guess value (= 1.2 in.), repeat substeps (i) and (j) with w = 0.70 in. (Trial 2). Table 2.7 shows that the value of w converges up to the second decimal place in five iterations. Thus, for an unfactored structural load Q of 22.5 kips, the total settlement w of footing 4, estimated using Lee and Salgado's method, is equal to 0.57 in. The iterative calculations can be performed in Microsoft Excel using one of its built-in functions (refer to Appendix C in Volume II).

Step 7: Total settlement check.

Since the total settlement w (= 0.57 in.) of footing 4, estimated using Lee and Salgado's method, is less than the maximum tolerable settlement w_{max} (= 1.2 in.) established in step 5, the footing design is satisfactory with respect to the serviceability limit state (i.e., excessive settlement) for the structural load under consideration.

TABLE 2.8
Calculation of angular distortion for each adjacent footing pair at Shenton Park for Q = 22.5 kips

Footing Pair	Predicted Differential Settlement Δw (in.)	Center-to-Center Distance Between Footings L_{cc} (ft)	Angular Distortion α (= $\Delta w/L_{cc}$)
1–2	0.10	18.0	0.00046
2–3	0.07	17.1	0.00034
3–4	0.31	13.5	0.0019

Note: The differential settlement between two adjacent footings was computed by taking the difference of their total settlements obtained using Lee and Salgado's method.

Step 8: Angular distortion check.

a. As an exercise, Table 2.8 summarizes the angular distortion, computed using Eq. 3.36 from Volume II, for each pair of adjacent footings at Shenton Park for Q = 22.5 kips.
b. All the footing pairs listed in Table 2.8 satisfy the maximum tolerable angular distortion criterion of 0.002 selected in step 5.

2.1.4 Estimation of Footing Bearing Capacity

Step 1: Determine the nominal or characteristic cone resistance $q_{c,\mathrm{CAM}}$.

All the footings at Shenton Park were embedded at a depth of 1 m (3.3 ft), except footing 3, which was embedded at a depth of 0.5 m (1.65 ft). Figure 2.8 shows the mean trend and bounds of the q_c data points between 1.0–4.0 m (3.3–13.1 ft) depth obtained from the four CPT soundings performed at the site. This depth range was chosen in order to include as many q_c data points below the footing base as possible while ignoring any outliers and regions (e.g., $z > 4$ m (13.1 ft)) where the data points tend to deviate from the mean trend.

Equation of the mean trendline obtained from the regression analysis:

$$E_{qc} = 2.435\left(\frac{\text{psi}}{\text{in.}}\right) \times z + 356.47(\text{psi})$$

Number n of q_c data points contained within the upper and lower bounds = 108.

Number N_σ of standard deviations of cone resistance = 5.05 (from Table 3.3 of Volume II).

Standard deviation of q_c (using Eq. 3.38 from Volume II):

$$\sigma_{qc} = \frac{(q_{c,\max} - q_{c,\min})_{\text{sample}}}{N_\sigma} = \frac{566.78 - 146.17}{5.05} = 83.29 \text{ psi}$$

Relationship of cone resistance with depth that is exceeded by 80% of the measurements (using Eq. 3.37 from Volume II):

$$q_{c,\mathrm{CAM}} = E_{q_c}(z) - 0.84\sigma_{q_c}$$
$$= 2.435z + 356.47 - 0.84(83.29) = 2.435z + 286.51$$

Step 2: Calculate the limit unit bearing capacity of the footing.

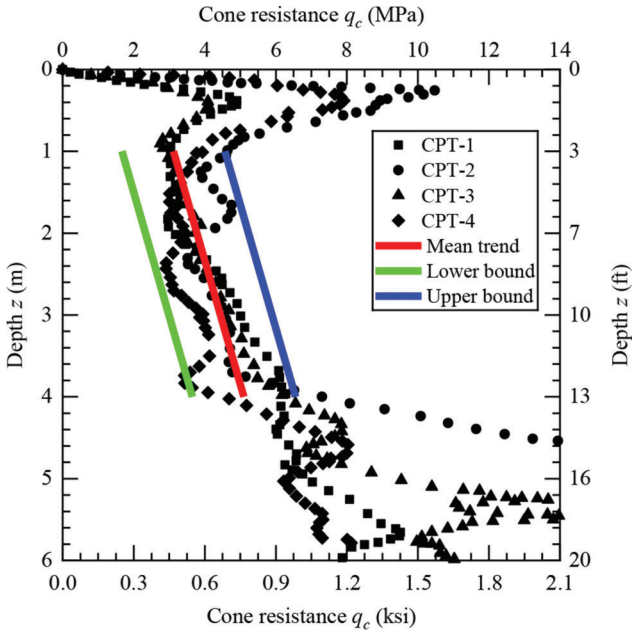

Figure 2.8 Four CPT logs in sand at Shenton Park with mean trendline and range lines.

An example calculation for footing 4, based on the procedure outlined in step 2 of Section 3.2 of Chapter 3 in Volume II, is shown as follows.

a. Since the groundwater table is deep, the unit weight γ to use in the bearing capacity equation is equal to γ_m (104.3 pcf).
b. Conservatively assessed mean (CAM) cone resistance at a depth of $B/2$ below the footing base:

$$q_{c,\mathrm{CAM}} = 2.435z + 286.51 = 2.435\left[D + \frac{B}{2}\right] + 286.51$$
$$= 2.435\left[3.3(12) + \frac{2.2(12)}{2}\right] + 286.51 = 415 \text{ psi}$$

In situ horizontal effective stress at a depth of $B/2$ below the footing base:

$$\sigma'_{h0} = K_0\sigma'_{v0} = K_0\gamma_m\left(D + \frac{B}{2}\right) = 0.565 \times 104.3$$
$$\times \left(3.3 + \frac{2.2}{2}\right) = 259.3 \text{ psf (or 1.8 psi)}$$

(Note: An average K_0 value between 0.43 and 0.70 was used in the calculation of σ'_{h0}).

Relative density at a depth of $B/2$ below the footing base (using Eq. 3.40 from Volume II):

$$D_R(\%) = \frac{\ln\left(\frac{q_{c,\mathrm{CAM}}}{p_A}\right) - 0.4947 - 0.1041\phi_c - 0.841\ln\left(\frac{\sigma'_{h0}}{p_A}\right)}{0.0264 - 0.0002\phi_c - 0.0047\ln\left(\frac{\sigma'_{h0}}{p_A}\right)}$$

$$= \frac{\ln\left(\frac{415}{14.5}\right) - 0.4947 - 0.1041(32) - 0.841\ln\left(\frac{1.8}{14.5}\right)}{0.0264 - 0.0002(32) - 0.0047\ln\left(\frac{1.8}{14.5}\right)} = 43\%$$

c. Representative mean effective stress (using Eq. 3.43 from Volume II):

$$\sigma'_{mp} = 20p_A\left(\frac{\gamma B}{p_A}\right)^{0.7}\left(1 - 0.32\frac{B}{L}\right) = 20 \times 14.5 \times \left(\frac{104.3 \times 2.2}{14.5 \times 144}\right)^{0.7} \times [1 - 0.32(1)] = 42.0 \text{ psi}$$

Peak friction angle (using Eq. 3.41 from Volume II):

$$\phi_p = \phi_c + A_\psi\left\{\frac{D_R}{100}\left[Q - \ln\left(\frac{100\sigma'_{mp}}{p_A}\right)\right] - R_Q\right\} = 32^\circ + 3\left\{\frac{43}{100}\left[10 - \ln\left(\frac{100 \times 42}{14.5}\right)\right] - 1\right\} = 34.6^\circ$$

d. Shape factors s_q and s_γ (using Eqs. 3.44 and 3.45 from Volume II):

$$s_q = 1 + (0.098\phi_p - 1.64)\left(\frac{D}{B}\right)^{0.7 - 0.01\phi_p}\left(\frac{B}{L}\right)^{1 - 0.16\left(\frac{D}{B}\right)} = 1 + [0.098(34.6) - 1.64]\left(\frac{3.3}{2.2}\right)^{0.7 - 0.01(34.6)} = 3.02$$

$$s_\gamma = 1 + (0.0336\phi_p - 1)\frac{B}{L} = 1 + [0.0336(34.6) - 1] = 1.16$$

e. Depth factor d_q (using Eq. 3.46 from Volume II):

$$d_q = 1 + (0.0036\phi_p + 0.393)\left(\frac{D}{B}\right)^{-0.27} = 1 + [0.0036(34.6) + 0.393]\left(\frac{3.3}{2.2}\right)^{-0.27} = 1.46$$

f. Bearing capacity factors N_q and N_γ (using Eqs. 3.47 and 3.48 from Volume II):

$$N_q = \frac{1 + \sin\phi_p}{1 - \sin\phi_p}e^{\pi\tan\phi_p} = \frac{1 + \sin 34.6^\circ}{1 - \sin 34.6^\circ} \times e^{\pi\tan 34.6^\circ} = 31.7$$

$$N_\gamma = (N_q - 0.6)\tan(1.33\phi_p)$$

$$= (31.7 - 0.6)\tan(1.33 \times 34.6^\circ) = 32.2$$

g. Surcharge (vertical effective stress) at the footing base level:

$$q_0 = \gamma_m D = 104.3 \times 3.3 = 344.19 \text{ psf (or 2.39 psi)}$$

Limit unit bearing capacity of the footing (using Eq. 3.49 from Volume II):

$$q_{bL} = (s_q d_q)q_0 N_q + 0.5(s_\gamma d_\gamma)\gamma B N_\gamma = (3.02 \times 1.46 \times 2.39 \times 31.7) + \left(0.5 \times 1.16 \times 1 \times \frac{104.3 \times 2.2}{144} \times 32.2\right) = 363.8 \text{ psi}$$

Net limit bearing capacity $q_{bL,\mathrm{net}}$ of the footing $= q_{bL} - q_0 = 363.8 - 2.39 = 361.4$ psi.

Assuming a factor of safety (FS) of 3, the net allowable bearing capacity of the footing is equal to $q_{bL,\mathrm{net}}/\mathrm{FS} = 361.4/3 = 120.5$ psi.

Table 2.9 summarizes the predicted limit unit bearing capacities of footings 1–4 at Shenton Park. As an example, for a settlement of 1 in., the net unit load $q_{b,\mathrm{net}}$ ($= q_b - \sigma'_{v0}$) at the base of footing 4 ($B = 2.2$ ft) obtained from Lee and Salgado's method is 46 psi. The estimated net limit bearing capacity $q_{bL,\mathrm{net}}$ ($= q_{bL} - q_0$) and net allowable bearing capacity ($q_{bL,\mathrm{net}}/\mathrm{FS}$) of this footing are 361 psi and 120 psi, respectively. Thus, the design of footing 4 is governed by the serviceability limit state (i.e., settlement criterion), which is usually the case for footings in sand.

2.1.5 Load and Resistance Factor Design

As an exercise, the following steps show how to use LRFD for the footings at Shenton Park based on the procedure outlined in Section 3.3 of Chapter 3 in Volume II.

Step 1: Obtain the nominal dead and live loads on the footing.

Both the nominal dead load DL_n and the nominal live load LL_n on each footing were assumed to be equal to 11.25 kips. This assumption was made just to illustrate how LRFD can be applied to the footings in this case history, but in reality, the nominal dead and live loads may be different for each footing and are usually provided by the structural engineer from the superstructure design.

Step 2: Set the load factors.

Load factor for dead load $LF_{DL} = 1.25$ and load factor for live load $LF_{LL} = 1.75$ (AASHTO, 2020).

Step 3: Calculate the nominal resistance of the footing.

Table 2.10 summarizes the nominal resistances R_n of footings 1–4 at Shenton Park. An example calculation for footing 4 is shown as follows.

Cross-sectional area A of the footing $= B^2 = 2.2 \times 2.2 = 4.84$ ft^2 (or 697 in.^{2}).

Nominal resistance of the footing (using Eq. 3.54 from Volume II):

$$R_n = q_{bL,\mathrm{net}}A = (q_{bL} - q_0)A = (363.8 - 2.39) \times 697 = 252 \text{ kips}$$

Step 4: Obtain the resistance factor.

Resistance factor $RF = 0.35$ for square footings in sand (Table 3.5 of Volume II).

Step 5: Verify whether the LRFD inequality is satisfied.

TABLE 2.9
Calculation of limit unit bearing capacities of footings 1–4 at Shenton Park

Parameter	Footing 1	Footing 2	Footing 3	Footing 4
Footing width B (ft)	4.9	3.3	3.3	2.2
Embedment depth D (ft)	3.3	3.3	1.65	3.3
Conservatively assessed mean cone resistance $q_{c,\mathrm{CAM}}$ (psi)	454	430	382	415
Relative density D_R (%)	40	42	46	43
Representative mean effective stress σ'_{mp} (psi)	74	56	56	42
Peak friction angle ϕ_p (°)	33.5	34.1	34.6	34.6
Shape factor s_q	2.42	2.70	2.37	3.02
Shape factor s_γ	1.13	1.15	1.16	1.16
Depth factor d_q	1.57	1.52	1.62	1.46
Depth factor d_γ	1.00	1.00	1.00	1.00
Bearing capacity factor N_q	27.9	29.7	31.8	31.7
Bearing capacity factor N_γ	26.9	29.5	32.4	32.2
Limit unit bearing capacity q_{bL} (psi)	306	329	191	364
Net allowable bearing capacity (psi)[1]	101	109	63	120
Net unit load $q_{b,\mathrm{net}}$ for 1 in. settlement (psi)[2]	35	43	34	46

Note: The values of $q_{c,\mathrm{CAM}}$, D_R, σ'_{mp}, q_{bL}, and $q_{b,\mathrm{net}}$ have been rounded to the nearest whole number.
[1]Assuming a factor of safety of 3 based on the Working Stress Design (WSD) method.
[2]Using Lee and Salgado's method.

TABLE 2.10
Calculation of resistances and equivalent factors of safety for footings 1–4 at Shenton Park for $DL_n = LL_n = 11.25$ kips

Parameter	Footing 1	Footing 2	Footing 3	Footing 4
Footing width B (ft)	4.9	3.3	3.3	2.2
Embedment depth D (ft)	3.3	3.3	1.65	3.3
Limit unit bearing capacity q_{bL} (psi)	306	329	191	364
Nominal resistance R_n (kips)	1,060	507	294	252
Factored resistance $(RF)R_n$ (kips)	371	177	103	88
Factored load $LF_{DL}DL_n + LF_{LL}LL_n$ (kips)	34	34	34	34
Mean resistance R (kips)	1,167	563	329	281
Bias factor b_R	1.10	1.11	1.12	1.12
Equivalent factor of safety	4.72	4.76	4.80	4.80

Note: Loads and resistances have been rounded to the nearest whole number.

Table 2.10 summarizes the results obtained for footings 1–4 at Shenton Park. An example calculation for footing 4 is shown as follows.

Factored load = $LF_{DL}DL_n + LF_{LL}LL_n$ = (1.25 × 11.25) + (1.75 × 11.25) = 33.75 kips ≈ 34 kips.

Factored resistance = $(RF)R_n$ = 0.35 × 252 = 88.2 kips ≈ 88 kips.

As the factored resistance of the footing is greater than the factored load applied on the footing, the LRFD inequality (Eq. 3.55 of Volume II) is satisfied, and thus the footing design is satisfactory with respect to the ultimate limit state (i.e., bearing capacity failure) for a target probability of failure of 10^{-3}.

Because LRFD is a more rational and evolved design method than Working Stress Design (WSD), there is no need to further calculate safety factors. However, as an example, the following calculations show how to obtain an equivalent factor of safety (FS), if needed, for the design of footing 4 produced using LRFD.

Footing width B = 2.2 ft.

Embedment depth D = 3.3 ft.

Mean cone resistance at a depth of $B/2$ below the footing base (Figure 2.8):

$$E_{qc} = 2.435z + 356.47 = 2.435\left[D + \frac{B}{2}\right] + 356.47$$

$$= 2.435\left[3.3(12) + \frac{2.2(12)}{2}\right] + 356.47 = 485 \text{ psi}$$

Using the mean cone resistance of 485 psi (instead of $q_{c,\mathrm{CAM}}$ (415 psi)) and following the steps for calculation of limit unit bearing capacity, we obtain D_R = 48%, σ'_{mp} = 42 psi, ϕ_p = 35.3°, s_q = 3.09, s_γ = 1.19, d_q = 1.47, d_γ = 1.00, N_q = 34.5, N_γ = 36.2, and q_{bL} = 405 psi.

Mean resistance R of the footing = $(q_{bL} - q_0)A$ = (405 – 2.39) × 697 = 281 kips.

Bias factor $b_R = R/R_n = 281/252 = 1.12$.

Ratio of nominal live load to nominal dead load $LL_n/DL_n = 11.25/11.25 = 1$.

Equivalent factor of safety (using Eq. 3.56 from Volume II):

$$\mathrm{FS} = b_R \frac{LF_{DL} + LF_{LL}\left(\frac{LL_n}{DL_n}\right)}{\left(\frac{LL_n}{DL_n} + 1\right)RF} = 1.12 \times \frac{1.25 + 1.75(1)}{(1+1)0.35} = 4.80$$

2.2 Square Footings in Silty Sand (College Station, TX, USA)

2.2.1 Site Description and Soil Profile

Briaud and Gibbens (1997) reported the results of five, instrumented, footing load tests performed at the National Geotechnical Experimentation Site on the Texas A&M University Riverside Campus near College Station, Texas, USA. Figure 2.9 shows the soil profile at the site, which consists predominantly of medium dense, silty silica sand of Pleistocene age up to a depth of 11 m (36.1 ft). Sieve analysis results showed the amount of fines content to vary with depth, from 2%–16% to 6%–35% nonplastic fines down to depths of 3 m (9.8 ft) and 9 m (29.5 ft), respectively. The sand layer is overconsolidated due to the desiccation of the fines and the removal of about 1 m (3.3 ft) of overburden prior to the construction of the footings. Below this sand layer, there is a very stiff, marine clay deposit of Eocene age extending down to a depth of about 33 m (108.3 ft). The liquid limit and plasticity index of the clay layer are 40% and 21%, respectively. The groundwater table was observed at a depth of 4.9 m (16.1 ft) from the ground surface. Table 2.11 summarizes the properties of the top 3.5-m-(11.5-ft)-thick silty sand layer, while Figure 2.10 shows the cone resistance profiles obtained from five CPT soundings performed at the site.

TABLE 2.11
Properties of silty sand layer at Texas A&M footing load test site (after Briaud & Gibbens, 1997)

Property	Units	Value
Specific gravity G_s	—	2.64–2.66
Mean particle size D_{50}	mm	0.15–0.20
	(mils)	(5.9–7.9)
Coefficient of uniformity C_U	—	1.8–2.4
Unit weight γ_m	kN/m^3	15.28–15.65
	(pcf)	(97.3–99.6)
Minimum void ratio $e_{\min}$	—	0.62–0.65
Maximum void ratio $e_{\max}$	—	0.91–0.94
Relative density D_R	%	55
Critical-state friction angle ϕ_c[1]	(°)	34.2

[1]Based on consolidated, drained triaxial compression test results.

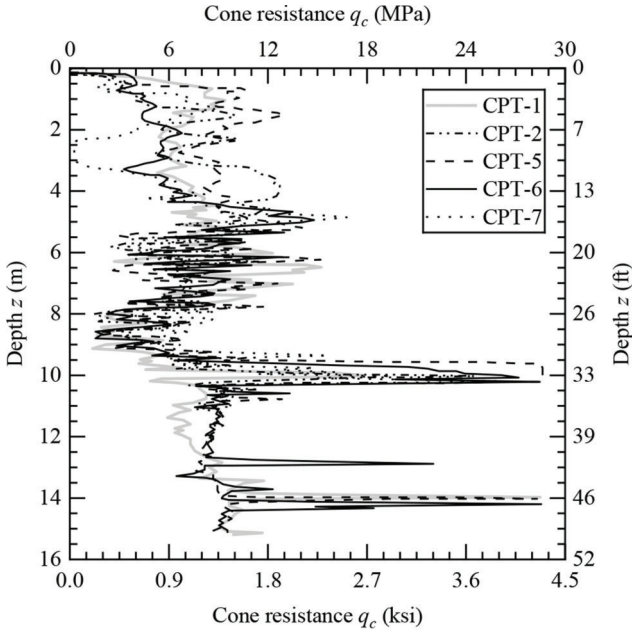

Figure 2.10 Cone resistance profiles obtained from five CPT soundings performed at Texas A&M footing load test site (digitized from Briaud & Gibbens, 1997).

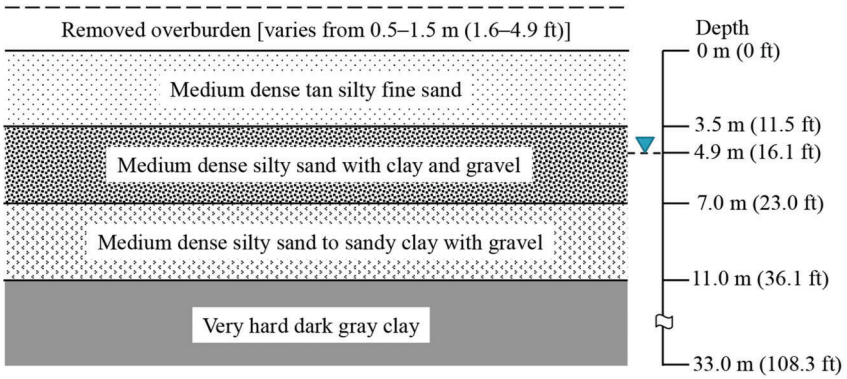

Figure 2.9 Soil profile at Texas A&M footing load test site (modified from Briaud & Gibbens, 1997).

2.2.2 Footing Dimensions and Loading Details

Figure 2.11 shows the layout of the footings and CPT soundings at the site, while Table 2.12 summarizes the as-built dimensions and embedment depth of the footings. The footings were loaded using the reaction provided by four 0.91-m-(3-ft)-diameter, 21.3-m-(70-ft)-long, belled drilled shafts with 60° under-reamed bells of 2.7 m (9 ft) base diameter and one 0.91-m-(3-ft)-diameter, 5-m-(16.5-ft)-long, cylindrical drilled shaft. The footings were loaded in increments equal to 1/10th of the footing capacity estimated by Briaud and Gibbens (1999) using traditional bearing capacity calculation methods. Each load increment was maintained for 30 minutes.

2.2.3 Estimation of Footing Settlement

Figure 2.12 to Figure 2.16 compare the load-settlement curves predicted using both the Lee and Salgado (2002) method and the traditional Schmertmann et al. (1978) method with those obtained from the static load test results reported by Briaud and Gibbens (1997) for footings 1–5, respectively. The measured data points, which correspond to the footing settlements obtained at the end of each load increment, were extracted from the footing load-settlement curves reported by Briaud and Gibbens (1997). An average unit weight of 15.5 kN/m^3 (98.45 pcf) (Table 2.11) was assigned to the silty sand layer above the water table, and a saturated unit weight γ_{sat} of 20.5 kN/m^3 (130.5 pcf) (Salgado, 2008) was assigned to the silty sand layer below the water table. The overconsolidation ratio (OCR) profile for the site was determined based on the removal of 1 m (3.3 ft) of overburden prior to footing construction; the unit weight of the overburden was assumed to be equal to 15.5 kN/m^3 (98.45 pcf). The coefficient of lateral earth pressure at-rest K_0 of each sublayer was determined from the values of $K_{0,NC}$ (taken as 0.45) and OCR using Eq. B.4 in Appendix B of Volume II. For overconsolidated silica sand, the parameter λ (Eq. 3.13 from Volume II) in Lee and Salgado's method was set to a value of 0.91, and the E/q_c ratio in Schmertmann's method was set to a value of 6.0 (Robertson & Campanella, 1989). Table 2.13 to Table 2.17 summarize the settlement calculations for footings 1–5, respectively, subjected to an unfactored structural load of 1 MN (225 kips).

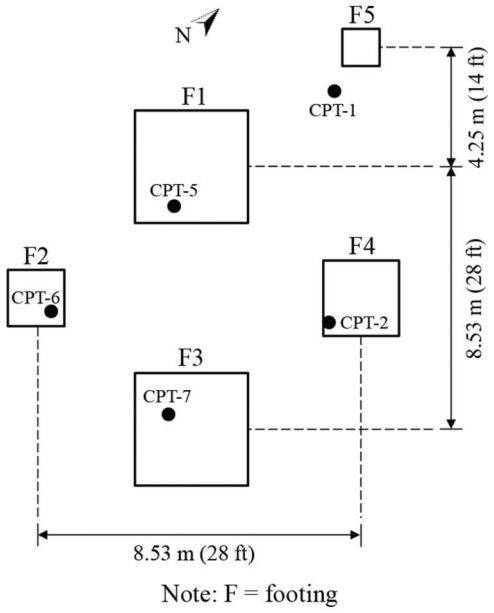

Figure 2.11 Layout of footings and CPT soundings at Texas A&M footing load test site (modified from Briaud & Gibbens, 1997).

Figure 2.14a shows that the cone resistance obtained from sounding CPT-7 is very low (≈ 300 kPa (43 psi)) at a depth of about 3 m (10 ft). The corresponding values of sleeve resistance f_s and friction ratio FR were also reported to be very low at this depth (Briaud & Gibbens, 1997). However, results obtained from adjacent CPT soundings (CPT-2 and CPT-6) reveal that the cone resistance at a depth of 3 m (10 ft) is about 6 MPa (870 psi), which is 20 times greater than that obtained from sounding CPT-7. In addition, results obtained from an SPT boring (SPT-1) adjacent to CPT-7 show that the SPT blow count at the same depth is about 22 (Briaud & Gibbens, 1997). Therefore, we believe that the very low cone resistance observed for sounding CPT-7 near a depth of 3 m (10 ft) may not reflect the true soil state below footing 3. Accordingly, for a depth of about 2.0–3.5 m (6.6–11.5 ft), instead of

TABLE 2.12
As-built dimensions of Texas A&M footings (Briaud & Gibbens, 1999)

Footing	Length L × Width B (as-built)	Embedment Depth D	Thickness t
1	3.004 m × 3.004 m (9.85 ft × 9.85 ft)	0.762 m (2.50 ft)	1.219 m (4.00 ft)
2	1.505 m × 1.492 m (4.94 ft × 4.90 ft)	0.762 m (2.50 ft)	1.219 m (4.00 ft)
3	3.023 m × 3.016 m (9.92 ft × 9.90 ft)	0.889 m (2.92 ft)	1.346 m (4.42 ft)
4	2.496 m × 2.489 m (8.19 ft × 8.17 ft)	0.762 m (2.50 ft)	1.219 m (4.00 ft)
5	0.991 m × 0.991 m (3.25 ft × 3.25 ft)	0.711 m (2.33 ft)	1.168 m (3.83 ft)

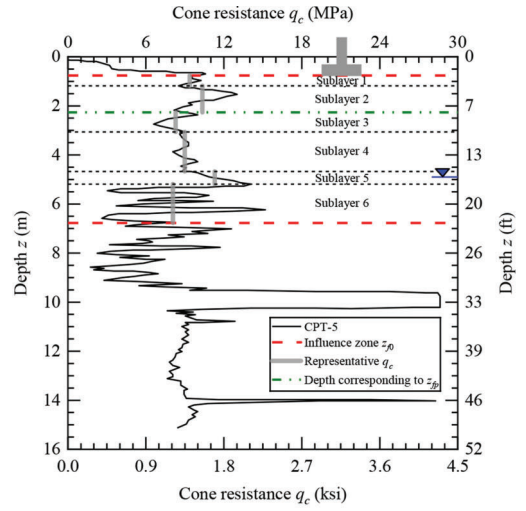

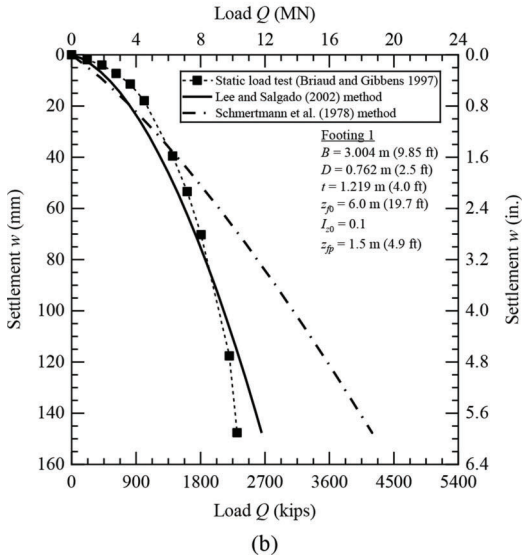

Figure 2.12 Analysis of footing 1 at Texas A&M: (a) discretization of q_c profile into sublayers and (b) comparison between predicted and measured load-settlement curves.

using the cone resistance profile obtained directly from sounding CPT-7, we considered the cone resistance to follow the trend indicated by the blue dashed line in Figure 2.14a.

Figure 2.17 compares the predicted and measured unit base loads (= Q/A) obtained for tolerable settlement levels of 25 mm (1 in.) and 50 mm (2 in.); Q = load applied on the footing, and A = area of the footing base. For a settlement of 25 mm (1 in.), the unit base loads obtained using both Lee and Salgado's method and Schmertmann's method are mostly conservative compared to those obtained from the static load test, with Lee and Salgado's method being slightly more conservative than Schmertmann's method. The ratio of the predicted to the measured unit base load, for 25 mm (1 in.) settlement, is in the range of 0.6–0.8 for Lee and Salgado's method and 0.7–1.0 for

TABLE 2.13
Calculation of $I_{zi}\Delta z_i/E_i$ using Lee and Salgado's method for footing 1 at Texas A&M for Q = 225 kips (1,000 kN)

Sublayer i	z_{top} (ft)	z_{bottom} (ft)	z_{middle} (ft)	Δz_i (ft)	q_{ci} (ksi)	γ_m (pcf)	σ_{v0} (psi)	u_0 (psi)	σ'_{v0} (psi)	σ'_{vp} (psi)	OCR	K_0	σ'_{h0} (psi)	D_R (%)	$\frac{E_i}{q_{ci}}$	E_i (ksi)	z_f (ft)	I_{zi}	$I_{zi}\Delta z_i/E_i$ (in./ksi)
1	2.5	3.9	3.2	1.4	1.36	98.4	2.2	0.0	2.2	4.4	2.03	0.64	1.4	80	8.8	11.9	0.7	0.183	0.25
2	3.9	7.4	5.7	3.5	1.50	98.4	3.9	0.0	3.9	6.1	1.58	0.57	2.2	76	9.1	13.6	3.2	0.479	1.50
3	7.4	10.1	8.7	2.6	1.20	98.4	6.0	0.0	6.0	8.2	1.38	0.53	3.2	62	10.4	12.5	6.2	0.630	1.58
4	10.1	15.3	12.7	5.3	1.30	98.4	8.7	0.0	8.7	10.9	1.26	0.50	4.4	58	10.9	14.2	10.2	0.445	1.99
5	15.3	17.0	16.2	1.7	1.64	130.5	11.1	0.04	11.0	13.3	1.20	0.49	5.4	62	10.4	17.0	13.7	0.282	0.33
6	17.0	22.2	19.6	5.2	1.17	130.5	14.2	1.53	12.7	14.9	1.18	0.49	6.2	45	12.8	15.0	17.1	0.121	0.50

Note: z_{top}, z_{bottom}, and z_{middle} = depth measured from the ground surface to the top, bottom and middle of the sublayer, respectively; Δz_i = thickness of the sublayer; q_{ci} = representative cone resistance of the sublayer; γ_m = unit weight; σ_{v0} = *in situ* vertical total stress at the middle of the sublayer; u_0 = hydrostatic pore water pressure at the middle of the sublayer; σ'_{v0} and σ'_{h0} = *in situ* vertical and horizontal effective stresses, respectively, at the middle of the sublayer; σ'_{vp} = preconsolidation stress; OCR = overconsolidation ratio; K_0 = coefficient of lateral earth pressure at-rest; D_R = relative density; E_i = elastic modulus of the sublayer; z_f = vertical distance from the footing base to the middle of the sublayer; and I_{zi} = strain influence factor for the sublayer.

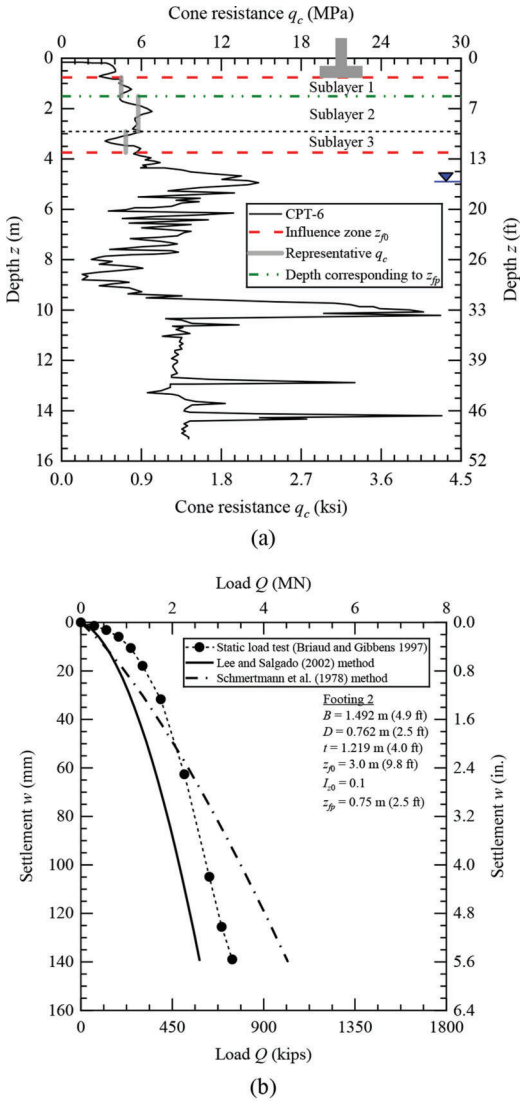

Figure 2.13 Analysis of footing 2 at Texas A&M: (a) discretization of q_c profile into sublayers and (b) comparison between predicted and measured load-settlement curves.

Schmertmann's method. In contrast, for a settlement of 50 mm (2 in.), Lee and Salgado's method predicts unit base loads that are in reasonable agreement with those obtained from the static load test, whereas Schmertmann's method overpredicts the unit base load. The ratio of the predicted to the measured unit base load, for 50 mm (2 in.) settlement, is in the range of 0.7–1.0 for Lee and Salgado's method and 1.0–1.4 for Schmertmann's method.

A step-by-step example calculation for footing 5, based on the procedure outlined in Section 3.1 of Chapter 3 of Volume II, is shown as follows.

Step 1: Obtain the site stratigraphy, the groundwater table depth, and the unit weight of the soil in each layer of the profile.

a. Figure 2.9 shows the soil profile at the site.
b. Depth z_w of groundwater table = 16.1 ft.

TABLE 2.14
Calculation of $I_{zi}\Delta z_i/E_i$ using Lee and Salgado's method for footing 2 at Texas A&M for Q = 225 kips (1,000 kN)

Sublayer i	z_{top} (ft)	z_{bottom} (ft)	z_{middle} (ft)	Δz_i (ft)	q_{ci} (ksi)	γ'_m (pcf)	σ_{v0} (psi)	u_0 (psi)	σ'_{v0} (psi)	σ'_{vp} (psi)	OCR	K_0	σ'_{h0} (psi)	D_R (%)	$\frac{E_i}{q_{ci}}$	E_i (ksi)	z_f (ft)	I_{zi}	$I_{zi}\Delta z_i/E_i$ (in./ksi)
1	2.5	4.9	3.7	2.4	0.65	98.4	2.5	0.0	2.5	4.8	1.88	0.62	1.6	54	4.5	2.9	1.2	0.523	5.25
2	4.9	9.6	7.3	4.6	0.84	98.4	5.0	0.0	5.0	7.2	1.45	0.54	2.7	52	4.6	3.9	4.8	0.649	9.27
3	9.6	12.3	10.9	2.7	0.70	98.4	7.5	0.0	7.5	9.7	1.30	0.51	3.8	36	5.8	4.1	8.4	0.176	1.42

Note: z_{top}, z_{bottom}, and z_{middle} = depth measured from the ground surface to the top, bottom and middle of the sublayer, respectively, Δz_i = thickness of the sublayer, q_{ci} = representative cone resistance of the sublayer, γ_m = unit weight, σ_{v0} = *in situ* vertical total stress at the middle of the sublayer, u_0 = hydrostatic pore water pressure at the middle of the sublayer, σ'_{v0} and σ'_{h0} = *in situ* vertical and horizontal effective stresses, respectively, at the middle of the sublayer, σ'_{vp} = preconsolidation stress, OCR = overconsolidation ratio, K_0 = coefficient of lateral earth pressure at-rest, D_R = relative density, E_i = elastic modulus of the sublayer, z_f = vertical distance from the footing base to the middle of the sublayer, and I_{zi} = strain influence factor for the sublayer.

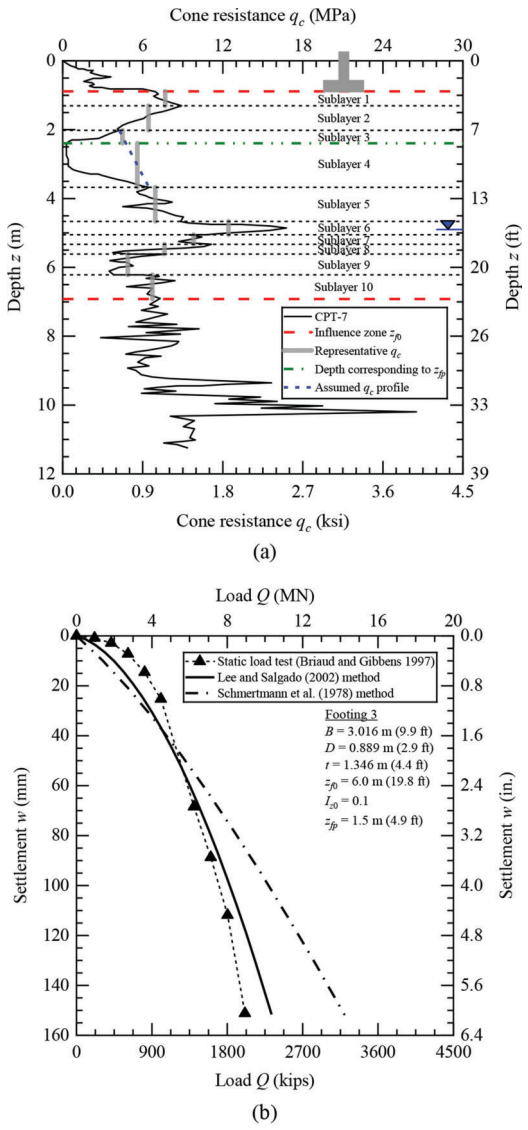

Figure 2.14 Analysis of footing 3 at Texas A&M: (a) discretization of q_c profile into sublayers and (b) comparison between predicted and measured load-settlement curves.

c. The unit weight γ_m of the silty sand layer is in the range of 97.3–99.6 pcf; an average value of 98.45 pcf was used in the calculations.

Step 2: Set the footing shape, geometry, and embedment depth.

a. Footing shape = square.
b. Footing width B = 3.25 ft and footing length L = 3.25 ft.
c. Footing thickness t = 3.83 ft.
d. Embedment depth D of the footing = 2.33 ft.

Step 3: Classify the soil layers for footing design.

The soil layer below the footing is silty silica sand with 2%–16% nonplastic fines.

Step 4: Correct the q_c data for pore pressure.

TABLE 2.15
Calculation of $I_{zi}\Delta z_i/E_i$ using Lee and Salgado's method for footing 3 at Texas A&M for Q = 225 kips (1,000 kN)

Sublayer i	z_{top} (ft)	z_{bottom} (ft)	z_{middle} (ft)	Δz_i (ft)	q_{ci} (ksi)	γ_m (pcf)	σ_{v0} (psi)	u_0 (psi)	σ'_{v0} (psi)	σ'_{vp} (psi)	OCR	K_0	σ'_{h0} (psi)	D_R (%)	$\frac{E_i}{q_{ci}}$	E_i (ksi)	z_f (ft)	I_{zi}	$I_{zi}\Delta z_i/E_i$ (in./ksi)
1	2.9	4.3	3.6	1.4	1.11	98.4	2.5	0.0	2.5	4.7	1.91	0.62	1.5	72	8.7	9.7	0.7	0.182	0.31
2	4.3	6.6	5.5	2.3	0.93	98.4	3.7	0.0	3.7	6.0	1.60	0.57	2.1	60	9.8	9.1	2.5	0.401	1.23
3	6.6	7.9	7.2	1.2	0.65	98.4	5.0	0.0	5.0	7.2	1.45	0.54	2.7	42	12.3	8.0	4.3	0.613	1.14
4	7.9	12.1	10.0	4.2	0.81	98.4	6.8	0.0	6.8	9.1	1.33	0.52	3.5	44	12.0	9.7	7.0	0.589	3.04
5	12.1	15.3	13.7	3.3	1.01	98.4	9.4	0.0	9.4	11.6	1.24	0.50	4.7	46	11.7	11.8	10.8	0.417	1.38
6	15.3	16.6	15.9	1.3	1.80	98.4	10.9	0.0	10.9	13.1	1.21	0.49	5.4	66	9.2	16.6	13.0	0.312	0.29
7	16.6	17.5	17.0	0.9	1.42	130.5	11.9	0.4	11.4	13.7	1.20	0.49	5.6	55	10.4	14.8	14.1	0.262	0.19
8	17.5	18.4	18.0	0.9	1.11	130.5	12.7	0.8	11.9	14.1	1.19	0.49	5.8	44	12.0	13.3	15.0	0.220	0.18
9	18.4	20.4	19.4	2.0	0.71	130.5	14.0	1.4	12.6	14.8	1.18	0.49	6.1	24	18.1	12.8	16.5	0.153	0.28
10	20.4	22.7	21.5	2.3	0.97	130.5	16.0	2.4	13.6	15.8	1.17	0.49	6.6	35	13.9	13.6	18.6	0.053	0.11

Note: z_{top}, z_{bottom}, and z_{middle} = depth measured from the ground surface to the top, bottom and middle of the sublayer, respectively; Δz_i = thickness of the sublayer; q_{ci} = representative cone resistance of the sublayer; γ_m = unit weight; σ_{v0} = *in situ* vertical total stress at the middle of the sublayer; u_0 = hydrostatic pore water pressure at the middle of the sublayer; σ'_{v0} and σ'_{h0} = *in situ* vertical and horizontal effective stresses, respectively, at the middle of the sublayer; σ'_{vp} = preconsolidation stress; OCR = overconsolidation ratio; K_0 = coefficient of lateral earth pressure at-rest; D_R = relative density; E_i = elastic modulus of the sublayer; z_f = vertical distance from the footing base to the middle of the sublayer; and I_{zi} = strain influence factor for the sublayer.

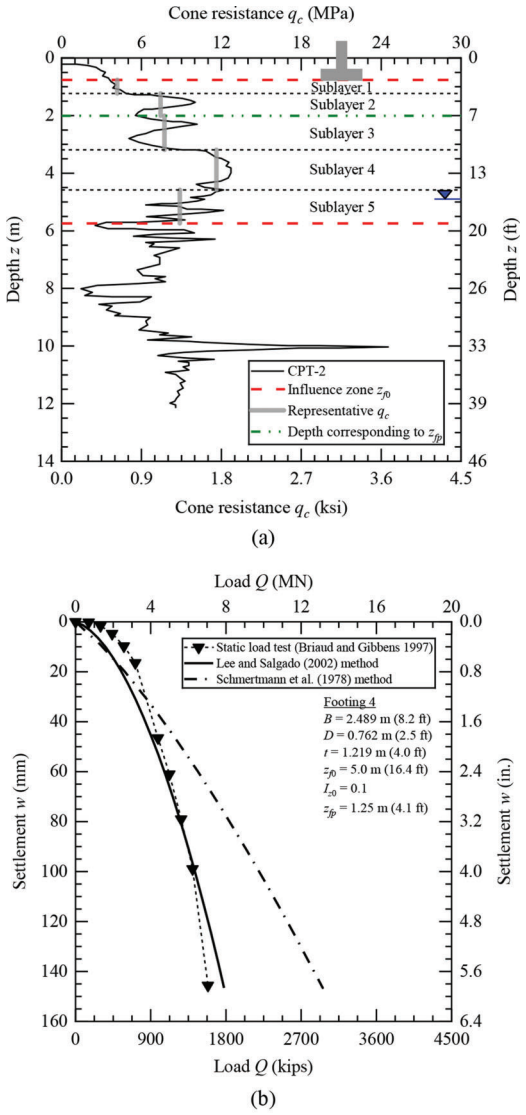

Figure 2.15 Analysis of footing 4 at Texas A&M: (a) discretization of q_c profile into sublayers and (b) comparison between predicted and measured load-settlement curves.

The pore water pressure correction to the q_c data was ignored because the location of the groundwater table is outside the zone of influence of the footing.

Step 5: Obtain the footing load and maximum tolerable settlement.

a. Unfactored structural load Q on the footing = 225 kips (assumed).
b. Maximum tolerable angular distortion α_{max} = 1/500 (or 0.002).
c. Maximum tolerable settlement of the footing (from Table 3.1 of Volume II):

$$w_{max} = 15 L_R \alpha_{max} = 15 \times 0.002 = 1.2 \text{ in.}$$

Step 6: Calculate the total settlement of the footing.

a. Critical-state friction angle ϕ_c = 34.2° (Table 2.11).

TABLE 2.16
Calculation of $I_z \Delta z_i / E_i$ using Lee and Salgado's method for footing 4 at Texas A&M for Q = 225 kips (1,000 kN)

Sublayer i	z_{top} (ft)	z_{bottom} (ft)	z_{middle} (ft)	Δz_i (ft)	q_{ci} (ksi)	γ_m (pcf)	σ_{v0} (psi)	u_0 (psi)	σ'_{v0} (psi)	σ'_{vp} (psi)	OCR	K_0	σ'_{h0} (psi)	D_R (%)	$\frac{E_i}{q_{ci}}$	E_i (ksi)	z_f (ft)	I_{zi}	$I_z \Delta z_i / E_i$ (in./ksi)
1	2.5	4.0	3.3	1.5	0.61	98.4	2.2	0.0	2.2	4.5	2.00	0.64	1.4	53	9.0	5.5	0.8	0.221	0.75
2	4.0	6.6	5.3	2.5	1.08	98.4	3.6	0.0	3.6	5.9	1.62	0.57	2.1	66	7.9	8.5	2.8	0.541	1.94
3	6.6	10.5	8.5	3.9	1.12	98.4	5.8	0.0	5.8	8.1	1.39	0.53	3.1	59	8.4	9.4	6.0	0.623	3.07
4	10.5	15.0	12.7	4.6	1.69	98.4	8.7	0.0	8.7	11.0	1.26	0.50	4.4	68	7.7	13.0	10.2	0.368	1.55
5	15.0	18.8	16.9	3.8	1.29	130.5	11.8	0.4	11.4	13.6	1.20	0.49	5.6	51	9.3	11.9	14.4	0.115	0.44

Note: z_{top}, z_{bottom}, and z_{middle} = depth measured from the ground surface to the top, bottom and middle of the sublayer, respectively; Δz_i = thickness of the sublayer; q_{ci} = representative cone resistance of the sublayer; γ_m = unit weight; σ_{v0} = *in situ* vertical total stress at the middle of the sublayer; u_0 = hydrostatic pore water pressure at the middle of the sublayer; σ'_{v0} and σ'_{h0} = *in situ* vertical and horizontal effective stresses; respectively, at the middle of the sublayer; σ'_{vp} = preconsolidation stress; OCR = overconsolidation ratio; K_0 = coefficient of lateral earth pressure at-rest; D_R = relative density; E_i = elastic modulus of the sublayer; z_f = vertical distance from the footing base to the middle of the sublayer; and I_{zi} = strain influence factor for the sublayer.

b. Cross-sectional area A of the footing = $L \times B = 3.25 \times 3.25 = 10.56$ ft^2.
Weight W_{ftg} of the footing = $\gamma_c A t = 150 \times 10.56 \times 3.83 = 6{,}066.72$ lb = 6.07 kips.
Weight W_{fill} of the backfill soil = $\gamma_{\text{fill}} A(D - t) = 0$ (since $D < t$).
Gross unit load on the footing base (using Eq. 3.3 from Volume II):

$$q_b = \frac{Q + W_{ftg} + W_{\text{fill}}}{A} = \frac{225 + 6.07 + 0}{10.56}$$

$$= 21.88 \text{ ksf (or } 151.8 \text{ psi)}$$

c. Influence depth measured from the footing base (using Eq. 3.5 from Volume II):

$$\frac{z_{f0}}{B} = 2 + 0.4\left[\min\left(\frac{L}{B}; 6\right) - 1\right]$$

$$= 2 + 0.4\left[\min\left(\frac{3.25}{3.25}; 6\right) - 1\right] = 2$$

$$\Rightarrow z_{f0} = 2B = 2 \times 3.25 = 6.5 \text{ ft}$$

d. Depth measured from the footing base at which the strain influence factor peaks (using Eq. 3.6 from Volume II):

$$\frac{z_{fp}}{B} = 0.5 + 0.1\left[\min\left(\frac{L}{B}; 6\right) - 1\right]$$

$$= 0.5 + 0.1\left[\min\left(\frac{3.25}{3.25}; 6\right) - 1\right] = 0.5$$

$$\Rightarrow z_{fp} = 0.5B = 0.5 \times 3.25 = 1.625 \text{ ft}$$

e. Based on the cone resistance profile, the silty sand layer below the footing was divided into three sublayers (Figure 2.16a), and representative (average) q_c values were assigned to each sublayer. The green dashed double dot line in Figure 2.16a indicates the depth z_{fp} below the footing base at which the strain influence factor peaks. It is useful to have a subdivision at the depth z_{fp} because the slope of the strain influence factor diagram (Figure 3.1 of Volume II) changes at this depth.

f. The following calculations are for sublayer $i = 3$ with results listed in Table 2.17.
Depth z_{top} measured from the ground surface to the top of the sublayer = 6.20 ft.
Depth z_{bottom} measured from the ground surface to the bottom of the sublayer = 8.84 ft.
Depth measured from the ground surface to the middle of the sublayer:

$$z_{\text{middle}} = \frac{z_{\text{top}} + z_{\text{bottom}}}{2} = \frac{6.20 + 8.84}{2} = 7.52 \text{ ft}$$

Thickness Δz of the sublayer = $z_{\text{bottom}} - z_{\text{top}} = 8.84 - 6.20 = 2.64$ ft (or 31.7 in.).
Vertical distance from the footing base to the middle of the sublayer:
$z_f = z_{\text{middle}} - D = 7.52 - 2.33 = 5.19$ ft
Strain influence factor at the footing base level (using Eq. 3.8 from Volume II):

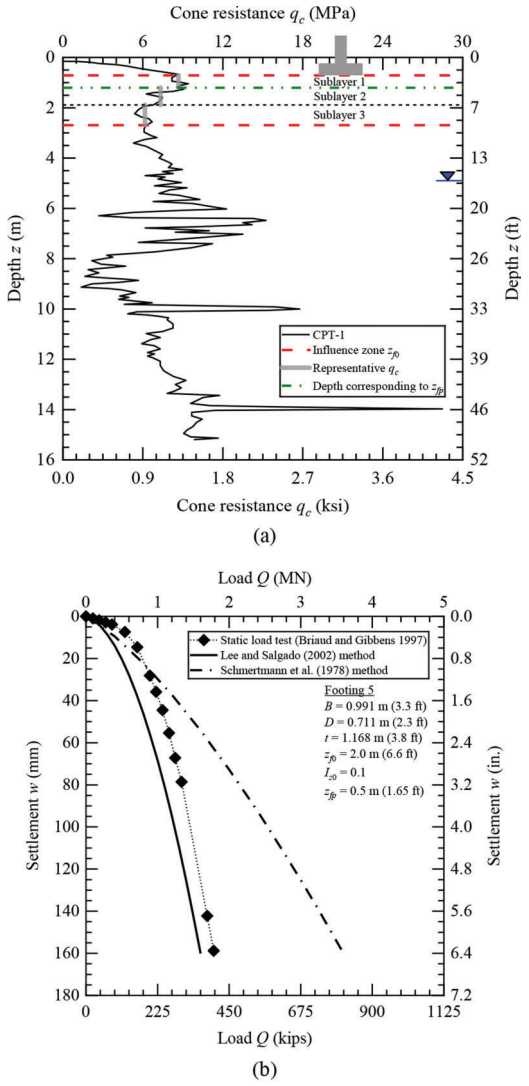

Figure 2.16 Analysis of footing 5 at Texas A&M: (a) discretization of q_c profile into sublayers, and (b) comparison between predicted and measured load-settlement curves.

$$I_{z0} = \min\left[0.1 + 0.0111\left(\frac{L}{B} - 1\right); 0.2\right]$$

$$= \min\left[0.1 + 0.0111\left(\frac{3.25}{3.25} - 1\right); 0.2\right] = 0.1$$

In situ vertical effective stress at the footing base level:

$$\sigma'_{v0}\big|_{z_f = 0} = \gamma_m D = 98.45 \times 2.33 = 229.4 \text{ psf (or } 1.59 \text{ psi)}$$

In situ vertical effective stress at the depth corresponding to z_{fp}:

$$\sigma'_{v0}\big|_{z_f = z_{fp}} = \gamma_m (D + z_{fp}) = 98.45 \times (2.33 + 1.625)$$

$$= 389.4 \text{ psf (or } 2.70 \text{ psi)}$$

TABLE 2.17
Calculation of $I_{zi}\Delta z_i/E_i$ using Lee and Salgado's method for footing 5 at Texas A&M for Q = 225 kips (1,000 kN)

Sublayer i	z_{top} (ft)	z_{bottom} (ft)	z_{middle} (ft)	Δz_i (ft)	q_{ci} (ksi)	γ_m (pcf)	σ_{v0} (psi)	u_0 (psi)	σ'_{v0} (psi)	σ'_{vp} (psi)	OCR	K_0	σ'_{h0} (psi)	D_R (%)	$\frac{E_i}{q_{ci}}$	E_i (ksi)	z_f (ft)	I_{zi}	$I_{zi}\Delta z_i/E_i$ (in./ksi)
1	2.3	4.0	3.1	1.6	1.26	98.4	2.2	0.0	2.2	4.4	2.04	0.64	1.4	78	2.3	2.9	0.8	0.673	4.56
2	4.0	6.2	5.1	2.2	1.06	98.4	3.5	0.0	3.5	5.7	1.65	0.58	2.0	66	2.5	2.7	2.7	0.959	9.53
3	6.2	8.8	7.5	2.6	0.89	98.4	5.1	0.0	5.1	7.4	1.44	0.54	2.8	53	2.9	2.6	5.2	0.337	4.07

Note: z_{top}, z_{bottom}, and z_{middle} = depth measured from the ground surface to the top, bottom and middle of the sublayer, respectively; Δz_i = thickness of the sublayer; q_{ci} = representative cone resistance of the sublayer; γ_m = unit weight; σ_{v0} = *in situ* vertical total stress at the middle of the sublayer; u_0 = hydrostatic pore water pressure at the middle of the sublayer; σ'_{v0} and σ'_{h0} = *in situ* vertical and horizontal effective stresses, respectively, at the middle of the sublayer; σ'_{vp} = preconsolidation stress; OCR = overconsolidation ratio; K_0 = coefficient of lateral earth pressure at-rest; D_R = relative density; E_i = elastic modulus of the sublayer; z_f = vertical distance from the footing base to the middle of the sublayer; and I_{zi} = strain influence factor for the sublayer.

Peak strain influence factor (using Eq. 3.9 from Volume II):

$$I_{zp} = 0.5 + 0.1\sqrt{\frac{q_b - \sigma'_{v0}\big|_{z_f=0}}{\sigma'_{v0}\big|_{z_f=z_{fp}}}} = 0.5 + 0.1\sqrt{\frac{151.8 - 1.59}{2.7}} = 1.246$$

Strain influence factor I_z for the sublayer (using Eq. 3.7 from Volume II):

$$I_z = \frac{z_{f0} - z_f}{z_{f0} - z_{fp}} I_{zp} = \frac{6.5 - 5.19}{6.5 - 1.625} \times 1.246 = 0.337$$

g. Coefficient of lateral earth pressure at-rest $K_{0,NC}$ of the sublayer if it were normally consolidated = 0.45 (assumed). Preconsolidation stress at the middle of the sublayer (before the removal of 1 m (3.28 ft) of overburden at the site):

$$\sigma'_{vp} = \gamma_m(z_{middle} + 3.28) = 98.45 \times (7.52 + 3.28)$$
$$= 1{,}063.3 \text{ psf (or 7.38 psi)}$$

Current vertical effective stress at the middle of the sublayer (after the removal of 1 m (3.28 ft) of overburden at the site):

$$\sigma'_v = \gamma_m z_{middle} = 98.45 \times 7.52 = 740.3 \text{ psf (or 5.14 psi)}$$

Overconsolidation ratio (OCR) of the sublayer due to the removal of 1 m (3.28 ft) of overburden at the site:

$$OCR = \frac{\sigma'_{vp}}{\sigma'_v} = \frac{7.38}{5.14} = 1.44$$

Coefficient of lateral earth pressure at-rest of the sublayer (using Eq. B.4 in Appendix B of Volume II):

$$K_0 = K_{0,NC}\sqrt{OCR} = 0.45 \times \sqrt{1.44} = 0.54$$

h. *In situ* horizontal effective stress at the middle of the sublayer:

$\sigma'_{h0} = K_0(\gamma_m z_{middle}) = 0.54 \times 98.45 \times 7.52 = 399.8$ psf (or 2.78 psi)

Representative cone resistance q_c of the sublayer = 892.6 psi (or 0.89 ksi).
Relative density of the sublayer (using Eq. 3.10 from Volume II):

$$D_R(\%) = \frac{\ln\left(\frac{q_c}{p_A}\right) - 0.4947 - 0.1041\phi_c - 0.841\ln\left(\frac{\sigma'_{h0}}{p_A}\right)}{0.0264 - 0.0002\phi_c - 0.0047\ln\left(\frac{\sigma'_{h0}}{p_A}\right)}$$
$$= \frac{\ln\left(\frac{892.6}{14.5}\right) - 0.4947 - 0.1041(34.2) - 0.841\ln\left(\frac{2.78}{14.5}\right)}{0.0264 - 0.0002(34.2) - 0.0047\ln\left(\frac{2.78}{14.5}\right)}$$
$$= 53.2\%$$

i. Initial guess value for footing settlement $w = w_{max}$ = 1.2 in. (Trial 1).

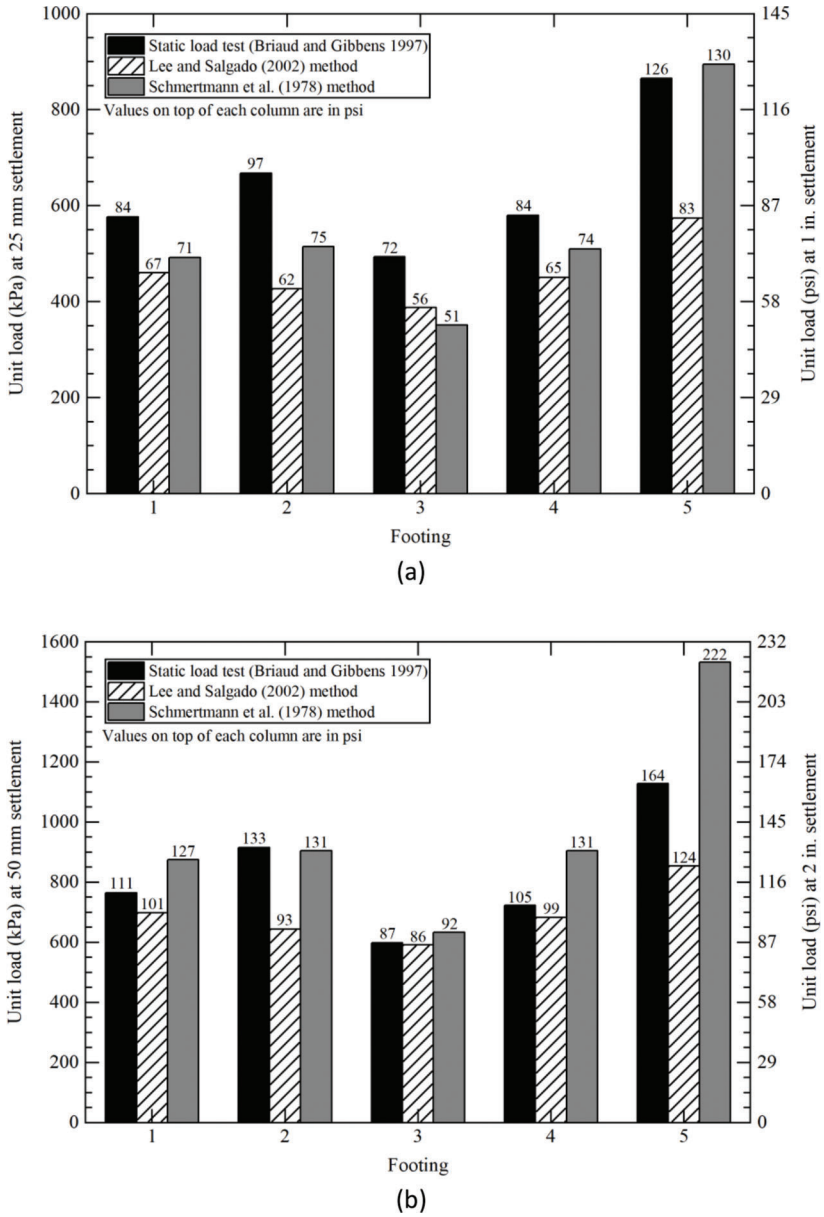

Figure 2.17 Comparison between predicted and measured unit base loads at Texas A&M for (a) 25 mm (1 in.) settlement and (b) 50 mm (2 in.) settlement.

Elastic modulus of the sublayer (using Eq. 3.12 from Volume II):

$$\frac{E}{q_c} = \lambda\left(\frac{w}{L_R}\right)^{-0.285}\left(\frac{B}{L_R}\right)^{0.4}\left(\frac{D_R}{100}\right)^{-0.65}$$

$$= 0.91\left(\frac{1.2}{39.4}\right)^{-0.285}\left(\frac{3.25}{3.28}\right)^{0.4}\left(\frac{53.2}{100}\right)^{-0.65} = 3.7$$

$$\Rightarrow E = 3.7q_c = 3.7 \times 892.6 = 3{,}303 \text{ psi}$$

Recall that the previous calculations were performed for sublayer 3. Repeating substeps f to i for sublayers 1 and 2, we obtain:
Sublayer 1 $\rightarrow \Delta z = 19.5$ in., $I_z = 0.673$, $D_R = 77.9\%$, and $E = 3{,}629$ psi

Sublayer 2 $\rightarrow \Delta z = 26.8$ in., $I_z = 0.959$, $D_R = 66.0\%$, and $E = 3{,}416$ psi

j. Depth factor (using Eq. 3.15 from Volume I):

$$C_1 = 1 - 0.5\left(\frac{\sigma'_{v0}\big|_{z_f=0}}{q_b - \sigma'_{v0}\big|_{z_f=0}}\right)$$

$$= 1 - 0.5\left(\frac{1.59}{151.8 - 1.59}\right) = 0.995$$

The time factor C_2 is taken as 1.0 because the footing is part of a load test program and not part of a superstructure that is designed to function for several years.

Total settlement of the footing (using Eq. 3.14 from Volume II):

$$w = C_1 C_2 \left(q_b - \sigma'_{v0}\big|_{z_f=0}\right) \sum_{i=1}^{n} \left(\frac{I_{zi}\Delta z_i}{E_i}\right)$$
$$= 0.995 \times 1 \times (151.8 - 1.59)$$
$$\times \left[\frac{0.673(19.5)}{3{,}629} + \frac{0.959(26.8)}{3{,}416} + \frac{0.337(31.7)}{3{,}303}\right]$$
$$= 2.15 \text{ in.}$$

k. As the calculated value of w (= 2.15 in.) is not equal to the initial guess value (= 1.2 in.), repeat substeps (i) and (j) with w = 2.15 in. (Trial 2). Table 2.18 shows that the value of w converges up to the second decimal place in six iterations. Thus, for an unfactored structural load Q of 225 kips, the total settlement w of footing 5, estimated using Lee and Salgado's method, is equal to 2.71 in. The iterative calculations can be performed in Microsoft Excel using one of its built-in functions (refer to Appendix C of Volume II).

Step 7: Total settlement check.

For an unfactored structural load of 225 kips, the total settlement w (= 2.71 in.) of footing 5, estimated using Lee and Salgado's method, is greater than the maximum tolerable settlement w_{max} (= 1.2 in.) established in step 5. The footing would thus have to be redesigned in order to satisfy the total settlement check for the structural load under consideration.

2.2.4 Estimation of Footing Bearing Capacity

Step 1: Determine the nominal or characteristic cone resistance $q_{c,CAM}$.

The footings at Texas A&M were embedded at depths ranging from 0.7–0.9 m (2.3–2.9 ft). Figure 2.18 shows the mean trend and bounds of the q_c data points between 0.7–8.0 m (2.3–26.2 ft) depth obtained from the five CPT soundings performed at the site. This depth range was chosen in order to include as many q_c data points below the footing base as possible while ignoring any outliers and regions (e.g., $z > 8$ m (26.2 ft)) where the data points tend to deviate from the mean trend.

Equation of the mean trendline obtained from the regression analysis:

$$E_{qc} = 0.097\left(\frac{\text{psi}}{\text{in.}}\right) \times z + 1{,}074.19(\text{psi})$$

Number n of q_c data points contained within the upper and lower bounds = 489.

Number N_σ of standard deviations of cone resistance = 6.06 (from Table 3.3 of Volume II).

Standard deviation of q_c (using Eq. 3.38 from Volume II):

$$\sigma_{qc} = \frac{(q_{c,max} - q_{c,min})_{sample}}{N_\sigma} = \frac{1{,}855.5 - 290.1}{6.06} = 263.27 \text{ psi}$$

Relationship of cone resistance with depth that is exceeded by 80% of the measurements (using Eq. 3.37 from Volume II):

$$q_{c,CAM} = E_{q_c}(z) - 0.84\sigma_{q_c} = 0.097z + 1{,}074.19$$
$$- 0.84(263.27) \;=\; 0.097z + 853.04$$

Step 2: Calculate the limit unit bearing capacity of the footing.

An example calculation for footing 5, based on the procedure outlined in step 2 of Section 3.2 of Chapter 3 in Volume II, is shown as follows.

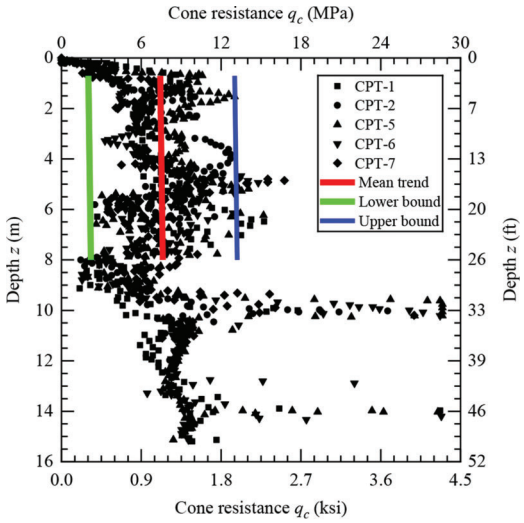

Figure 2.18 Five CPT logs in sand at Texas A&M with mean trendline and range lines.

TABLE 2.18
Iterative calculation of total settlement of footing 5 at Texas A&M for Q = 225 kips

Trial	Initial Guess Value for Settlement w_{guess} (in.)	Elastic Modulus E (psi)			Calculated Settlement $w_{calculated}$ (in.)
		Sublayer 1	Sublayer 2	Sublayer 3	
1	1.20	3,629	3,416	3,303	2.15
2	2.15	3,073	2,893	2,791	2.54
3	2.54	2,931	2,759	2,662	2.66
4	2.66	2,891	2,722	2,626	2.70
5	2.70	2,880	2,712	2,616	2.71
6	2.71	2,877	2,709	2,613	2.71

Note: Values of elastic modulus have been rounded to the nearest whole number.

a. Since the groundwater table is deep, the unit weight γ to use in the bearing capacity equation is equal to γ_m (98.45 pcf).
b. Conservatively assessed mean (CAM) cone resistance at a depth of $B/2$ below the footing base:

$$q_{c,\mathrm{CAM}} = 0.097z + 853.04 = 0.097\left[D + \frac{B}{2}\right] + 853.04$$
$$= 0.097\left[2.33(12) + \frac{3.25(12)}{2}\right] + 853.04 = 857.6 \text{ psi}$$

Preconsolidation stress at a depth of $B/2$ below the footing base (before the removal of 1 m (3.28 ft) of overburden):

$$\sigma'_{vp} = \gamma_m\left(D + \frac{B}{2} + 3.28\right) = 98.45 \times \left(2.33 + \frac{3.25}{2} + 3.28\right)$$
$$= 712.3 \text{ psf (or 4.95 psi)}$$

Current vertical effective stress at a depth of $B/2$ below the footing base (after the removal of 1 m (3.28 ft) of overburden):

$$\sigma'_v = \gamma_m\left(D + \frac{B}{2}\right) = 98.45 \times \left(2.33 + \frac{3.25}{2}\right)$$
$$= 389.4 \text{ psf (or 2.70 psi)}$$

Overconsolidation ratio (OCR) at a depth of $B/2$ below the footing base due to the removal of 1 m (3.28 ft) of overburden:

$$\mathrm{OCR} = \frac{\sigma'_{vp}}{\sigma'_v} = \frac{4.95}{2.70} = 1.83$$

Coefficient of lateral earth pressure at-rest (using Eq. B.4 in Appendix B of Volume II):

$$K_0 = K_{0,\mathrm{NC}}\sqrt{\mathrm{OCR}} = 0.45 \times \sqrt{1.83} = 0.61$$

In situ horizontal effective stress at a depth of $B/2$ below the footing base:

$$\sigma'_{h0} = K_0\gamma_m\left(D + \frac{B}{2}\right) = 0.61 \times 98.45$$
$$\times \left(2.33 + \frac{3.25}{2}\right) = 237.5 \text{ psf (or 1.65 psi)}$$

Relative density at a depth of $B/2$ below the footing base (Eq. 3.40 from Volume II):

$$D_R(\%) = \frac{\ln\left(\frac{q_{c,\mathrm{CAM}}}{p_A}\right) - 0.4947 - 0.1041\phi_c - 0.841\ln\left(\frac{\sigma'_{h0}}{p_A}\right)}{0.0264 - 0.0002\phi_c - 0.0047\ln\left(\frac{\sigma'_{h0}}{p_A}\right)}$$
$$= \frac{\ln\left(\frac{857.6}{14.5}\right) - 0.4947 - 0.1041(34.2) - 0.841\ln\left(\frac{1.65}{14.5}\right)}{0.0264 - 0.0002(34.2) - 0.0047\ln\left(\frac{1.65}{14.5}\right)}$$
$$= 62.2\%$$

c. Representative mean effective stress (using Eq. 3.43 from Volume II):

$$\sigma'_{mp} = 20p_A\left(\frac{\gamma B}{p_A}\right)^{0.7}\left(1 - 0.32\frac{B}{L}\right) = 20 \times 14.5$$
$$\times \left(\frac{98.45 \times 3.25}{14.5 \times 144}\right)^{0.7} \times [1 - 0.32(1)] = 53.1 \text{ psi}$$

Peak friction angle (using Eq. 3.41 from Volume II):

$$\phi_p = \phi_c + A_\psi\left\{\frac{D_R}{100}\left[Q - \ln\left(\frac{100\sigma'_{mp}}{p_A}\right)\right] - R_Q\right\}$$
$$= 34.2^\circ + 3\left\{\frac{62.2}{100}\left[10 - \ln\left(\frac{100 \times 53.1}{14.5}\right)\right] - 1\right\} = 38.85^\circ$$

d. Shape factors s_q and s_γ (using Eqs. 3.44 and 3.45 from Volume II):

$$s_q = 1 + (0.098\phi_p - 1.64)\left(\frac{D}{B}\right)^{0.7 - 0.01\phi_p}\left(\frac{B}{L}\right)^{1 - 0.16\left(\frac{D}{B}\right)}$$
$$= 1 + [0.098(38.85) - 1.64]\left(\frac{2.33}{3.25}\right)^{0.7 - 0.01(38.85)}$$
$$= 2.95$$

$$s_\gamma = 1 + (0.0336\phi_p - 1)\frac{B}{L} = 1 + [0.0336(38.85) - 1] = 1.31$$

e. Depth factor d_q (using Eq. 3.46 from Volume II):

$$d_q = 1 + (0.0036\phi_p + 0.393)\left(\frac{D}{B}\right)^{-0.27}$$
$$= 1 + [0.0036(38.85) + 0.393]\left(\frac{2.33}{3.25}\right)^{-0.27} = 1.58$$

f. Bearing capacity factors N_q and N_γ (using Eqs. 3.47 and 3.48 from Volume II):

$$N_q = \frac{1 + \sin\phi_p}{1 - \sin\phi_p}e^{\pi\tan\phi_p} = \frac{1 + \sin 38.85^\circ}{1 - \sin 38.85^\circ} \times e^{\pi\tan 38.85^\circ} = 54.9$$

$$N_\gamma = (N_q - 0.6)\tan(1.33\phi_p)$$
$$= (54.9 - 0.6)\tan(1.33 \times 38.85^\circ) = 68.7$$

g. Surcharge (vertical effective stress) at the footing base level:

$$q_0 = \gamma_m D = 98.45 \times 2.33 = 229.4 \text{ psf (or 1.59 psi)}$$

Limit unit bearing capacity of the footing (using Eq. 3.49 from Volume II):

$$q_{bL} = (s_q d_q)q_0 N_q + 0.5(s_\gamma d_\gamma)\gamma B N_\gamma$$
$$= (2.95 \times 1.58 \times 1.59 \times 54.9)$$
$$+ \left(0.5 \times 1.31 \times 1 \times \frac{98.45 \times 3.25}{144} \times 68.7\right)$$
$$= 506.8 \text{ psi}$$

Net limit bearing capacity $q_{bL,\mathrm{net}}$ of the footing = $q_{bL} - q_0$ = 506.8 – 1.59 = 505.2 psi.

Assuming a factor of safety (FS) of 3, the net allowable bearing capacity of the footing is equal to $q_{bL,net}$/FS = 505.2/3 = 168.4 psi.

Table 2.19 summarizes the predicted limit unit bearing capacities of footings 1–5 at the Texas A&M site. For a settlement of 1 in., the net unit load $q_{b,net}$ (= $q_b - \sigma'_{v0}$) at the base of footing 5 (B = 3.25 ft) obtained from Lee and Salgado's method is 86 psi. The estimated net limit bearing capacity $q_{bL,net}$ (= $q_{bL} - q_0$) and net allowable bearing capacity ($q_{bL,net}$/FS) of this footing are 503 psi and 168 psi, respectively. Thus, the design of footing 5 is governed by the serviceability limit state (i.e., settlement criterion), which is usually the case for footings in sand.

2.2.5 Load and Resistance Factor Design

As an exercise, the following steps show how to use LRFD for the footings at Texas A&M based on the procedure outlined in Section 3.3 of Chapter 3 in Volume II.

Step 1: Obtain the nominal dead and live loads on the footing.

Both the nominal dead load DL_n and the nominal live load LL_n on each footing were assumed to be equal to 112.5 kips. This assumption was made just to illustrate how LRFD can be applied to the footings in this case history, but in reality, the nominal dead and live loads may be different for each footing and are usually provided by the structural engineer from the superstructure design.

Step 2: Set the load factors.

Load factor for dead load LF_{DL} = 1.25 and load factor for live load LF_{LL} = 1.75 (AASHTO, 2020).

Step 3: Calculate the nominal resistance of the footing.

Table 2.20 summarizes the nominal resistances R_n of footings 1–5 at Texas A&M. An example calculation for footing 5 is shown as follows.

Cross-sectional area A of the footing = $L \times B$ = 3.25 × 3.25 = 10.56 ft^2 (or 1,521 in.^{2}).

Nominal resistance of the footing (using Eq. 3.54 from Volume II):

$$R_n = q_{bL,net}A = (q_{bL} - q_0)A$$
$$= (506.8 - 1.59) \times 1{,}521 = 768 \text{ kips}$$

Step 4: Obtain the resistance factor.

Resistance factor RF = 0.35 for square footings in sand (Table 3.5 of Volume II).

Step 5: Verify whether the LRFD inequality is satisfied.

Table 2.20 summarizes the results obtained for footings 1–5 at Texas A&M. An example calculation for footing 5 is shown as follows.

Factored load = $LF_{DL}DL_n + LF_{LL}LL_n$ = (1.25 × 112.5) + (1.75 × 112.5) = 338 kips.

Factored resistance = $(RF)R_n$ = 0.35 × 768 = 269 kips.

As the factored resistance of the footing is less than the factored load applied on the footing, the LRFD inequality (Eq. 3.55 of Volume II) is not satisfied, and thus the footing has to be redesigned for the structural load under consideration. However, the other footings (footings 1–4) satisfy the LRFD inequality, as shown in Table 2.20.

TABLE 2.19
Calculation of limit unit bearing capacities of footings 1–5 at Texas A&M

Parameter	Footing 1	Footing 2	Footing 3	Footing 4	Footing 5
Footing width B (ft)	9.85	4.90	9.90	8.17	3.25
Footing length L (ft)	9.85	4.94	9.92	8.19	3.25
Embedment depth D (ft)	2.50	2.50	2.92	2.50	2.33
Conservatively assessed mean cone resistance $q_{c,CAM}$ (psi)	862	859	862	861	858
Relative density D_R (%)	52	59	51	54	62
Representative mean effective stress σ'_{mp} (psi)	115	71	116	101	53
Peak friction angle ϕ_p (°)	36.4	37.9	36.3	36.8	38.9
Shape factor s_q	2.22	2.66	2.27	2.33	2.95
Shape factor s_γ	1.22	1.27	1.22	1.24	1.31
Depth factor d_q	1.76	1.63	1.73	1.72	1.58
Depth factor d_γ	1.00	1.00	1.00	1.00	1.00
Bearing capacity factor N_q	39.7	48.5	39.2	42.0	54.9
Bearing capacity factor N_γ	44.1	58.1	43.3	47.6	68.7
Limit unit bearing capacity q_{bL} (psi)	446	485	485	452	507
Net allowable bearing capacity (psi)[1]	148	161	161	150	168
Net unit load $q_{b,net}$ for 1 in. settlement (psi)[2]	69	64	59	68	86

Note: The values of B and L represent the as-built dimensions of the footing. The values of $q_{c,CAM}$, D_R, σ'_{mp}, q_{bL}, and $q_{b,net}$ have been rounded to the nearest whole number.

[1]Assuming a factor of safety of 3 based on the Working Stress Design (WSD) method.

[2]Using Lee and Salgado's method.

TABLE 2.20
Calculation of nominal and factored resistances of footings 1–5 at Texas A&M for $DL_n = LL_n = 112.5$ kips

Parameter	Footing 1	Footing 2	Footing 3	Footing 4	Footing 5
Footing width B (ft)	9.85	4.90	9.90	8.17	3.25
Footing length L (ft)	9.85	4.94	9.92	8.19	3.25
Embedment depth D (ft)	2.50	2.50	2.92	2.50	2.33
Limit unit bearing capacity q_{bL} (psi)	446	485	485	452	507
Nominal resistance R_n (kips)	6,221	1,681	6,819	4,334	768
Factored resistance $(RF)R_n$ (kips)	2,177	588	2,387	1,517	269
Factored load $LF_{DL}DL_n + LF_{LL}LL_n$ (kips)	338	338	338	338	338

Note: The values of B and L represent the as-built dimensions of the footing. The loads and resistances have been rounded to the nearest whole number.

2.3 Rectangular Footing in Clay (Shell Haven, UK)

2.3.1 Site Description and Soil Profile

Schnaid et al. (1993) reported the results of an instrumented footing load test performed at the Shell Haven refinery on the north bank of the river Thames in Essex, England. Figure 2.19 shows the soil profile at the site and the depth profiles of net cone resistance, plastic limit PL, water content wc, liquid limit LL, and undrained shear strength s_u (measured from field vane shear tests, unconsolidated-undrained triaxial compression (UUTXC) tests, and isotropically-consolidated, undrained triaxial compression (CIUTXC) tests). The site consists of soft, normally consolidated (NC), estuarine clay up to a depth of 10–15 m (33–49 ft), generally overlain by a 1.5-m-(5-ft)-thick crust. Dense gravel lies below the clay. According to Schnaid et al. (1993), limited *in situ* and laboratory tests were performed on the crust material because of the need to excavate inspection pits to search for underground utilities. However, based on a few CPTs, field vane shear tests, and hand tests carried out in some of the inspection pits, they found that the undrained shear strength s_u of the crust varies from 20–40 kPa (3–6 psi). For the clay layer, the s_u/σ'_{v0} ratio is in the range of 0.2–0.3 and the cone factor N_k [$(= (q_t - \sigma_{v0})/s_u$] is equal to 12.4 (Figure 2.20).

2.3.2 Footing Dimensions and Loading Details

A static load test was performed on a rectangular footing with dimensions of 14 m × 5 m × 175 mm (45.9 ft × 16.4 ft × 6.9 in.). The footing was cut from a reinforced concrete pavement that already existed at the site; the pavement was built so that multi-wheeled transporters could carry major components of a Naphtha Minus Plant that were fabricated offsite. Cubical concrete blocks, each weighing 20 kN (4.5 kips), were used to load the footing. The blocks were placed on the footing in a predefined order, starting in the center and moving to the edges of the loaded area. The settlement of the footing was monitored after the placement of every 5 blocks, i.e., after every 100 kN (22.5 kips) of applied load. At a limit load Q_L of 6,000 kN (1350 kips), which corresponds to a limit unit bearing capacity q_{bL} of about 85 kPa (12.3 psi), the footing experienced a rotational failure accompanied by toppling of the concrete blocks. Based on the piezometer readings recorded during the test, Schnaid et al. (1993) concluded that the footing failed under essentially undrained conditions.

2.3.3 Estimation of Footing Settlement

Figure 2.21 shows that the predicted immediate settlements of the footing using the Foye et al. (2008) method are in reasonable agreement with the measured settlements obtained from the footing load test. The predicted footing load-settlement curves, using s_u values obtained from both *in situ* and laboratory shear test results (i.e., field vane shear, UUTXC and CIUTXC) as well as those back-calculated from CPT data with $N_k = 12.4$, bound most of the measured data points. For a tolerable settlement of 50 mm (2 in.) for isolated footings in clay, the difference between the predicted and measured unit load is less than 10%.

A step-by-step example calculation, based on the procedure outlined in Section 3.1 of Chapter 3 of Volume II, is shown as follows.

Step 1: Obtain the site stratigraphy, the groundwater table depth, and the unit weight of the soil in each layer of the profile.

a. The site stratigraphy is described in Section 2.3.1.
b. The groundwater table is assumed to be at the ground surface because the site is located on a riverbank.
c. The saturated unit weight γ_{sat} of clay typically ranges from 95–115 pcf (Salgado, 2008); an average value of 105 pcf was used in the calculations.

Step 2: Set the footing shape, geometry, and embedment depth.

a. Footing shape = rectangular.
b. Footing width $B = 16.40$ ft and footing length $L = 45.93$ ft.
c. Footing thickness $t = 6.89$ in.
d. Embedment depth D of the footing = 0.574 ft.

Step 3: Classify the soil layers for footing design.

The soil profile below the footing consists of a firm top crust followed by soft, normally consolidated clay.

Step 4: Correct the q_c data for pore pressure.

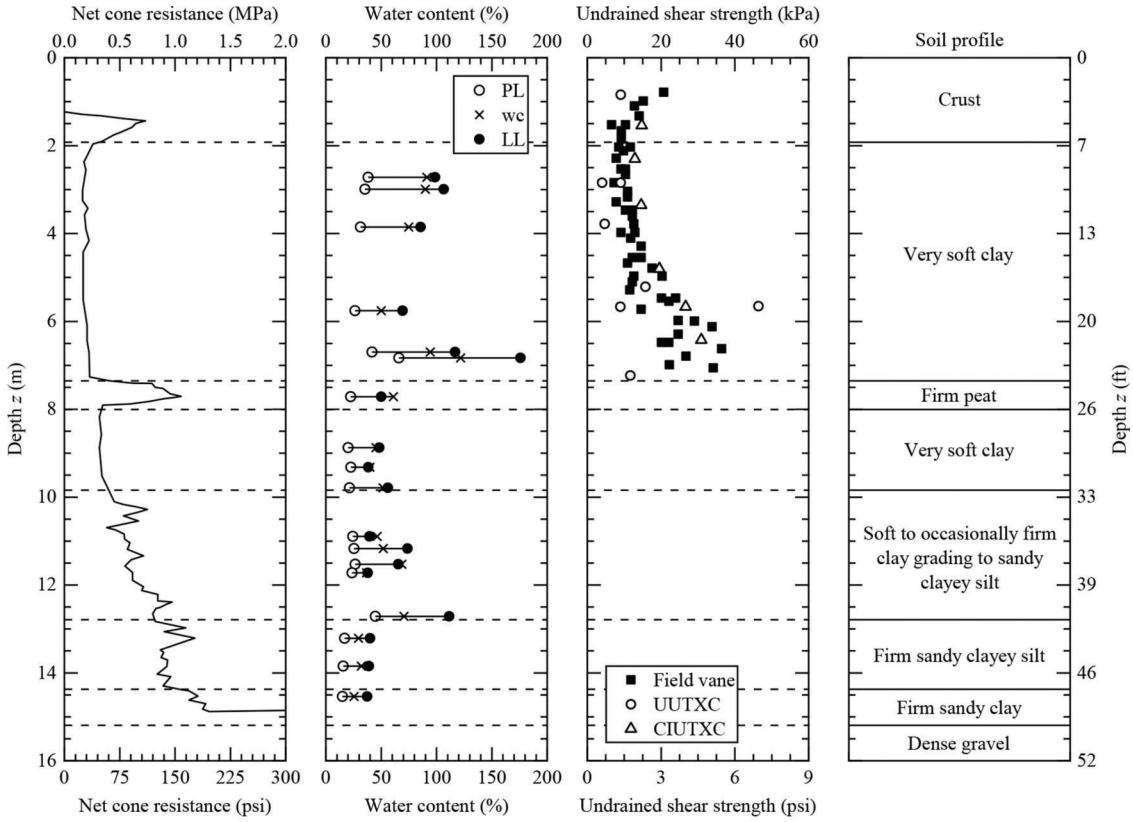

Figure 2.19 Net cone resistance, Atterberg limits, undrained shear strength, and soil profile at Shell Haven (Schnaid et al., 1993).

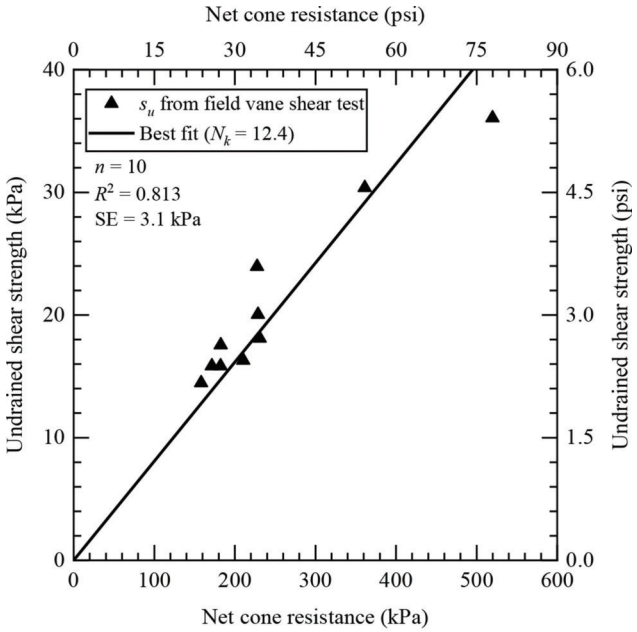

Figure 2.20 Estimation of cone factor N_k from CPT and field vane shear test data at Shell Haven (modified from Schnaid et al., 1993).

Figure 2.19 shows the depth profile of the corrected, net cone resistance.

Step 5: Obtain the footing load and maximum tolerable settlement.

a. Unfactored structural load Q on the footing = 550 kips (assumed).
b. Maximum tolerable angular distortion α_{max} = 1/500 (or 0.002).
c. Maximum tolerable settlement of the footing (from Table 3.1 of Volume II):

$$w_{max} = 25 L_R \alpha_{max} = 25 \times 39.4 \times 0.002 = 2 \text{ in.}$$

Step 6: Calculate the total settlement of the footing.

Calculation of Immediate Settlement

a. Figure 2.22 shows how to determine a representative undrained shear strength $\bar{s}_u$ over a vertical distance of B (= 16.4 ft) below the footing base using (a) data obtained from field vane shear, UUTXC and CIUTXC tests, and (b) CPT data with N_k = 12.4 (Eq. 3.17 from Volume II).
b. The representative undrained shear strength $\bar{s}_u$ of clay below the footing base is equal to 1.80 psi and 2.25 psi based on *in situ* + laboratory shear test data (field vane, UUTXC and CIUTXC) and CPT data (N_k = 12.4), respectively.
c. Influence depth $z_{\bar{G}_0}$ below the footing base within which most of the strains develop (using Eq. 3.18 from Volume II):

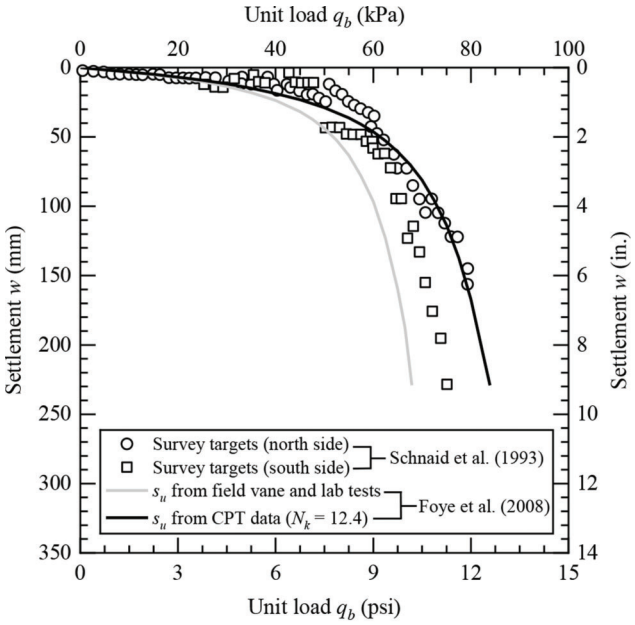

Figure 2.21 Comparison between predicted and measured footing load-settlement curves at Shell Haven.

$$\frac{z_{\bar{G}_0}}{B} = \min\left[1+0.111\left(\frac{L}{B}-1\right);2\right]$$
$$= \min\left[1+0.111\left(\frac{45.93}{16.40}-1\right);2\right]=1.2$$
$$\Rightarrow z_{\bar{G}_0}=1.2B=1.2\times 16.4=19.7 \text{ ft}$$

d. Table 2.21 summarizes the values of the small-strain shear modulus G_0 within the influence depth $z_{\bar{G}_0}$ below the footing base. The coefficient of lateral earth pressure at-rest K_0 typically ranges from 0.50–0.75 for normally consolidated clay (Appendix B of Volume II); an average value of 0.625 was used in the analysis.
An example calculation for one set of values (row 4 of Table 2.21) is shown as follows.
Depth z at which the LL and PL values were reported = 18.9 ft.
Plasticity index PI = LL – PL = 69 – 26 = 43%.
In situ vertical total stress at the depth being considered:

$$\sigma_{v0}=\gamma_{sat}z=105\times 18.9=1{,}984.5 \text{ psf (or } 13.8 \text{ psi)}$$

Hydrostatic pore water pressure at the depth being considered:

$$u_0=\gamma_w z=62.45\times 18.9=1{,}180.3 \text{ psf (or } 8.2 \text{ psi)}$$

In situ vertical effective stress at the depth being considered (using Eq. 3.11 from Volume II):

$$\sigma'_{v0}=\sigma_{v0}-u_0=13.8-8.2=5.6 \text{ psi}$$

In situ horizontal effective stress at the depth being considered:

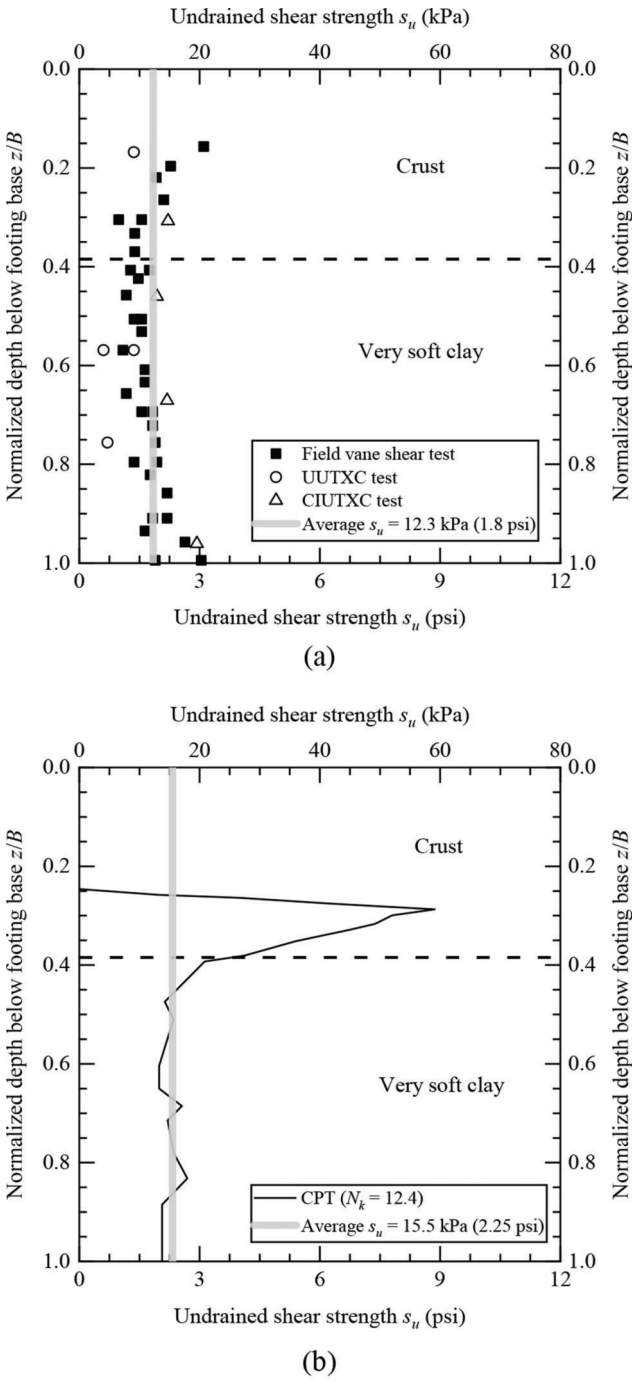

Figure 2.22 Representative undrained shear strength within depth B below the footing base using (a) field vane shear, UUTXC and CIUTXC data and (b) CPT data (N_k = 12.4).

$$\sigma'_{h0}=K_0\sigma'_{v0}=0.625\times 5.6=3.5 \text{ psi}$$

In situ mean effective stress at the depth being considered (using Eq. 3.25 from Volume II):

$$\sigma'_{m0}=\frac{1}{k+1}\left(\sigma'_{v0}+k\sigma'_{h0}\right)=\frac{1}{2+1}\left[5.6+(2\times 3.5)\right]=4.2 \text{ psi}$$

TABLE 2.21
Calculation of small-strain shear modulus G_0 for Shell Haven site

z (ft)	LL (%)	PL (%)	PI (%)	σ'_{v0} (psi)	σ'_{h0} (psi)	σ'_{m0} (psi)	C_g	n_g	m_g	G_0 (psi)
8.9	99	38	61	2.6	1.6	2.0	2.47	0.88	0.28	362
9.8	107	35	72	2.9	1.8	2.2	1.54	0.90	0.29	257
12.6	86	31	55	3.7	2.3	2.8	3.29	0.87	0.27	632
18.9	69	26	43	5.6	3.5	4.2	5.47	0.85	0.25	1,373

Note: z = depth, LL = liquid limit, PL = plastic limit, PI = plasticity index, σ'_{v0} = *in situ* vertical effective stress at the depth being considered, σ'_{h0} = *in situ* horizontal effective stress at the depth being considered (= $K_0\sigma'_{v0}$), K_0 = coefficient of lateral earth pressure at-rest, σ'_{m0} = *in situ* mean effective stress at the depth being considered, and C_g, n_g and m_g = parameters that depend on the plasticity index.

Parameters C_g, n_g, and m_g (using Eqs. 3.22, 3.23, and 3.24 from Volume II):

$$C_g = 37.9\exp(-0.045\text{PI}) = 37.9\exp(-0.045\times 43) = 5.47$$

$$n_g = 0.109\ln(\text{PI}) + 0.4374 = 0.109\ln(43) + 0.4374 = 0.847$$

$$m_g = 0.0015\text{PI} + 0.1863 = 0.0015(43) + 0.1863 = 0.251$$

Small-strain shear modulus (using Eq. 3.20 from Volume II):

$$\frac{G_0}{p_A} = C_g\left(\frac{100\sigma'_{m0}}{p_A}\right)^{n_g} R_0^{m_g} = 5.47\times\left(\frac{100\times 4.2}{14.5}\right)^{0.847} \times 1^{0.251} = 94.7 \Rightarrow G_0 = 94.7p_A = 94.7\times 14.5 = 1{,}373 \text{ psi}$$

e. The representative small-strain shear modulus $\bar{G}_0$ is calculated by taking the average of the G_0 values within the influence depth $z_{\bar{G}_0}$ below the footing base:

$$\bar{G}_0 = \frac{362+257+632+1{,}373}{4} = 656 \text{ psi}$$

f. Area A of the footing base = $L \times B$ = 45.93 × 16.40 = 753.3 ft^2.
Weight W_{ftg} of the footing = $\gamma_c At$ = 150 × 753.3 × 0.574 = 64,859 lb = 65 kips.
Weight W_{fill} of the backfill soil = $\gamma_{\text{fill}}A(D-t)$ = 0 (since $D = t$ = 0.574 ft).
Gross unit load on the footing base (using Eq. 3.3 from Volume II):

$$q_b = \frac{Q + W_{\text{ftg}} + W_{\text{fill}}}{A} = \frac{550+65+0}{753.3} = 0.82 \text{ ksf (or 5.67 psi)}$$

Net unit load on the footing base (using Eq. 3.27 from Volume II):

$$q_{b,\text{net}} = q_b - \gamma_m D = 5.67 - \left(\frac{105\times 0.574}{144}\right) = 5.25 \text{ psi}$$

g. Although the soil layers between depths of 32–50 ft are not pure clay but consist of sand-silt-clay mixtures (Figure 2.19), they are nonetheless considered to be part of the total thickness H of the clay layer below the footing base because these layers consist of fines that are plastic in nature with PI > 14%. Accordingly, the total thickness H of the clay layer below the footing base is equal to 49.3 ft.
Normalized thickness H/B of the clay layer below the footing base = 49.3/16.4 = 3.0.
Using the representative undrained shear strength obtained from *in situ* + laboratory shear test data (field vane, UUTXC and CIUTXC), $\frac{q_{b,\text{net}}}{\bar{s}_u} = \frac{5.25}{1.80} = 2.92$.
Using the representative undrained shear strength obtained from CPT data (N_k = 12.4), $\frac{q_{b,\text{net}}}{\bar{s}_u} = \frac{5.25}{2.25} = 2.33$.
Aspect ratio L/B of the footing = 45.9/16.4 = 2.8.
From Figure 3.2c of Volume II, the influence factor I_q, for H/B = 3, is equal to 1.34 and 1.11 for $\frac{q_{b,\text{net}}}{\bar{s}_u}$ equal to 2.92 and 2.33, respectively. The values of I_q, for H/B = 3, were obtained by linear interpolation between the curves given for H/B = 2 and H/B = 5. Although Figure 3.2c of Volume II was developed for rectangular footings with L/B = 2, it was used to obtain values of I_q for the footing in this case history because influence factor charts for $L/B > 2$ are currently unavailable. Alternatively, the value of I_q, for rectangular footings with $2 < L/B < 10$, may be interpolated between that for rectangular footings with L/B = 2 (Figure 3.2c of Volume II) and strip footings with $L/B \geq 10$ (Figure 3.2a of Volume II).

h. Poisson's ratio ν = 0.5 (for undrained conditions).
Representative small-strain Young's modulus of clay below the footing base (using Eq. 3.28 from Volume II):

$$\bar{E}_0 = 2(1+\nu)\bar{G}_0 = 2\times(1+0.5)\times 656 = 1{,}968 \text{ psi}$$

i. Immediate settlement of the footing (using Eq. 3.29 from Volume II):

$$w_i = I_q\frac{q_{b,\text{net}}B}{\bar{E}_0} = 1.34\times\frac{5.25\times(16.4\times 12)}{1{,}968} = 0.7 \text{ in.}$$

(using s_u values obtained from field vane shear, UUTXC and CIUTXC test results)

$$w_i = I_q\frac{q_{b,\text{net}}B}{\bar{E}_0} = 1.11\times\frac{5.25\times(16.4\times 12)}{1{,}968} = 0.58 \text{ in.} (\approx 0.6 \text{ in.})$$

(using s_u values back-calculated from CPT data considering N_k = 12.4).

Calculation of Primary Consolidation Settlement

a. Based on the depth profiles of water content and plasticity index (Figure 2.19), the approximately 15-m-(49-ft)-thick clay layer below the footing base was divided into 10 sublayers.

b. Table 2.22 summarizes the results obtained for each sublayer. An example calculation for sublayer 10 is shown as follows.
Depth z_{top} measured from the ground surface to the top of the sublayer = 47.15 ft.
Depth z_{bottom} measured from the ground surface to the bottom of the sublayer = 49.84 ft.
Depth measured from the ground surface to the middle of the sublayer:

$$z_{middle} = \frac{z_{top} + z_{bottom}}{2} = \frac{47.15 + 49.84}{2} = 48.495 \text{ ft}$$

Thickness Δz of the sublayer = $z_{bottom} - z_{top}$ = 49.84 – 47.15 = 2.69 ft (or 32.3 in.).
Vertical distance from the footing base to the middle of the sublayer:
$z_f = z_{middle} - D$ = 48.495 – 0.574 = 47.92 ft
Vertical stress increment at the middle of the sublayer (using Eq. 3.30 from Volume II):

$$\Delta\sigma_v = \frac{Q}{(B+z_f)(L+z_f)} = \frac{550}{(16.40+47.92)\times(45.93+47.92)} = 0.091 \text{ ksf (or 0.63 psi)}$$

c. Water content wc of the sublayer = 25.4%.
The specific gravity G_s of clay typically ranges from 2.60–2.80; an average value of 2.70 was used in the analysis.
Degree of saturation S = 100% (since the groundwater table is assumed to be at the ground surface).
Initial void ratio e_0 of the sublayer = wcG_s/S = (25.4 × 2.7)/100 = 0.69.

d. Liquid limit LL of the sublayer = 37.3%.
Plastic limit PL of the sublayer = 15.0%.
Plasticity index PI of the sublayer = LL – PL = 37.3 – 15.0 = 22.3%.
Compression index of the sublayer (using Eq. 3.32 from Volume II):

$$C_c = \frac{1}{200} G_s \text{PI}(\%) = \frac{2.7 \times 22.3}{200} = 0.30$$

Initial (*in situ*) vertical effective stress at the middle of the sublayer before the stress increment is applied (using Eq. 3.11 from Volume II):

$$\sigma'_{v0} = \sigma_{v0} - u_0 = (105 \times 48.495) - (62.45 \times 48.495) = 2{,}063.5 \text{ psf (or 14.33 psi)}$$

Current vertical effective stress at the middle of the sublayer after the stress increment is applied and full primary consolidation has taken place:

$$\sigma'_v = \sigma'_{v0} + \Delta\sigma_v = 14.33 + 0.63 = 14.96 \text{ psi}$$

Vertical compressive strain of the NC sublayer (using Eq. 3.31 from Volume II):

$$\Delta\varepsilon_z = \frac{C_c}{1+e_0} \log\left(\frac{\sigma'_v}{\sigma'_{v0}}\right) = \frac{0.30}{1+0.69} \times \log\left(\frac{14.96}{14.33}\right) = 0.0033$$

Vertical compression of the sublayer: $\Delta\varepsilon_z \Delta z = 0.0033 \times 32.3 = 0.11$ in.

e. 1D consolidation settlement w_{c1D} of the clay layer below the footing base (using Eq. 3.33 from Volume II):

$w_{c1D} = \sum_{i=1}^{n} \Delta\varepsilon_{z,i} \Delta z_i = 23.08$ in (obtained by summing the last column of Table 2.22).

TABLE 2.22
Calculation of 1D primary consolidation settlement w_{c1D} at Shell Haven for Q = 550 kips

Sublayer *i*	z_{top} (ft)	z_{bottom} (ft)	z_{middle} (ft)	Δz (ft)	z_f (ft)	wc (%)	PI (%)	e_0	C_c	σ'_{v0} (psi)	$\Delta\sigma_v$ (psi)	σ'_v (psi)	$\Delta\varepsilon_z$	$\Delta\varepsilon_z\Delta z$ (in.)
1	0.6	11.2	5.9	10.7	5.3	91	66	2.45	0.89	1.7	3.4	5.2	0.122	15.59
2	11.2	15.8	13.5	4.5	12.9	75	54	2.02	0.73	4.0	2.2	6.2	0.047	2.53
3	15.8	20.4	18.1	4.7	17.5	50	43	1.35	0.58	5.4	1.8	7.1	0.031	1.72
4	20.4	24.1	22.3	3.7	21.7	108	93	2.92	1.25	6.6	1.5	8.1	0.028	1.25
5	24.1	26.3	25.2	2.1	24.6	61	28	1.65	0.37	7.5	1.3	8.8	0.010	0.25
6	26.3	32.3	29.3	6.0	28.7	46	26	1.23	0.35	8.7	1.1	9.8	0.008	0.62
7	32.3	39.4	35.8	7.1	35.3	51	29	1.38	0.39	10.6	0.9	11.5	0.006	0.50
8	39.4	42.0	40.7	2.6	40.1	71	67	1.91	0.90	12.0	0.8	12.8	0.009	0.26
9	42.0	47.1	44.6	5.2	44.0	31	23	0.83	0.31	13.2	0.7	13.9	0.004	0.24
10	47.1	49.8	48.5	2.7	47.9	25	22	0.69	0.30	14.3	0.6	15.0	0.003	0.11

Note: z_{top}, z_{bottom}, and z_{middle} = depth measured from the ground surface to the top, bottom and middle of the sublayer, respectively; Δz = thickness of the sublayer; z_f = vertical distance from the footing base to the middle of the sublayer; wc = water content; PI = plasticity index; e_0 = initial void ratio; C_c = compression index; σ'_{v0} and σ'_v = initial (*in situ*) and current vertical effective stresses, respectively, at the middle of the sublayer; $\Delta\sigma_v$ = vertical stress increment at the middle of the sublayer; and $\Delta\varepsilon_z$ = vertical compressive strain of the sublayer.

f. Skempton's pore pressure parameter A typically ranges from 0.50–0.75 for normally consolidated clay; an average value of 0.625 was used in the analysis.
Normalized thickness H/B of the clay layer below the footing base = 49.3/16.4 = 3.0.
Aspect ratio B/L of the footing = 16.40/45.93 = 0.36.
For H/B = 3.0 and B/L = 0.36, the coefficient α is equal to 0.25 (from Table 3.2 of Volume II).
Primary consolidation settlement of the footing (using Eq. 3.34 from Volume II):

$$w_c = [A + \alpha(1-A)]w_{c1D}$$
$$= [0.625 + 0.25(1-0.625)] \times 23.08 = 16.6 \text{ in.}$$

g. Total settlement w of the footing for an unfactored structural load Q of 550 kips:

$$w = w_i + w_c = 0.7 + 16.6 = 17.3 \text{ in.}$$

(using s_u values obtained from field vane shear, UUTXC and CIUTXC test results)

$$w = w_i + w_c = 0.6 + 16.6 = 17.2 \text{ in.}$$

(using s_u values back-calculated from CPT data considering N_k = 12.4).
Note that the immediate settlement w_i of the footing is just a small fraction (in this case, of the order of 4%) of the total settlement w.

Step 7: Total settlement check.

For an unfactored structural load of 550 kips, the estimated total settlement w of the footing is much greater than the maximum tolerable settlement $w_{\max}$ established in step 5. The footing would thus have to be redesigned in order to satisfy the serviceability limit state (i.e., excessive settlement) for the structural load under consideration. Alternative design solutions, such as ground improvement or a transition to pile foundations, may also be explored.

2.3.1 Estimation of Footing Bearing Capacity

Step 1: Determine the nominal or characteristic cone resistance $q_{c,\text{CAM}}$.

Figure 2.23a,b show the idealized profiles of net cone resistance and undrained shear strength at Shell Haven. As only one CPT sounding was performed at the site, the gradient of net cone resistance with depth, obtained from regression analysis, is as follows.

$$q_{c,\text{CAM}} - \sigma_{v0} = 0.0822\left(\frac{\text{psi}}{\text{in.}}\right) \times z + 14.85(\text{psi})$$

Step 2: Calculate the limit unit bearing capacity of the footing.

a. Table 2.23 summarizes the predicted limit unit bearing capacity of the footing at Shell Haven. A step-by-step example calculation using CPT data is shown as follows.
Cone factor N_k = 12.4 (Figure 2.20).
Undrained shear strength profile back-calculated from CPT data (using Eq. 3.50 from Volume II):

$$s_u = \frac{q_{c,\text{CAM}} - \sigma_{v0}}{N_k} = \frac{0.0822z + 14.85}{12.4}$$
$$= 0.00663\left(\frac{\text{psi}}{\text{in.}}\right) \times z + 1.198(\text{psi})$$

b. The gradient ρ of undrained shear strength with depth and the undrained shear strength s_{u0} at the footing base level are the following.

$$\rho = 0.00663 \text{ psi/in.}$$

$$s_{u0} = \frac{23.92}{12.4} = 1.93 \text{ psi}$$

Recall that the footing base is 0.175 m (6.89 in.) below the ground surface. The net cone resistance at that depth is equal to 23.92 psi (Figure 2.23a).

$$\frac{\rho B}{s_{u0}} = \frac{0.00663 \times 196.85}{1.93} = 0.68$$

Recall that the footing width B is 5 m (196.85 in.).

c. The net cone resistance and undrained shear strength profiles shown in Figure 2.23 resemble profile 2 in Figure 3.4 of Volume II. Therefore, the correction factor F is equal to 0.973 for $\rho B/s_{u0}$ = 0.68.

d. Aspect ratio B/L of the footing = 16.40/45.93 = 0.36.
Coefficient C_1 = 0.159 and coefficient C_2 = 0.143 (from Table 3.4 of Volume II).
Shape factor (using Eq. 3.51 from Volume II):

$$s_{su} = 1 + C_1\frac{B}{L}\left\{\frac{2.3}{\exp\left[0.353\left(\frac{\rho B}{s_{u0}}\right)^{0.509}\right]} - 1.3\right\} + C_2\sqrt{\frac{D}{B}}$$
$$= 1 + (0.159 \times 0.36)\left\{\frac{2.3}{\exp\left[0.353(0.68)^{0.509}\right]} - 1.3\right\}$$
$$+ 0.143\sqrt{\frac{6.89}{196.85}} = 1.05$$

Depth factor (using Eq. 3.52 from Volume II):

$$d_{su} = 1 + 0.27\sqrt{\frac{D}{B}} = 1 + 0.27\sqrt{\frac{6.89}{196.85}} = 1.05$$

e. Surcharge (vertical total stress) at the footing base level:

$$q_0 = \gamma_{sat}D = 105 \times 0.574 = 60.3 \text{ psf (or } 0.42 \text{ psi)}$$

Bearing capacity factor $N_c = 2 + \pi \approx 5.14$.
Limit unit bearing capacity q_{bL} of the footing (using Eq. 3.53 of Volume II):

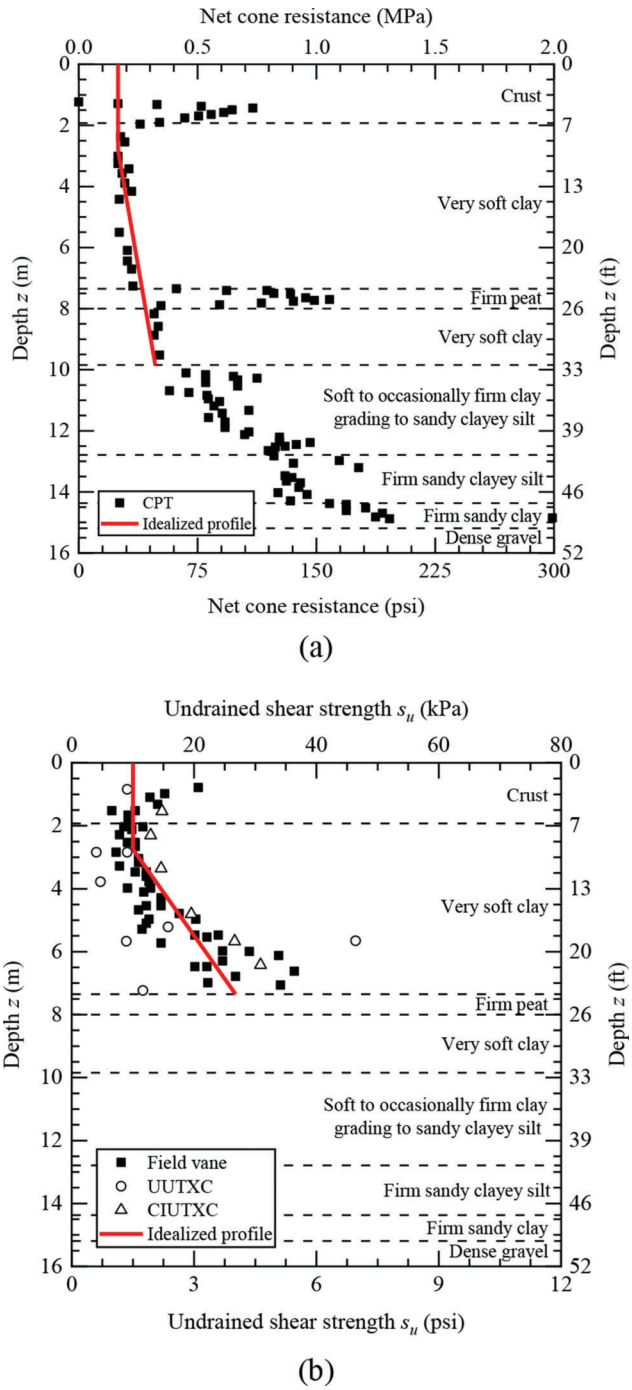

Figure 2.23 Best fit lines to (a) CPT data and (b) s_u data obtained from field vane, UUTXC and CIUTXC tests at Shell Haven.

$$q_{bL} = Fs_{su}d_{su}\left[1+\frac{\rho B}{4s_{u0}N_c}\right]s_{u0}N_c + q_0$$

$$= 0.973 \times 1.05 \times 1.05 \times \left[1+\frac{0.68}{4\times 5.14}\right]$$

$$\times 1.93 \times 5.14 + 0.42 = 11.4 \text{ psi}$$

The predicted limit unit bearing capacity q_{bL} of the footing is in good agreement with the value of q_{bL} (= 12.3 psi) obtained from the static load test.

2.3.2 Load and Resistance Factor Design

As an exercise, the following steps show how to use LRFD for the footing at Shell Haven based on the procedure outlined in Section 3.3 of Chapter 3 in Volume II.

Step 1: Obtain the nominal dead and live loads on the footing.

Both the nominal dead load DL_n and the nominal live load LL_n on the footing were assumed to be equal to 275 kips. This assumption was made just to illustrate how LRFD can be applied to the footing in this case history, but in reality, the nominal dead and live loads may be different and are usually provided by the structural engineer from the superstructure design.

Step 2: Set the load factors.

Load factor for dead load LF_{DL} = 1.25 and load factor for live load LF_{LL} = 1.75 (AASHTO, 2020).

Step 3: Calculate the nominal resistance of the footing.

Cross-sectional area A of the footing = $L \times B$ = 45.93 × 16.40 = 753.3 ft^2.

Nominal resistance of the footing (using Eq. 3.54 from Volume II):

$$R_n = q_{bL,\text{net}}A = (q_{bL} - q_0)A$$

$$= (11.4 - 0.42) \times 753.3 \times 144 = 1{,}191 \text{ kips}$$

Step 4: Obtain the resistance factor.

Resistance factor RF = 0.75 for rectangular footings in clay (Table 3.5 of Volume II).

Step 5: Verify whether the LRFD inequality is satisfied.

Factored load = $LF_{DL}DL_n + LF_{LL}LL_n$ = (1.25 × 275) + (1.75 × 275) = 825 kips.

Factored resistance = $(RF)R_n$ = 0.75 × 1,191 = 893 kips.

As the factored resistance of the footing is greater than the factored load applied on the footing, the LRFD inequality (Eq. 3.55 of Volume II) is satisfied, and thus the footing design is satisfactory with respect to the ultimate limit state (i.e., bearing capacity failure) for a target probability of failure of 10^{-3}.

TABLE 2.23
Calculation of limit unit bearing capacity of footing at Shell Haven from both CPT data and laboratory/field shear test data

Parameter	From CPT Data	From Field Vane, UUTXC and CIUTXC Test Data
Strength gradient ρ (psi/in.)	0.0066	0.0134
Undrained shear strength at the footing base level s_{u0} (psi)	1.93	1.45
$\rho B/s_{u0}$	0.68	1.82
Correction factor F	0.97	0.93
Shape factor s_{su}	1.05	1.03
Depth factor d_{su}	1.05	1.05
Bearing capacity factor N_c	5.14	5.14
Limit unit bearing capacity q_{bL} (psi)	11.4	8.7

3. PILE FOUNDATIONS

3.1 Closed-Ended Pipe Pile in Silty Sand (Marshall County, IN, USA)

Han et al. (2017) reported the results of a static axial load test performed on an instrumented, driven, closed-ended steel pipe pile at a bridge construction site located at the intersection of 7th Road with U.S. 31 in Marshall County, Indiana. Figure 3.1 shows the soil profile at the site and the depth profiles of (a) uncorrected SPT blow count N_{SPT} obtained from two SPT borings, S1 and S2, using an automatic trip hammer, and (b) cone resistance q_c obtained from two CPT soundings, C1 and C2, performed at a distance of about 3–12 m (10–39 ft) from the test pile location. The soil profile consists primarily of layers of medium-dense-to-dense silty sand and stiff-to-hard silt and sand mixtures. The CPTs were terminated at depths of about 16–17 m (53–56 ft), where a hard layer consisting of a mixture of silt and sand was found—this layer extends down to a depth of 24.7 m (81 ft). The groundwater table was located at a depth of 4.3 m (14.1 ft) from the ground surface.

The outer diameter and wall thickness of the closed-ended pipe (CEP) pile are 356 mm (14 in.) and 9.53 mm (0.375 in.), respectively. The pile was driven using a single-acting impact hammer, with a ram weight of 29.4 kN (6.6 kips) and a maximum hammer stroke of 3.2 m (10.5 ft), down to a depth of 15.42 m (50.6 ft) from the ground surface. The base of the pile was embedded in the hard silt with sand layer, as shown in Figure 3.1.

A slow, maintained static load test was performed on the closed-ended pipe pile 9 days after pile driving. The ultimate load Q_{ult} corresponding to a pile head settlement of 35.6 mm (1.4 in.) (= 0.1B) was 3,275 kN (736 kips), whereas the load Q_L and pile head settlement required for the pile to start plunging into the ground were 3,394 kN (763 kips) and 48.3 mm (1.9 in.) (= 0.136B), respectively. The following steps show how to estimate the limit shaft capacity Q_{sL}, the ultimate base capacity $Q_{b,ult}$, and the ultimate load capacity Q_{ult} of the pile using CPT results.

3.1.1 Estimation of Limit Shaft Capacity

Step 1: Obtain the site stratigraphy, the groundwater table depth, and the unit weight of the soil in each layer of the profile.

a. Figure 3.1 shows the soil profile obtained from the SPT boring logs.
b. Depth z_w of groundwater table = 14.1 ft (according to the SPT boring logs). This depth was also confirmed by groundwater monitoring data collected by the Indiana Department of Natural Resources.
c. Table 3.1 summarizes the unit weights of the soil layers from the boring logs.

Step 2: Select the pile type and decide the pile length.
Pile type = closed-ended pipe (CEP) pile.
Outer diameter B of the pile = 14 in.
Embedded length L of the pile = 50.6 ft.
Bearing layer for placement of the pile base = hard silt with sand.

Step 3: Classify the soil layers for pile design.
Classify the soil layers in contact with the pile as either "sand" or "clay," as shown in Table 3.1.

Step 4: Correct the q_c data for pore pressure.
The q_c data recorded within the saturated "clay" layer (layer 4 in Table 3.1) was corrected for the pore water pressure generated during cone penetration (calculations are presented in step 8(c)(i)).

Step 5: Divide the soil profile into sublayers.
Figure 3.2 shows the discretization of the q_c profile obtained from CPT sounding C1 into 14 sublayers up to a depth equal to the embedded length of the pile (= 50.6 ft). The grey vertical bars indicate the representative (average) q_c values within each sublayer. Four q_c data points at depths of 22.1 ft, 26.4 ft, 38.4 ft, and 42.8 ft were considered to be outliers and thus not included in the analysis.

Step 6: Calculate vertical effective stresses.
Table 3.2 summarizes the *in situ* vertical effective stress at the middle of each sublayer.

Step 7: Calculate the limit unit shaft resistance of pile segments in contact with "sand" sublayers.

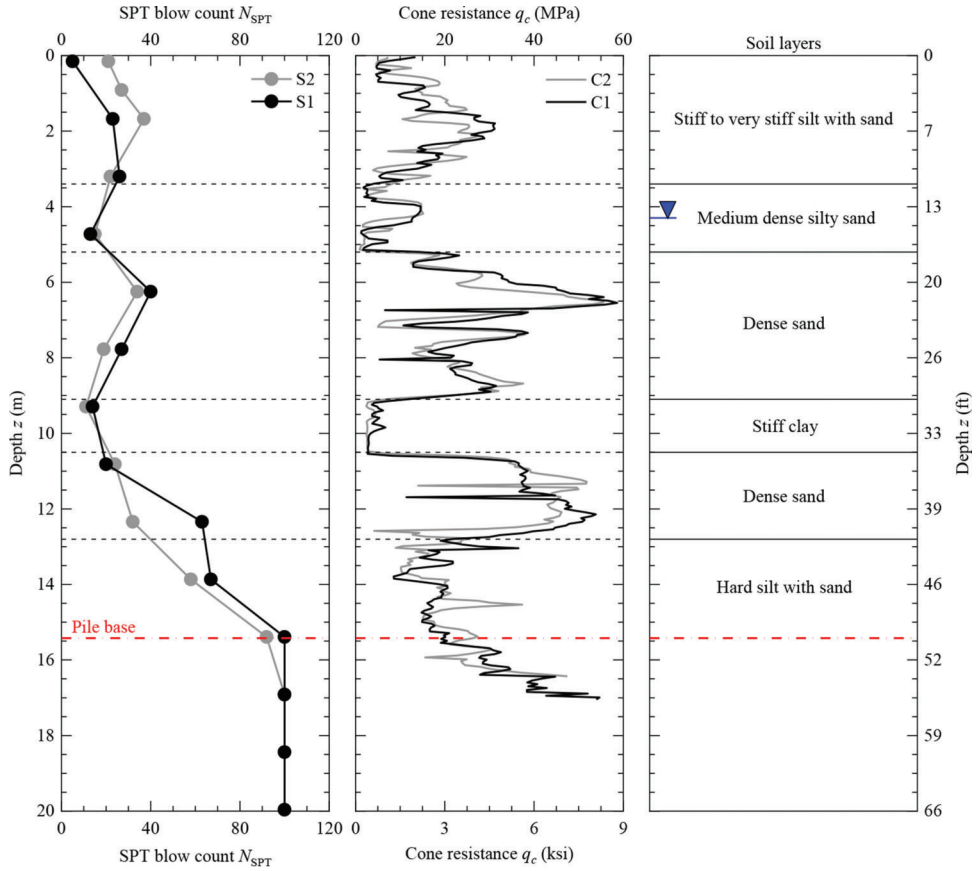

Figure 3.1 N_{SPT}, q_c, and soil profiles at CEP pile test site in Marshall County, Indiana (after Han et al., 2017).

Table 3.2 summarizes the results obtained for all the sublayers using the Purdue pile design method (PPDM). An example calculation for sublayer 10, which is a "sand" sublayer, is shown in the following.

a. Depths from the ground surface to the top and bottom of the sublayer:

$$z_{top} = 23.43 \text{ ft and } z_{bottom} = 29.86 \text{ ft}$$

Depth from the ground surface to the middle of the sublayer:

$$z_{middle} = \frac{z_{top} + z_{bottom}}{2} = \frac{23.43 + 29.86}{2} = 26.65 \text{ ft}$$

Thickness of the sublayer $\Delta z = z_{bottom} - z_{top} = 29.86 - 23.43 = 6.43$ ft.
Representative cone resistance of the sublayer q_c = 3,617.1 psi (Figure 3.2).
In situ vertical total stress at the middle of the sublayer:

$\sigma_{v0} = 123.5(11.2) + 135(17.1 - 11.2) + 131.8(26.65 - 17.1)$ = 3,438.39 psf (or 23.88 psi)

Hydrostatic pore water pressure at the middle of the sublayer:

$u_0 = \gamma_w(z_{middle} - z_w) = 62.45 \times (26.65 - 14.1) = 783.75$ psf (or 5.44 psi)

In situ vertical effective stress at the middle of the sublayer (using Eq. 4.2 from Volume II):

$$\sigma'_{v0} = \sigma_{v0} - u_0 = 23.88 - 5.44 = 18.44 \text{ psi}$$

The coefficient of lateral earth pressure at-rest K_0 was taken as 0.45 for the medium dense silty sand layer and 0.4 for the other stiff/dense sand layers.
In situ horizontal effective stress at the middle of the sublayer:

$$\sigma'_{h0} = K_0\sigma'_{v0} = 0.4 \times 18.44 = 7.38 \text{ psi}$$

b. In the absence of gradation, morphology and laboratory shear test results for this site, the critical-state friction angle ϕ_c of all the "sand" layers was taken as 33°, which is near the middle of the 28°–36° range for silica sands.
c. Critical-state interface friction angle δ_c of the sublayer = $0.85\phi_c = 0.85 \times 33^\circ = 28.05^\circ$.
d. Ignore this substep as the pile is not an H-pile.
e. Vertical distance from the middle of the sublayer to the pile base:

$$h = L - z_{middle} = 50.6 - 26.65 = 23.95 \text{ ft}$$

Coefficient of lateral earth pressure (using Eq. 4.9 from Volume II):

TABLE 3.1
Classification of soil layers at CEP pile test site as "sand" or "clay" (after Han et al., 2017)

Layer	z (ft)	Soil Type	Soil Classification for Pile Design	γ_m (pcf)
1	0.0–11.2	Stiff to very stiff silt with sand	Sand	123.5
2	11.2–17.1	Medium dense silty sand	Sand	135.0
3	17.1–29.9	Dense sand	Sand	131.8
4	29.9–34.4	Silty clay	Clay	136.9
5	34.4–42.0	Dense sand	Sand	131.8
6	42.0–81.0	Hard silt with sand	Sand	131.8

Note: Layers of silt with sand were classified as "sand" for the purpose of pile capacity analysis because the silt was nonplastic; z = depth from the ground surface; and γ_m = unit weight (= γ_{sat} if the soil is saturated). Values of z and γ_m have been converted from SI units and rounded to the first decimal place.

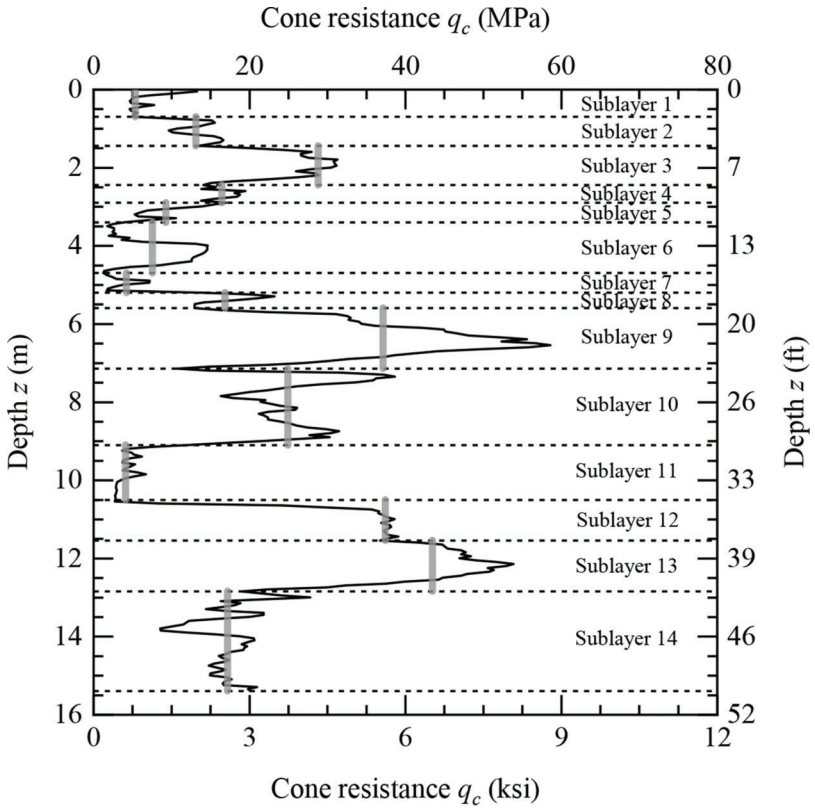

Figure 3.2 Discretization of q_c profile obtained from CPT sounding C1 into 14 sublayers at CEP pile test site in Marshall County, Indiana.

$$K = 0.2 + \left[\frac{0.01\left(\frac{q_c}{p_A}\right)}{\sqrt{\frac{\sigma'_{h0}}{p_A}}} - 0.2\right] \exp\left(\frac{-0.14h}{L_R}\right)$$

$$= 0.2 + \left[\frac{0.01 \times \left(\frac{3{,}617.1}{14.5}\right)}{\sqrt{\frac{7.38}{14.5}}} - 0.2\right] \exp\left(\frac{-0.14 \times 23.95}{3.28}\right)$$

$$= 1.39$$

Limit unit shaft resistance of the pile segment in contact with sublayer 10 (using Eq. 4.8 from Volume II):

$$q_{sLi} = F_{\text{load}} K \sigma'_{v0} \tan \delta_c$$

$$= 1 \times 1.39 \times 18.44 \times \tan 28.05^{\circ} = 13.66 \text{ psi}$$

Pile shaft area interfacing with sublayer 10 (from Table 4.1 of Volume II):

$$A_{si} = \pi B \Delta z_i = \pi \times 1.17 \times 6.43 = 23.63 \text{ ft}^2$$

Limit shaft capacity of the pile segment in contact with sublayer 10:

TABLE 3.2
Calculation of limit shaft capacity of CEP pile in Marshall County, Indiana

Sublayer i	Soil Type	z_{top} (ft)	z_{bottom} (ft)	Δz (ft)	z_{middle} (ft)	q_c (psi)	σ_{v0} (psi)	σ'_{v0} (psi)	K_0	σ'_{h0} (psi)	h (ft)	K	s_u (psi)	α	q_{sLi} (psi)	A_{si} (ft^2)	Q_{sLi} (kips)
1	Sand	0.0	2.3	2.3	1.1	776	1.0	1.0	0.40	0.4	49.5	0.57	—	—	0.3	8.3	0.4
2	Sand	2.3	4.7	2.5	3.5	1,905	3.0	3.0	0.40	1.2	47.1	0.79	—	—	1.3	9.0	1.6
3	Sand	4.7	8.0	3.3	6.4	4,179	5.5	5.5	0.40	2.2	44.2	1.29	—	—	3.8	12.0	6.5
4	Sand	8.0	9.5	1.5	8.8	2,389	7.5	7.5	0.40	3.0	41.8	0.77	—	—	3.1	5.4	2.4
5	Sand	9.5	11.2	1.7	10.3	1,348	8.9	8.9	0.40	3.5	40.3	0.50	—	—	2.4	6.1	2.1
6	Sand	11.2	15.4	4.2	13.3	1,098	11.6	11.6	0.45	5.2	37.3	0.42	—	—	2.6	15.6	5.8
7	Sand	15.4	17.1	1.7	16.2	612	14.3	13.4	0.45	6.0	34.4	0.30	—	—	2.2	6.1	1.9
8	Sand	17.1	18.4	1.3	17.7	2,446	15.7	14.1	0.40	5.7	32.9	0.81	—	—	6.1	4.7	4.2
9	Sand	18.4	23.4	5.1	20.9	5,387	18.6	15.7	0.40	6.3	29.7	1.73	—	—	14.5	18.6	38.9
10	Sand	23.4	29.9	6.4	26.6	3,617	23.9	18.4	0.40	7.4	23.9	1.39	—	—	13.6	23.6	46.2
11	Clay	29.9	34.4	4.6	32.2	614	29.0	21.2	—	—	—	—	48.7	0.43	20.9	16.9	50.8
12	Sand	34.4	37.9	3.4	36.2	5,430	32.7	23.2	0.40	9.3	14.4	2.62	—	—	32.4	12.6	58.5
13	Sand	37.9	42.1	4.3	40.0	6,309	36.3	25.0	0.40	10.0	10.6	3.41	—	—	45.4	15.7	102.5
14	Sand	42.1	50.6	8.5	46.4	2,494	42.1	28.1	0.40	11.2	4.2	1.66	—	—	24.9	31.0	111.2

Note: z_{top}, z_{bottom}, and z_{middle} = depth measured from the ground surface to the top, bottom and middle of the sublayer, respectively; Δz = thickness of the sublayer; q_c = representative cone resistance of the sublayer; σ_{v0} and σ'_{v0} = *in situ* vertical total and effective stresses, respectively, at the middle of the sublayer; σ'_{h0} = *in situ* horizontal effective stress at the middle of the sublayer; h = vertical distance from the middle of the sublayer to the pile base; K = coefficient of lateral earth pressure; s_u = undrained shear strength; q_{sLi} = limit unit shaft resistance of pile segment in contact with sublayer i; A_{si} = pile shaft area interfacing with sublayer i; and Q_{sLi} = limit shaft capacity of pile segment in contact with sublayer i.

$$Q_{sLi} = q_{sLi}A_{si} = 13.66 \times 23.63 \times 144 = 46.5 \text{ kips}$$

Step 8: Calculate the limit unit shaft resistance of pile segments in contact with "clay" sublayers.

Table 3.2 summarizes the results obtained for all the sublayers using the Purdue pile design method (PPDM). An example calculation for sublayer 11, which is a "clay" sublayer, is shown in the following.

a. In the absence of laboratory shear test results, the critical-state friction angle ϕ_c of the "clay" sublayer was taken as 24°, which is near the middle of the 15°–30° range for clays.
b. In the absence of ring shear test results, the minimum residual-state friction angle $\phi_{r,\min}$ of the "clay" sublayer was taken as 12°, which is within the 5°–15° range for clays.
c. Depths from the ground surface to the top and bottom of the sublayer:

$$z_{top} = 29.86 \text{ ft and } z_{bottom} = 34.45 \text{ ft}$$

Depth from the ground surface to the middle of the sublayer:

$$z_{middle} = \frac{z_{top} + z_{bottom}}{2} = \frac{29.86 + 34.45}{2} = 32.15 \text{ ft}$$

Thickness of the sublayer $\Delta z = z_{bottom} - z_{top} = 34.45 - 29.86 = 4.59$ ft.
Representative cone resistance of the sublayer $q_c = 598.2$ psi (Figure 3.2).
In situ vertical total stress at the middle of the sublayer:

$$\sigma_{v0} = 123.5(11.2) + 135(17.1 - 11.2) + 131.8(29.9 - 17.1) + 136.9(32.15 - 29.9) = 4{,}174.8 \text{ psf (or 28.99 psi)}$$

Hydrostatic pore water pressure at the middle of the sublayer:

$$u_0 = \gamma_w(z_{middle} - z_w) = 62.45 \times (32.15 - 14.1) = 1{,}127.22 \text{ psf (or 7.83 psi)}$$

In situ vertical effective stress at the middle of the sublayer (using Eq. 4.2 from Volume II):

$$\sigma'_{v0} = \sigma_{v0} - u_0 = 28.99 - 7.83 = 21.16 \text{ psi}$$

i. Pore water pressure u_2 at the shoulder position behind the cone face = 77.2 psi.
Corrected, total cone resistance of the sublayer (using Eq. 4.1 from Volume II):

$$q_t = q_c + (1-a)u_2 = 598.2 + (1-0.8)(77.2) = 613.6 \text{ psi}$$

The cone factor N_k was taken as 12, which is in the middle of the 9–15 range for undrained penetration in clay.
Undrained shear strength of the sublayer (using Eq. 4.11 from Volume II):

$$s_u = \frac{q_t - \sigma_{v0}}{N_k} = \frac{613.6 - 28.99}{12} = 48.72 \text{ psi}$$

ii. Difference between the critical-state and minimum residual-state friction angles of the sublayer $\phi_c - \phi_{r,\min} = 24° - 12° = 12°$.

Coefficient A_1 (using Eq. 4.14 from Volume II):

$$A_1 = 0.43 \text{ (for } \phi_c - \phi_{r,\min} \geq 12^\circ)$$

Coefficient A_2 (using Eq. 4.15 from Volume II):

$$A_2 = 0.55 + 0.43 \ln\left(\frac{s_u}{\sigma'_{v0}}\right) = 0.55 + 0.43 \ln\left(\frac{48.72}{21.16}\right) = 0.91$$

Parameter α (using Eq. 4.13 from Volume II):

$$\alpha = A_1 + (1 - A_1) \exp\left[-\left(\frac{\sigma'_{v0}}{p_A}\right)(\phi_c - \phi_{r,\min})^{A_2}\right]$$
$$= 0.43 + (1 - 0.43) \exp\left[-\left(\frac{21.16}{14.5}\right)(24 - 12)^{0.91}\right]$$
$$= 0.43$$

Limit unit shaft resistance of the pile segment in contact with sublayer 11 (using Eq. 4.12 from Volume II):

$$q_{sLi} = \alpha s_u = 0.43 \times 48.72 = 20.95 \text{ psi}$$

Pile shaft area interfacing with sublayer 11 (from Table 4.1 of Volume II):

$$A_{si} = \pi B \Delta z_i = \pi \times 1.17 \times 4.59 = 16.87 \text{ ft}^2$$

Limit shaft capacity of the pile segment in contact with sublayer 11:

$$Q_{sLi} = q_{sLi} A_{si} = 20.95 \times 16.87 \times 144 = 50.9 \text{ kips}$$

Step 9: Repeat steps 7 and 8 for all sublayers in contact with the pile shaft.

Table 3.2 summarizes the results obtained for all the sublayers in contact with the pile shaft.

Step 10: Compute the limit shaft capacity Q_{sL} of the pile.

Limit shaft capacity of the pile (using Eq. 4.23 from Volume II):

$$Q_{sL} = \sum_{i=1}^{14} Q_{sLi} = \sum_{i=1}^{14} q_{sLi} A_{si} = 433 \text{ kips}$$

(obtained by summing the last column of Table 3.2)

3.1.2 Estimation of Ultimate Base Capacity

Step 1: Estimate the average cone resistance q_{cb} at the pile base.

a. Depth corresponding to $L - B = 50.6 - 1.17 = 49.43$ ft. Depth corresponding to $L + 2B = 50.6 + 2(1.17) = 52.94$ ft. Depth corresponding to $L + (B/2) = 50.6 + (1.17/2) = 51.18$ ft.

   i. Following the Purdue pile design method (PPDM), the representative cone resistance q_{cb} for use in pile base capacity calculation is obtained by averaging the q_c values between $1B$ above and $2B$ below the pile base, corresponding to a 49.43–52.94 ft depth range. This yields $q_{cb} = 3{,}480$ psi.

Step 2: Calculate the ultimate unit base resistance $q_{b,ult}$ of the pile.

a. The bearing layer for the pile base, which consists of hard silt with sand, is classified as "sand" for the purpose of pile base capacity calculation because the silt is nonplastic.
   In situ vertical total stress at the depth corresponding to $L + (B/2)$:

   $\sigma_{v0} = 123.5(11.2) + 135(17.1 - 11.2) + 131.8(29.9 - 17.1) + 136.9(34.4 - 29.9) + 131.8(42.0 - 34.4) + 131.8(51.18 - 42.0) = 6{,}694.4$ psf (or 46.49 psi)

   Hydrostatic pore water pressure at the depth corresponding to $L + (B/2)$:

   $u_0 = \gamma_w(z - z_w) = 62.45 \times (51.18 - 14.1) = 2{,}315.6$ psf (or 16.08 psi)

   In situ vertical effective stress at the depth corresponding to $L + (B/2)$:

   $$\sigma'_{v0} = \sigma_{v0} - u_0 = 46.49 - 16.08 = 30.41 \text{ psi}$$

   In situ horizontal effective stress at the depth corresponding to $L + (B/2)$:

   $$\sigma'_{h0} = K_0 \sigma'_{v0} = 0.4 \times 30.41 = 12.16 \text{ psi}$$

   Critical-state friction angle $\phi_c = 33^\circ$.
   Relative density (using Eq. 4.30 from Volume II):

$$D_R = \frac{\ln\left(\frac{q_{cb}}{p_A}\right) - 0.4947 - 0.1041\phi_c - 0.841 \ln\left(\frac{\sigma'_{h0}}{p_A}\right)}{0.0264 - 0.0002\phi_c - 0.0047 \ln\left(\frac{\sigma'_{h0}}{p_A}\right)}$$
$$= \frac{\ln\left(\frac{3{,}480}{14.5}\right) - 0.4947 - 0.1041(33) - 0.841 \ln\left(\frac{12.16}{14.5}\right)}{0.0264 - 0.0002(33) - 0.0047 \ln\left(\frac{12.16}{14.5}\right)}$$
$$= 82.3\%$$

   Ultimate unit base resistance of the pile (using Eq. 4.28 from Volume II):

$$q_{b,ult} = (1 - 0.0058 D_R) q_{cb}$$
$$= [1 - 0.0058(82.3)] \times 3{,}480 = 1{,}818.9 \text{ psi}$$

Step 3: Compute the ultimate base capacity $Q_{b,ult}$ of the pile.

Cross-sectional area of the pile base (from Table 4.2 of Volume II):

$$A_b = \frac{\pi B^2}{4} = \frac{\pi \times 14^2}{4} = 153.94 \text{ in.}^2$$

Ultimate base capacity of the pile (using Eq. 4.34 from Volume II):

$$Q_{b,ult} = q_{b,ult} A_b = 1{,}818.9 \times 153.94 = 280 \text{ kips}$$

Step 4: Compute the ultimate load capacity Q_{ult} of the pile.

Ultimate load capacity of the pile (using Eq. 4.35 from Volume II):

$$Q_{ult} = Q_{sL} + Q_{b,ult} = 433 + 280 = 713 \text{ kips}$$

3.1.3 Comparison Between Predicted and Measured Pile Capacities

Table 3.3 compares the shaft, base and total capacities of the CEP pile obtained from the static load test (after correction for residual loads) with those predicted using the Purdue pile design method (PPDM) and the DrivenPiles program (version 1.3.7) (MDSC, Inc., 2018). The DrivenPiles program is based on the semi-empirical, limit equilibrium-based methods proposed by Nordlund (1963, 1979) and Tomlinson (1980, 1986) for driven piles in coarse-grained and fine-grained soils, respectively; the main input parameter for coarse-grained soil is the friction angle ϕ, which is limited to a maximum of 36° in the program (IN.gov, 2019), while that for fine-grained soil is the undrained shear strength s_u. The equations for the pile shaft and base resistances in Nordlund's and Tomlinson's methods are summarized in the INDOT (IN.gov, 2019) and DrivenPiles (MDSC, Inc., 2018) manuals. For a given soil layer, the value of ϕ can be entered manually into the program or it can be computed from the SPT blow count (i.e., the user inputs the SPT blow counts obtained within the layer and the program automatically computes the friction angle using the Peck et al., 1974 relationship). Unlike ϕ_p and ϕ_c, the friction angle ϕ has no physical meaning and is simply a fitting parameter obtained from a linear approximation of the nonlinear Mohr-Coulomb strength envelope in σ'-τ space.

The SPT blow counts obtained from boring S1 were entered into the DrivenPiles program, and the option "correct the N values for the influence of the effective overburden pressure" was selected to then obtain the corresponding values of ϕ for each of the "sand" layers listed in Table 3.1. The ϕ values obtained for each layer are 34.1° for layer 1, 31° for layer 2, 36.6° (limited to 36°) for layer 3, and 41.6° (limited to 36°) for layers 5 and 6. For the 4.5-ft-thick "clay" layer (layer 4), an s_u value of 48.7 psi was entered into the program, and the option "piles driven through overlying sands or sandy gravels" was selected for the adhesion type (Tomlinson, 1980).

For a pile head settlement of $0.1B$ (= 1.4 in.), the ultimate load capacity Q_{ult} of the pile predicted using the PPDM (= 713 kips) is in good agreement with that obtained from the static load test (= 736 kips). The DrivenPiles program predicts a nominal pile capacity of 523 kips.

3.2 H-Pile in Clayey Silt (Jasper County, IN, USA)

Seo et al. (2009) reported the results of two static axial load tests performed on an instrumented, driven, steel H-pile at a test site located on State Road 49 (on the north side of Oliver Ditch) in Jasper County, Indiana. Figure 3.3 shows the soil profile at the site and the depth profiles of uncorrected SPT blow counts N_{SPT} (obtained from SPT borings S3 and S4), cone resistance q_c and sleeve resistance f_s (obtained from CPT soundings C3 and C4). The soil profile consists of 11 different layers of sand, silt and clay; each layer has different percentages of these three main soil types. The two CPTs were terminated at a depth of about 18 m (59 ft), one meter (3 ft) into an extremely dense, nonplastic silt layer with an average q_c value of 50 MPa (7,252 psi). Additional boring logs at the site indicated the presence of a 7.6-m-(25 ft)-thick soft silty clay layer with an average q_c value of 1.5 MPa (218 psi) below this silt layer. The groundwater table and bedrock were located at depths of 1 m (3 ft) and 26 m (85 ft), respectively, from the ground surface. Table 3.4 summarizes the properties of each soil layer in contact with the H-pile at the site.

The H-pile (HP 310×110) had a flange width b_f of 310 mm (12.2 in.), section depth d of 308 mm (12.1 in.), and flange and web thicknesses, t_f and t_w, of 15 mm (0.6 in.). The equivalent diameter B of the pile, obtained by equating the gross cross-sectional area ($b_f \times d$) of the pile with that of an equivalent circle, was 0.349 m (13.7 in.). The pile was driven using a single-acting diesel hammer, with a ram weight of 18.2 kN (4.1 kips) and maximum hammer stroke of 3.12 m (10.2 ft), down to a depth of 17.4 m (57 ft) from the ground surface. The base of the pile was embedded in the very dense, nonplastic silt layer, as shown in Figure 3.3.

The first static load test was performed on the H-pile 63 days after pile driving, and the second test was performed 99 days after driving. The results obtained from the first static load test are summarized as follows:

TABLE 3.3
Comparison between predicted and measured capacities of CEP pile in Marshall County, Indiana

Source of Capacity	Test/Design Method/Program	Shaft Capacity (kips)	Base Capacity (kips)	Total Capacity (kips)
Measurement (static load test)	Ultimate load at pile head settlement of $0.1B$[1]	460	276	736
Prediction	PPDM	433	280	713[2]
	DrivenPiles program	360	163	523

[1]After correction for residual loads (Han et al., 2017).
[2]Ultimate load Q_{ult} corresponding to a pile head settlement of $0.1B$ (= 1.4 in).

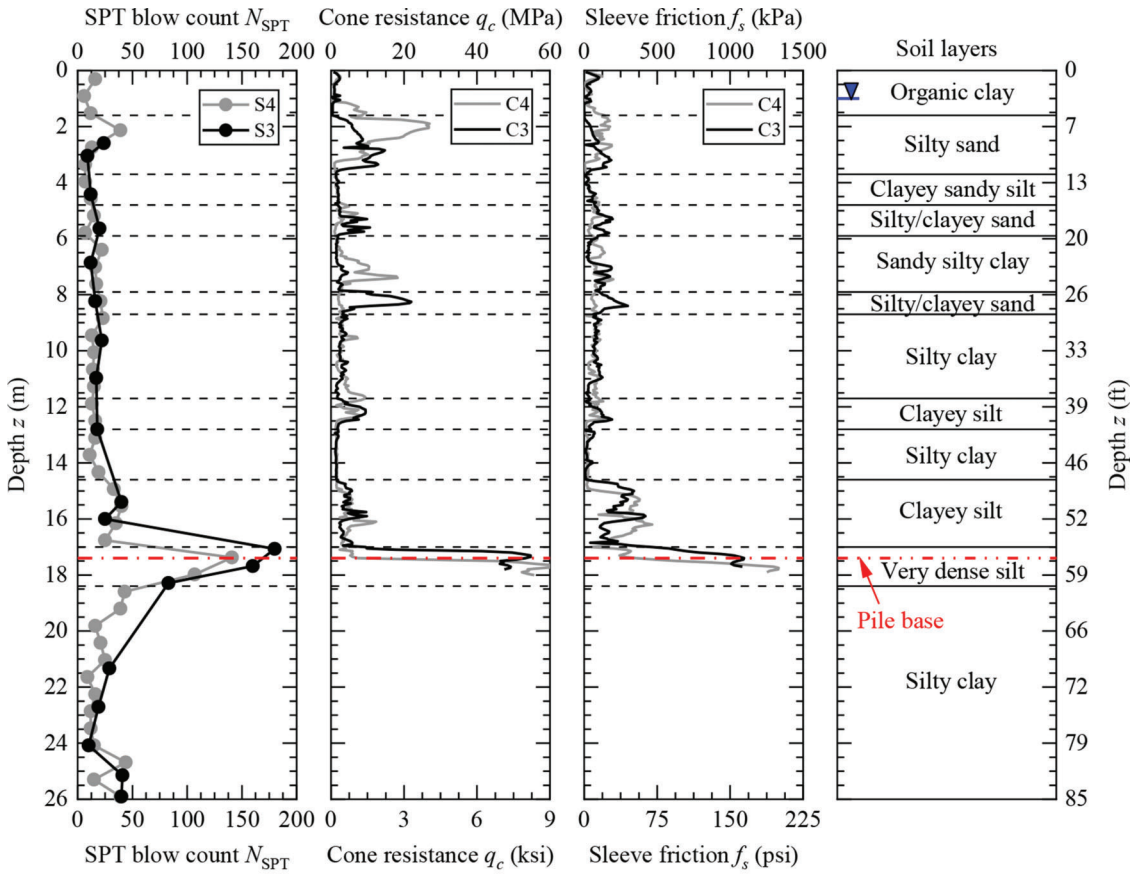

Figure 3.3 Profiles of N_{SPT}, q_c, f_s and soil layers at H-pile test site in Jasper County, Indiana (after Seo et al., 2009).

(a) the ultimate load Q_{ult} corresponding to a pile head settlement of 34.9 mm (1.37 in.) (= 0.1B) was 1,839 kN (414 kips), and (b) the pile almost plunged into the ground at an applied load of 2,092 kN (470 kips) and a corresponding pile head settlement of 114.5 mm (4.5 in.) (= 0.33B). The following steps show how to estimate the limit shaft capacity Q_{sL}, the ultimate base capacity $Q_{b,ult}$, and the ultimate load capacity Q_{ult} of the pile using CPT results.

3.2.1 Estimation of Limit Shaft Capacity

Step 1: Obtain the site stratigraphy, the groundwater table depth, and the unit weight of the soil in each layer of the profile.

a. Figure 3.3 shows the soil profile at the site; the soil layers were classified based on laboratory test results (i.e., Atterberg limits and sieve/hydrometer analysis).
b. Depth z_w of groundwater table = 3.3 ft.
c. Table 3.4 summarizes the unit weights of the soil layers. The unit weights of layers 1, 3, and 7–10 were obtained from consolidation test results, while the unit weights of the other layers were determined based on the typical range of values given in Section 4.1 of Volume II.

Step 2: Select the pile type and decide the pile length.
Pile type = H-pile.
Flange width b_f = 310 mm (12.2 in.) and depth of H-section d = 308 mm (12.1 in.).
Flange and web thickness t_f and t_w = 15 mm (0.6 in.).
Embedded length L of the pile = 17.4 m (57.1 ft).
Bearing layer for placement of the pile base = very dense silt.

Step 3: Classify the soil layers for pile design.
Classify the soil layers in contact with the pile as either "sand" or "clay," as shown in Table 3.4. Soil layers containing mixtures of sand and nonplastic fines were classified as "sand," whereas soil layers containing mixtures of sand and plastic fines with fines content FC $\geq$ 20% and plasticity index PI $\geq$ 8% were classified as "clay."

Step 4: Correct the q_c data for pore pressure.
The q_c data recorded within the saturated "clay" layers were corrected for the pore water pressure generated during cone penetration (calculations are presented in step 8(d)(i)).

Step 5: Divide the soil profile into sublayers.
Figure 3.4 shows the discretization of the q_c profile obtained from CPT sounding C3 into 11 sublayers up to a depth equal to the embedded length of the pile

TABLE 3.4
Properties of soil layers at H-pile test site in Jasper County, Indiana (after Seo et al., 2009)

Layer	z (ft)	Soil Type	Soil Classification for Pile Design	γ_m (pcf)	wc (%)	LL (%)	PI (%)	ϕ_c (°)	OCR	s_u (psi)	Particle Size Distribution			
											% Gravel	% Sand	% Silt	% Clay
1	0.0–5.2	Organic clay	—	85.3	96	138	89	—	—	—	—	—	—	—
2	5.2–12.1	Silty sand	Sand	140.0[1]	15	—	—	31[2]	—	—	3	91	6	—
3	12.1–15.7	Clayey sandy silt	Clay	137.5	19	18	8	28.7	5.6	11.3	—	29	42	29
4	15.7–19.4	Silty/clayey sand	Sand	140.0[1]	—	—	—	29[2]	—	—	—	—	—	—
5	19.4–25.9	Sandy silty clay	Clay	133.7[1]	—	—	—	31[1]	6.3	14.9	5	45	39	11
6	25.9–28.5	Silty/clayey sand	Sand	140.0[1]	—	—	—	29[2]	—	—	—	—	—	—
7	28.5–38.4	Silty clay	Clay	128.0	25	37	19	34.6	3.2	31.9	—	2	82	16
8	38.4–42.0	Clayey silt	Clay	131.1	23	29	10	31.4	1.9	46.4	—	2	83	15
9	42.0–47.9	Silty clay	Clay	139.4	15	21	9	31	4.9	14.9	—	15	64	21
10	47.9–55.8	Clayey silt	Clay	137.5	11	22	10	31.6	2.0	42.4	—	5	65	30
11	55.8–60.4	Very dense silt	Sand	133.7[1]	—	—	—	30[2]	—	—	—	1	94	5

Note: z = depth from the ground surface; γ_m = unit weight; wc = water content; LL = liquid limit; PI = plasticity index; ϕ_c = critical-state friction angle; OCR = overconsolidation ratio (obtained from the results of consolidation tests performed on Shelby tube samples recovered from the soil layer); and s_u = undrained shear strength (obtained from the results of isotropically-consolidated, undrained triaxial compression (CIUC) tests).

[1]Assumed values.

[2]Values estimated based on silty sand research by Salgado et al. (2000) and Lee et al. (2004).

(= 57.1 ft); the number of sublayers is equal to the number of soil layers listed in Table 3.4. The grey vertical bars indicate the representative (average) q_c values within each layer. One q_c data point at a depth of 2.75 m (9.0 ft) was considered to be an outlier and thus not included in the analysis.

Step 6: Calculate vertical effective stresses.

Table 3.5 summarizes the *in situ* vertical effective stress at the middle of each sublayer.

Step 7: Calculate the limit unit shaft resistance of pile segments in contact with "sand" sublayers.

Table 3.5 summarizes the results obtained for all the sublayers using the Imperial College pile design method (ICPDM). An example calculation for sublayer 2, which is a "sand" sublayer, is shown as follows.

a. Depths from the ground surface to the top and bottom of the sublayer:

$$z_{top} = 5.25 \text{ ft and } z_{bottom} = 12.14 \text{ ft}$$

Depth from the ground surface to the middle of the sublayer:

$$z_{middle} = \frac{z_{top} + z_{bottom}}{2} = \frac{5.25 + 12.14}{2} = 8.695 \text{ ft}$$

Thickness of the sublayer $\Delta z = z_{bottom} - z_{top} = 12.14 - 5.25 = 6.89$ ft.
Representative cone resistance of the sublayer q_c = 1,094.2 psi (Figure 3.4).
In situ vertical total stress at the middle of the sublayer:

$\sigma_{v0} = 85.3(5.25) + 140(8.695 - 5.25) = 930.13$ psf (or 6.46 psi)

Hydrostatic pore water pressure at the middle of the sublayer:

$u_0 = \gamma_w(z_{middle} - z_w) = 62.45 \times (8.695 - 3.3) = 336.92$ psf (or 2.34 psi)

In situ vertical effective stress at the middle of the sublayer (using Eq. 4.2 from Volume II):

$$\sigma'_{v0} = \sigma_{v0} - u_0 = 6.46 - 2.34 = 4.12 \text{ psi}$$

b. Critical-state friction angle ϕ_c of the sublayer = 31° (Table 3.4).
c. Critical-state interface friction angle δ_c of the sublayer = $0.85\phi_c = 0.85 \times 31° = 26.35°$.
d. Flange width b_f = 12.2 in. and depth of H-section d = 12.1 in.
Flange and web thickness t_f and t_w = 0.6 in.

$$d - 2t_f = 12.1 - 2(0.6) = 10.9 \text{ in.}$$

Since $b_f/2 < (d - 2t_f) < b_f$, therefore $X_p = b_f/8 = 12.2/8 = 1.525$ in.
Cross-sectional area of the pile base (from Table 4.2 of Volume II):

$A_b = 2b_f t_f + (2X_p + t_w)(d - 2t_f) = (2 \times 12.2 \times 0.6) + [2(1.525) + 0.6](10.9) = 54.4 \text{ in.}^2$

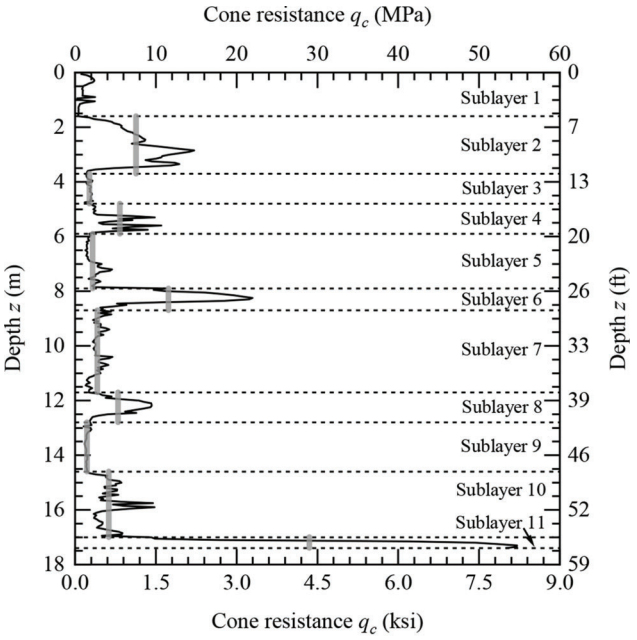

Figure 3.4 Discretization of q_c profile obtained from CPT sounding C3 into 11 sublayers at H-pile test site in Jasper County, Indiana.

Stress-normalized cone resistance (using Eq. 4.7 from Volume II):

$$\eta = \frac{\frac{q_c}{p_A}}{\sqrt{\frac{\sigma'_{v0}}{p_A}}} = \frac{\frac{1{,}094.2}{14.5}}{\sqrt{\frac{4.12}{14.5}}} = 141.6$$

Vertical distance from the middle of the sublayer to the pile base:

$h = L - z_{middle} = 57.1 - 8.695 = 48.4$ ft (or 580.8 in.)

Local radial effective stress acting on the pile segment after installation (using Eq. 4.5 from Volume II):

$$\sigma'_{rc} = 0.029 q_c \left(\frac{\sigma'_{v0}}{p_A}\right)^{0.13} \left(\max\left[\frac{h}{\sqrt{\frac{A_b}{\pi}}}; 8\right]\right)^{-0.38}$$

$$= 0.029 \times 1{,}094.2 \times \left(\frac{4.12}{14.5}\right)^{0.13} \times \left(\max\left[\frac{580.8}{\sqrt{\frac{54.4}{\pi}}}; 8\right]\right)^{-0.38}$$

$= 4.12$ psi

Increase in local radial effective stress associated with constrained dilation during pile loading (using Eq. 4.6 from Volume II):

TABLE 3.5
Calculation of limit shaft capacity of H-pile in Jasper County, Indiana

Sublayer i	Soil Type	z_{top} (ft)	z_{bottom} (ft)	Δz (ft)	z_{middle} (ft)	q_t (psi)	σ'_{v0} (psi)	η	σ'_{rc} (psi)	σ'_{rd} (psi)	$\left(\frac{s_u}{\sigma'_{v0}}\right)$	OCR	s_u (psi)	K	$\delta_{c,r}$ (°)	q_{sLi} (psi)	A_{si} (ft^2)	Q_{sLi} (kips)
1[1]	—	0.0	5.2	5.2	2.6	—	1.6	—	—	—	—	—	—	—	—	—	—	—
2	Sand	5.2	12.1	6.9	8.7	1,094	4.1	141.7	4.1	2.4	—	—	—	—	26.4	3.2	27.9	13.0
3	Clay	12.1	15.7	3.6	13.9	260	6.9	—	—	—	0.29	14.9	17.2	0.73	25.7	1.9	14.6	4.1
4	Sand	15.7	19.4	3.6	17.6	805	8.8	71.2	3.6	3.0	—	—	—	—	24.7	3.0	14.6	6.4
5	Clay	19.4	25.9	6.6	22.6	314	11.4	—	—	—	0.31	8.9	20.4	0.85	25.4	3.7	26.6	14.1
6	Sand	25.9	28.5	2.6	27.2	1,677	13.7	118.7	8.9	4.2	—	—	—	—	24.7	6.0	10.6	9.2
7	Clay	28.5	38.4	9.8	33.5	400	16.7	—	—	—	0.35	6.5	25.7	1.55	23.1	8.8	39.9	50.7
8	Clay	38.4	42.0	3.6	40.2	771	19.8	—	—	—	0.31	13.9	51.1	2.02	20.1	11.7	14.6	24.6
9	Clay	42.0	47.9	5.9	44.9	227	22.2	—	—	—	0.31	2.2	13.0	1.30	21.2	8.9	23.9	30.9
10	Clay	47.9	55.8	7.9	51.8	606	25.9	—	—	—	0.32	7.0	38.8	3.05	18.1	20.6	31.9	94.7
11	Sand	55.8	57.1	1.3	56.4	4,207	28.2	207.9	60.4	7.0	—	—	—	—	25.5	32.1	5.3	24.6

Note: z_{top}, z_{bottom}, and z_{middle} = depth measured from the ground surface to the top, bottom and middle of the sublayer, respectively; Δz = thickness of the sublayer; q_t = corrected, total cone resistance (= q_c for the sand sublayers); σ'_{v0} = *in situ* vertical effective stress at the middle of the sublayer; OCR = overconsolidation ratio (estimated from CPT results); s_u = undrained shear strength (estimated from CPT results using N_k = 14.4); K = coefficient of lateral earth pressure; $\delta_{c,r}$ = critical-state/residual interface friction angle (δ_c for sand and δ_r for clay); q_{sLi} = limit unit shaft resistance of pile segment in contact with sublayer i; A_{si} = pile shaft area interfacing with sublayer i; and Q_{sLi} = limit shaft capacity of pile segment in contact with sublayer i.

[1]The top 5.2-ft-thick organic clay layer was included in the vertical effective stress calculations but was excluded from the pile shaft resistance analysis due to the very low q_c values obtained in this layer.

$$\Delta\sigma'_{rd} = 2q_c \begin{bmatrix} 0.0203 + 0.00125\eta \\ -1.216 \times 10^{-6}\eta^2 \end{bmatrix}^{-1} \left(\frac{\Delta r}{\sqrt{\frac{A_b}{\pi}}} \right)$$

$$= 2 \times 1{,}094.2 \times \begin{bmatrix} 0.0203 + 0.00125(141.6) \\ -1.216 \times 10^{-6}(141.6)^2 \end{bmatrix}^{-1} \times \left(\frac{0.0008}{\sqrt{\frac{54.4}{\pi}}} \right) = 2.43 \text{ psi}$$

Limit unit shaft resistance of the pile segment in contact with sublayer 2 (using Eq. 4.4 from Volume II):

$$q_{sLi} = \left(F_{\text{load}}\sigma'_{rc} + \Delta\sigma'_{rd} \right) \tan\delta_c$$

$$= (4.12 + 2.43) \times \tan 26.35 = 3.24 \text{ psi}$$

Pile shaft area interfacing with sublayer 2 (from Table 4.1 of Volume II):

$A_{si} = 2(b_f + d)\Delta z_i = 2 \times (12.2 + 12.1) \times 6.89 \times 12 = 4{,}018.25$ in.^{2} (or 27.9 ft^2)

Limit shaft capacity of the pile segment in contact with sublayer 2:

$$Q_{sLi} = q_{sLi}A_{si} = 3.24 \times 4{,}018.25 = 13.0 \text{ kips}$$

Step 8: Calculate the limit unit shaft resistance of pile segments in contact with "clay" sublayers.

Table 3.5 summarizes the results obtained for all the sublayers using the Imperial College pile design method (ICPDM). An example calculation for sublayer 9, which is a "clay" sublayer, is shown as follows.

a. Critical-state friction angle ϕ_c of the sublayer = 31° (Table 3.4).
b. Minimum residual-state friction angle $\phi_{r,\min}$ of the sublayer = 15° (assumed).
c. Ignore this substep as the pile is not a CEP pile or a drilled shaft.
d. Depths from the ground surface to the top and bottom of the sublayer:

$$z_{\text{top}} = 42.0 \text{ ft and } z_{\text{bottom}} = 47.9 \text{ ft}$$

Depth from the ground surface to the middle of the sublayer:

$$z_{\text{middle}} = \frac{z_{\text{top}} + z_{\text{bottom}}}{2} = \frac{42.0 + 47.9}{2} = 44.95 \text{ ft}$$

Thickness of the sublayer $\Delta z = z_{\text{bottom}} - z_{\text{top}} = 47.9 - 42.0 = 5.9$ ft.
Representative cone resistance of the sublayer $q_c = 214.6$ psi (Figure 3.4).
In situ vertical total stress at the middle of the sublayer:

$\sigma_{v0} = 85.3(5.2) + 140(12.1 - 5.2) + 137.5(15.7 - 12.1) + 140(19.4 - 15.7) + 133.7(25.9 - 19.4) + 140(28.5 - 25.9) + 128(38.4 - 28.5) + 131.1(42.0 - 38.4) + 139.4(44.95 - 42.0) = 5{,}806$ psf (or 40.3 psi)

Hydrostatic pore water pressure at the middle of the sublayer:

$u_0 = \gamma_w(z_{\text{middle}} - z_w) = 62.45 \times (44.95 - 3.3) = 2{,}601$ psf (or 18.1 psi)

In situ vertical effective stress at the middle of the sublayer (using Eq. 4.2 from Volume II):

$$\sigma'_{v0} = \sigma_{v0} - u_0 = 40.3 - 18.1 = 22.2 \text{ psi}$$

i. Pore water pressure u_2 at the shoulder position behind the cone face = 63.5 psi.
Corrected, total cone resistance of the sublayer (using Eq. 4.1 from Volume II):

$$q_t = q_c + (1 - a)u_2 = 214.6 + (1 - 0.8)(63.5) = 227.3 \text{ psi}$$

Normalized cone resistance of the sublayer:

$$q_{tn} = \frac{q_t - \sigma_{v0}}{\sigma'_{v0}} = \frac{227.3 - 40.3}{22.2} = 8.4$$

Normalized undrained strength ratio of the sublayer if it were normally consolidated (Appendix B of Volume II):

$$\left(\frac{s_u}{\sigma'_{v0}} \right)_{\text{NC}} = \frac{\phi_c}{100} = \frac{31}{100} = 0.31$$

By plotting the net cone resistance $q_t - \sigma_{v0}$ of the "clay" layers versus the undrained shear strength s_u determined from CIUC test results, the cone factor N_k was found to be equal to 14.4 for the site. This value of N_k is reasonable given that the site consists of overconsolidated, clayey/silty soil layers.
Overconsolidation ratio (OCR) of the sublayer (using Eq. B.1 from Appendix B of Volume II):

$$\text{OCR} = \max\left\{ \left[\frac{q_{tn}/N_k}{\left(\frac{s_u}{\sigma'_{v0}} \right)_{\text{NC}}} \right]^{1.25}; 1 \right\}$$

$$= \max\left\{ \left[\frac{8.4/14.4}{0.31} \right]^{1.25}; 1 \right\} = 2.2$$

ii. *In situ* undrained shear strength of the sublayer (using Eq. 4.11 from Volume II):

$$s_u = \frac{q_t - \sigma_{v0}}{N_k} = \frac{227.3 - 40.3}{14.4} = 13.0 \text{ psi}$$

The plastic limit PL, water content wc, and liquid limit LL of the sublayer are 12%, 15%, and 21%, respectively.
Plasticity index PI of the sublayer = LL – PL = 21 – 12 = 9%.
Liquidity index LI of the sublayer = (wc – PL)/PI = (15 – 12)/9 = 0.33.

Remolded undrained shear strength of the sublayer (using Eq. 4.17 from Volume II):

$$\frac{s_{ur}}{p_A} = 0.017 \times 10^{2(1-\mathrm{LI})} = 0.017 \times 10^{2(1-0.33)} = 0.37$$

$$\Rightarrow s_{ur} = 0.37 p_A = 0.37 \times 14.5 = 5.4 \text{ psi}$$

Sensitivity of the sublayer (using Eq. 4.16 from Volume II):

$$S_t = \frac{s_u}{s_{ur}} = \frac{13.0}{5.4} = 2.41$$

iii. Equivalent pile radius (using Eq. 4.19 from Volume II):

$$R = \sqrt{\frac{A_b}{\pi}} = \sqrt{\frac{54.4}{\pi}} = 4.16 \text{ in.}$$

Vertical distance from the middle of the sublayer to the pile base:

$h = L - z_{\text{middle}} = 57.1 - 44.95 = 12.15$ ft (or 145.8 in.)

Lateral earth pressure coefficient of the sublayer (using Eq. 4.18 from Volume II):

$$K = [2.2 + 0.016 \text{ OCR} - 0.87 \log S_t] \text{OCR}^{0.42} \left(\max \left[\frac{h}{R}; 8 \right] \right)^{-0.20}$$

$$= [2.2 + 0.016(2.2) - 0.87 \log(2.41)] \times 2.2^{0.42} \times \left(\max \left[\frac{145.8}{4.16}; 8 \right] \right)^{-0.20} = 1.30$$

iv. Value of σ' at which the friction angle is equal to the average of $\phi_{r,\min}$ and ϕ_c:
$\sigma'_{\text{median}} = 14.5$ psi (assumed)
Normal effective stress σ' ($= \sigma'_h$) on the pile operative at the time of shearing (using Eq. 4.21 from Volume II):

$$\sigma' \left(= \sigma'_h \right) = F_{\text{load}} K \sigma'_{v0} = 0.8 \times 1.3 \times 22.2 = 23.1 \text{ psi}$$

Residual interface friction angle of the sublayer (using Eq. 4.20 from Volume II):

$$\delta_r \approx \phi_r = \phi_{r,\min} + \frac{\phi_c - \phi_{r,\min}}{1 + \frac{\sigma'}{\sigma'_{\text{median}}}} = 15^\circ + \frac{31^\circ - 15^\circ}{1 + \frac{23.1}{14.5}} = 21.2^\circ$$

v. Limit unit shaft resistance of the pile segment in contact with sublayer 9 (using Eq. 4.22 from Volume II):

$$q_{sLi} = F_{\text{load}} K \sigma'_{v0} \tan \delta_r = 0.8 \times 1.3 \times 22.2 \times \tan 21.2^\circ = 8.96 \text{ psi}$$

Pile shaft area interfacing with sublayer 9 (from Table 4.1 of Volume II):

$A_{si} = 2(b_f + d)\Delta z_i = 2 \times (12.2 + 12.1) \times (5.9 \times 12) = 3{,}440.88$ in.^{2} (or 23.9 ft^2)

Limit shaft capacity of the pile segment in contact with sublayer 9:

$$Q_{sLi} = q_{sLi} A_{si} = 8.96 \times 3{,}440.88 = 30.8 \text{ kips}$$

Step 9: Repeat steps 7 and 8 for all sublayers in contact with the pile shaft.

Table 3.5 summarizes the results obtained for all the sublayers in contact with the pile shaft.

Step 10: Compute the limit shaft capacity Q_{sL} of the pile.

Limit shaft capacity of the pile (using Eq. 4.23 from Volume II):

$$Q_{sL} = \sum_{i=1}^{11} Q_{sLi} = \sum_{i=1}^{11} q_{sLi} A_{si} = 272 \text{ kips}$$

(obtained by summing the last column of Table 3.5).

3.2.2 Estimation of Ultimate Base Capacity

Step 1: Estimate the average cone resistance q_{cb} at the pile base.

a. Figure 3.3 shows that a 7.6-m-(24.9-ft)-thick weak, silty clay layer lies below the bearing layer (i.e., the 1.4-m-(4.6-ft)-thick very dense, nonplastic silt layer) in which the pile base is embedded. Therefore, execute the following substeps.

i. Representative (steady-state) cone resistance of the strong (very dense silt) layer $q_{c,s} = 7{,}251.9$ psi.
Representative (steady-state) cone resistance of the weak (silty clay) layer $q_{c,w} = 227.3$ psi and $q_{c,w}/q_{c,s} = 227.3/7{,}251.9 = 0.031$.
As the CPT sounding C3 was terminated at a depth of 17.8 m (58.4 ft) from the ground surface, the value of $q_{c,w}$ (= 227.3 psi) for the weak silty clay layer, which lies between depths of 18.4 m (60.4 ft) and 26 m (85.3 ft), was assigned based on the q_c values obtained for a similar layer between depths of 12.8 m (42.0 ft) and 14.6 m (47.9 ft).

ii. Flange width $b_f = 12.2$ in. and depth of H-section $d = 12.1$ in.
Flange and web thickness t_f and $t_w = 0.6$ in.
Equivalent diameter of H-pile:

$$B = \sqrt{\frac{4 \times b_f \times d}{\pi}} = \sqrt{\frac{4 \times 12.2 \times 12.1}{\pi}} = 13.71 \text{ in.} (\text{or } 1.14 \text{ ft})$$

Sensing distance H_s (using Eq. 4.24 from Volume II):

$$\frac{H_s}{B} = 1.41 - 2.52 \ln \left(\frac{q_{c,w}}{q_{c,s}} \right) = 1.41 - 2.52 \ln(0.031) = 10.16$$

$$\Rightarrow H_s = 10.16 B = 10.16 \times 13.71 = 139.3 \text{ in.} (\text{or } 11.6 \text{ ft})$$

iii. Embedded length L of the pile = 57.1 ft.
Vertical distance H from the pile base to the interface between the strong and weak layers = 60.4 – 57.1 = 3.3 ft.

iv. $$\text{Coefficient } A_1 = \min\left[-0.22\ln\left(\frac{q_{c,w}}{q_{c,s}}\right)+0.11;\,1.5\right]$$
$$= \min\left[-0.22\ln(0.031)+0.11;\,1.5\right] = 0.87$$
$$\text{Coefficient } A_2 = \min\left[-0.11\ln\left(\frac{q_{c,w}}{q_{c,s}}\right)-0.79;\,-0.2\right]$$
$$= \min\left[-0.11\ln(0.031)-0.79;\,-0.2\right] = -0.41$$

Since $H < H_s$, the average cone resistance q_{cb} at the pile base is obtained using Eq. 4.25 from Volume II:

$$\frac{q_{cb}}{q_{c,s}} = \frac{q_{c,w}}{q_{c,s}} + \left(1-\frac{q_{c,w}}{q_{c,s}}\right)\exp\left\{-\exp\left[A_1 + A_2\left(\frac{H}{B}\right)\right]\right\}$$
$$= 0.031 + (1-0.031)\exp\left\{-\exp\left[0.87-0.41\left(\frac{3.3}{1.14}\right)\right]\right\}$$
$$= 0.495 \Rightarrow q_{cb} = 0.495 q_{c,s} = 0.495 \times 7{,}251.9 = 3{,}589.7 \text{ psi}$$

Step 2: Calculate the ultimate unit base resistance $q_{b,ult}$ of the pile.

From Eq. 4.28 of Volume II, the ultimate unit base resistance $q_{b,ult}$ of the H-pile is equal to the average cone resistance q_{cb} (= 3,589.7 psi) at the pile base.

Step 3: Compute the ultimate base capacity $Q_{b,ult}$ of the pile.

Cross-sectional area of the pile base (from Table 4.2 of Volume II):

$A_b = 2b_f t_f + (2X_p + t_w)(d - 2t_f) = (2 \times 12.2 \times 0.6) + [2(1.525) + 0.6](10.9) = 54.4$ in.^{2}

Ultimate base capacity of the pile (using Eq. 4.34 from Volume II):

$$Q_{b,ult} = q_{b,ult} A_b = 3{,}589.7 \times 54.4 = 195 \text{ kips}$$

Step 4: Compute the ultimate load capacity Q_{ult} of the pile.

Ultimate load capacity of the pile (using Eq. 4.35 from Volume II):

$$Q_{ult} = Q_{sL} + Q_{b,ult} = 272 + 195 = 467 \text{ kips}$$

3.2.3 Comparison Between Predicted and Measured Pile Capacities

Table 3.6 compares the shaft, base and total capacities of the H-pile obtained from the static load test (without correcting for residual loads) with those predicted using the Imperial College pile design method (ICPDM) for two cases: Case 1 (OCR and s_u estimated from CPT results) and Case 2 (OCR and s_u determined from laboratory test results). Predictions obtained for Case 2 are in better agreement with the static load test results than those obtained for Case 1. For Case 1, the predicted ultimate load capacity Q_{ult} of the pile is greater than the measured capacity by about 13%, whereas for Case 2, the predicted value of Q_{ult} is almost equal to the measured value.

If the effect of the weak silty clay layer below the pile base is not considered, and the value of q_{cb} is estimated by taking the average of the q_c values over a vertical distance of $1.5B$ above and below the pile base, then the predicted ultimate base capacity of the pile is equal to 305 kips, which is greater than the measured base capacity by about 50%. However, by considering the effect of the weak silty clay layer using the equations proposed by Xu and Lehane (2008), the predicted ultimate base capacity is equal to 195 kips, which is less than the measured base capacity by about 4%. The DrivenPiles program (see Section 3.1.3) was not used to estimate the capacity of the H-pile because the pile dimensions and the s_u values at the site were not compatible with the pile adhesion charts incorporated in the program.

3.3 Drilled Shaft in Clayey Silt (Jasper County, IN, USA)

This example problem shows how to calculate the limit shaft capacity, the ultimate base capacity, and the ultimate load capacity of a 17.4-m-(57.1-ft)-long, 350-mm-(13.8-in.)-diameter drilled shaft installed in the same soil profile as that shown in Figure 3.3. Consider the coefficient of lateral earth pressure at-rest K_0 of the "sand" layers to be 0.45 and the minimum residual-state friction angle $\phi_{r,\min}$ of the "clay" layers to be 15°.

TABLE 3.6
Comparison between predicted and measured capacities of H-pile in Jasper County, Indiana

Source of Capacity	Test/Design Method	Shaft Capacity (kips)	Base Capacity (kips)	Total Capacity (kips)
Measurement	Ultimate load at pile head	210	204	414
(1st static load test)	settlement of $0.1B$[1]			
Prediction	ICPDM (Case 1)[2]	272	195	467
	ICPDM (Case 2)[3]	218	195	413

[1]Not accounting for residual load (Seo et al., 2009).
[2]Using the values of OCR and s_u estimated from CPT results with N_k = 14.4.
[3]Using the values of OCR and s_u determined from laboratory test results.

3.3.1 Estimation of Limit Shaft Capacity

Steps 1–6 are the same as those detailed in Section 3.2.1, except that the pile is a drilled shaft with L = 17.4 m (57.1 ft) and B = 350 mm (13.8 in.). Calculations from step 7 onward are shown as follows.

Step 7: Calculate the limit unit shaft resistance of pile segments in contact with "sand" sublayers.

Table 3.7 summarizes the results obtained for all the sublayers using the Purdue pile design method (PPDM). An example calculation for sublayer 2, which is a "sand" sublayer, is shown in the following.

a. Recall from step 7 of Section 3.2.1 that z_{top} = 5.25 ft, z_{bottom} = 12.14 ft, z_{middle} = 8.695 ft, Δz = 6.89 ft, q_c = 1,094.2 psi, and σ'_{v0} = 4.12 psi.
Coefficient of lateral earth pressure at-rest K_0 = 0.45.
In situ horizontal effective stress at the middle of the sublayer:
$$\sigma'_{h0} = K_0\sigma'_{v0} = 0.45 \times 4.12 = 1.85 \text{ psi}.$$

b. Critical-state friction angle ϕ_c of the sublayer = 31° (Table 3.4).
c. Critical-state interface friction angle δ_c of the sublayer = ϕ_c = 31°.
d. Ignore this substep as the pile is not an H-pile.
e. Relative density of the sublayer (using Eq. 4.10 from Volume II):

$$D_R(\%) = \frac{\ln\left(\frac{q_c}{p_A}\right) - 0.4947 - 0.1041\phi_c - 0.841\ln\left(\frac{\sigma'_{h0}}{p_A}\right)}{0.0264 - 0.0002\phi_c - 0.0047\ln\left(\frac{\sigma'_{h0}}{p_A}\right)}$$
$$= \frac{\ln\left(\frac{1{,}094.2}{14.5}\right) - 0.4947 - 0.1041(31) - 0.841\ln\left(\frac{1.85}{14.5}\right)}{0.0264 - 0.0002(31) - 0.0047\ln\left(\frac{1.85}{14.5}\right)}$$
$$= 78.1\%$$

Coefficient of lateral earth pressure K (using Eq. 4.9 from Volume II):

$$K = \frac{0.67K_0}{\exp\left[0.3\sqrt{K_0 - 0.4}\right]}\exp\left\{\frac{D_R}{100}\left[1.5 - 0.35\ln\left(\frac{\sigma'_{v0}}{p_A}\right)\right]\right\}$$
$$= \frac{0.67 \times 0.45}{\exp\left[0.3\sqrt{0.45 - 0.4}\right]} \times \exp\left\{\frac{78.1}{100}\left[1.5 - 0.35\ln\left(\frac{4.12}{14.5}\right)\right]\right\}$$
$$= 1.28$$

Limit unit shaft resistance of the pile segment in contact with sublayer 2 (using Eq. 4.8 from Volume II):

$$q_{sLi} = K\sigma'_{v0}\tan\delta_c = 1.28 \times 4.12 \times \tan 31^\circ = 3.17 \text{ psi}$$

Pile shaft area interfacing with sublayer 2 (from Table 4.1 of Volume II):

$A_{si} = \pi B\Delta z_i = \pi \times 13.8 \times 6.89 \times 12 = 3{,}584.51$ in.^{2} (or 24.9 ft^2)

Limit shaft capacity of the pile segment in contact with sublayer 2:

$$Q_{sLi} = q_{sLi}A_{si} = 3.17 \times 3{,}584.51 = 11.4 \text{ kips}$$

Step 8: Calculate the limit unit shaft resistance of pile segments in contact with "clay" sublayers.

Table 3.7 summarizes the results obtained for all the sublayers using the Purdue pile design method (PPDM). An example calculation for sublayer 9, which is a "clay" sublayer, is shown in the following.

a. Critical-state friction angle ϕ_c of the sublayer = 31° (Table 3.4).
b. Minimum residual-state friction angle $\phi_{r,min}$ of the sublayer = 15°.
c. Recall from step 8 of Section 3.2.1 that z_{top} = 42.0 ft, z_{bottom} = 47.9 ft, z_{middle} = 44.95 ft, Δz = 5.9 ft, q_c = 214.6 psi, σ_{v0} = 40.3 psi, and σ'_{v0} = 22.2 psi.

i. Recall from step 8 of Section 3.2.1 that q_t = 227.3 psi, N_k = 14.4, and s_u = 13.0 psi.
ii. Difference between the critical-state and minimum residual-state friction angles of the sublayer $\phi_c - \phi_{r,min}$ = 31° − 15° = 16°.
Coefficient A_1 (using Eq. 4.14 from Volume II):

$$A_1 = 0.40 \ \left(\text{for } \phi_c - \phi_{r,\min} \geq 12^\circ\right)$$

Coefficient A_2 (using Eq. 4.15 from Volume II):

$$A_2 = 0.40 + 0.30\ln\left(\frac{s_u}{\sigma'_{v0}}\right) = 0.40 + 0.30\ln\left(\frac{13.0}{22.2}\right) = 0.24$$

Parameter α (using Eq. 4.13 from Volume II):

$$\alpha = \left(\frac{s_u}{\sigma'_{v0}}\right)^{-0.05}\left\{A_1 + (1 - A_1)\exp\left[-\left(\frac{\sigma'_{v0}}{p_A}\right)(\phi_c - \phi_{r,\min})^{A_2}\right]\right\}$$
$$= \left(\frac{13.0}{22.2}\right)^{-0.05}\left\{0.4 + (1 - 0.4)\exp\left[-\left(\frac{22.2}{14.5}\right) \times (16)^{0.24}\right]\right\}$$
$$= 0.44$$

Limit unit shaft resistance of the pile segment in contact with sublayer 9 (using Eq. 4.12 from Volume II):

$$q_{sLi} = \alpha s_u = 0.44 \times 13 = 5.72 \text{ psi}$$

Pile shaft area interfacing with sublayer 9 (from Table 4.1 of Volume II):

$A_{si} = \pi B\Delta z_i = \pi \times 13.8 \times (5.9 \times 12) = 3{,}069.46$ in.^{2} (or 21.3 ft^2)

Limit shaft capacity of the pile segment in contact with sublayer 9:

$$Q_{sLi} = q_{sLi}A_{si} = 5.72 \times 3{,}069.46 = 17.6 \text{ kips}$$

Step 9: Repeat steps 7 and 8 for all sublayers in contact with the pile shaft.

TABLE 3.7
Calculation of limit shaft capacity of drilled shaft in Jasper County, Indiana

Sublayer i	Soil Type	z_{top} (ft)	z_{bottom} (ft)	Δz (ft)	z_{middle} (ft)	q_t (psi)	σ'_{v0} (psi)	σ'_{h0} (psi)	D_R (%)	K	δ_c (°)	s_u (psi)	A_1	A_2	α	q_{sLi} (psi)	A_{si} (ft^2)	Q_{sLi} (kips)
1[1]	—	0.0	5.2	5.2	2.6	—	1.6	—	—	—	—	—	—	—	—	—	—	—
2	Sand	5.2	12.1	6.9	8.7	1,094	4.1	1.9	78	1.28	31.0	—	—	—	—	3.2	24.9	11.4
3	Clay	12.1	15.7	3.6	13.9	260	6.9	—	—	—	—	17.2	0.40	0.67	0.42	7.2	13.0	13.5
4	Sand	15.7	19.4	3.6	17.6	805	8.8	4.0	60	0.77	29.0	—	—	—	—	3.7	13.0	7.0
5	Clay	19.4	25.9	6.6	22.6	314	11.4	—	—	—	—	20.4	0.40	0.57	0.40	8.2	23.7	27.9
6	Sand	25.9	28.5	2.6	27.2	1,677	13.7	6.2	79	0.94	29.0	—	—	—	—	7.2	9.5	9.8
7	Clay	28.5	38.4	9.8	33.5	400	16.7	—	—	—	—	25.7	0.40	0.53	0.39	10.1	35.5	51.7
8	Clay	38.4	42.0	3.6	40.2	771	19.8	—	—	—	—	51.1	0.40	0.68	0.38	19.5	13.0	36.5
9	Clay	42.0	47.9	5.9	44.9	227	22.2	—	—	—	—	13.0	0.40	0.24	0.44	5.7	21.3	17.6
10	Clay	47.9	55.8	7.9	51.8	606	25.9	—	—	—	—	38.8	0.40	0.52	0.39	15.2	28.4	62.3
11	Sand	55.8	57.1	1.3	56.4	4,207	28.2	12.7	100	1.00	30.0	—	—	—	—	16.3	4.7	11.1

Note: z_{top}, z_{bottom}, and z_{middle} = depth measured from the ground surface to the top, bottom and middle of the sublayer, respectively; Δz = thickness of the sublayer; q_t = corrected, total cone resistance (= q_c for the sand sublayers); σ'_{v0} and σ'_{h0} = *in situ* vertical and horizontal effective stresses, respectively, at the middle of the sublayer; D_R = relative density (estimated from CPT results); K = coefficient of lateral earth pressure, δ_c = critical-state interface friction angle, s_u = undrained shear strength (estimated from CPT results using N_k = 14.4), q_{sLi} = limit unit shaft resistance of pile segment in contact with sublayer i, A_{si} = pile shaft area interfacing with sublayer i, and Q_{sLi} = limit shaft capacity of pile segment in contact with sublayer i.

[1]The top 5.2-ft-thick organic clay layer was included in the vertical effective stress calculations but was excluded from the pile shaft resistance analysis due to the very low q_c values obtained in this layer.

Table 3.7 summarizes the results obtained for all the sublayers in contact with the pile shaft.

Step 10: Compute the limit shaft capacity Q_{sL} of the pile.

Limit shaft capacity of the pile (using Eq. 4.23 from Volume II):

$$Q_{sL} = \sum_{i=1}^{11} Q_{sLi} = \sum_{i=1}^{11} q_{sLi} A_{si} = 249 \text{ kips}$$

(obtained by summing the last column of Table 3.7)

3.3.2 Estimation of Ultimate Base Capacity

Step 1: Estimate the average cone resistance q_{cb} at the pile base. Recall from step 1 of Section 3.2.2 that q_{cb} = 3,589.7 psi.

Step 2: Calculate the ultimate unit base resistance $q_{b,ult}$ of the pile.

a. Depth corresponding to $L + (B/2)$ = 57.1 + (1.15/2) = 57.675 ft.
In situ vertical total stress at the depth corresponding to $L + (B/2)$:

σ_{v0} = 85.3(5.2) + 140(12.1 – 5.2) + 137.5(15.7 – 12.1) + 140(19.4 – 15.7) + 133.7(25.9 – 19.4) + 140(28.5 – 25.9) + 128(38.4 – 28.5) + 131.1(42.0 – 38.4) + 139.4(47.9 – 42.0) + 137.5(55.8 – 47.9) + 133.7(57.675 – 55.8) = 7,554.17 psf (or 52.46 psi)

Hydrostatic pore water pressure at the depth corresponding to $L + (B/2)$:

$u_0 = \gamma_w(z - z_w)$ = 62.45 × (57.675 – 3.3) = 3,395.72 psf (or 23.58 psi)

In situ vertical effective stress at the depth corresponding to $L + (B/2)$:

$$\sigma'_{v0} = \sigma_{v0} - u_0 = 52.46 - 23.58 = 28.88 \text{ psi}$$

In situ horizontal effective stress at the depth corresponding to $L + (B/2)$:

$$\sigma'_{h0} = K_0 \sigma'_{v0} = 0.45 \times 28.88 = 12.99 \text{ psi}$$

Critical-state friction angle $\phi_c = 30^\circ$.
Relative density (using Eq. 4.30 from Volume II):

$$D_R = \frac{\ln\left(\frac{q_{cb}}{p_A}\right) - 0.4947 - 0.1041\phi_c - 0.841\ln\left(\frac{\sigma'_{h0}}{p_A}\right)}{0.0264 - 0.0002\phi_c - 0.0047\ln\left(\frac{\sigma'_{h0}}{p_A}\right)}$$

$$= \frac{\ln\left(\frac{3{,}589.7}{14.5}\right) - 0.4947 - 0.1041(30) - 0.841\ln\left(\frac{12.99}{14.5}\right)}{0.0264 - 0.0002(30) - 0.0047\ln\left(\frac{12.99}{14.5}\right)}$$

$$= 95\%$$

Ultimate unit base resistance of the pile (using Eq. 4.28 from Volume II):

$$q_{b,ult} = 62 p_A \left(\frac{D_R}{100}\right)^{1.83} \left(\frac{\sigma'_{h0}}{p_A}\right)^{0.4}$$

$$= 62 \times 14.5 \times \left(\frac{95}{100}\right)^{1.83} \times \left(\frac{12.99}{14.5}\right)^{0.4} = 783.2 \text{ psi}$$

Step 3: Compute the ultimate base capacity $Q_{b,ult}$ of the pile.

Cross-sectional area of the pile base (from Table 4.2 of Volume II):

$$A_b = \frac{\pi B^2}{4} = \frac{\pi \times 13.8^2}{4} = 149.57 \text{ in.}^2$$

Ultimate base capacity of the pile (using Eq. 4.34 from Volume II):

$$Q_{b,ult} = q_{b,ult} A_b = 783.2 \times 149.57 = 117 \text{ kips}$$

Step 4: Compute the ultimate load capacity Q_{ult} of the pile.

Ultimate load capacity of the pile (using Eq. 4.35 from Volume II):

$$Q_{ult} = Q_{sL} + Q_{b,ult} = 249 + 117 = 366 \text{ kips}$$

3.3.3 Comparison Between Predicted Capacities of H-pile and Drilled Shaft

Table 3.8 summarizes the predicted shaft, base and total capacities of both the H-pile and the drilled shaft for two cases: Case 1 (soil properties estimated from CPT results) and Case 2 (soil properties determined from laboratory test results). For an H-pile and a drilled shaft with similar dimensions (L and B) installed in the same soil profile (Jasper County, Indiana), the predicted ultimate load capacity Q_{ult} of the H-pile, which is a partial-displacement pile, is greater than that of the drilled shaft, which is a nondisplacement pile, by about 11%–28%; the difference being greater in terms of their base capacities as opposed to their shaft capacities.

3.4 Open-Ended Pipe Pile in Gravelly Sand (Tippecanoe County, IN, USA)

Han et al. (2019b, 2020) reported the results of a static axial load test performed on an instrumented, driven, double-wall, open-ended steel pipe pile at a bridge construction site located on the east bank of the Wabash River at its intersection with Sagamore Parkway in Lafayette, Tippecanoe County, Indiana. Figure 3.5 shows the soil profile at the site, the SPT blow counts N_{SPT} obtained from two SPT borings S1 and S2 (using an automatic trip hammer), the cone resistance q_c values obtained from CPT sounding C3 (using a 44.6-mm-(1.75 in.)-diameter cone), and the mean particle size D_{50} and gravel content of the soil layers. The two SPTs, S1 and S2, were performed at radial distances of about 23 m (75.5 ft) and 15 m (49 ft), respectively, from the center of the

test pile, while the CPT was performed 3.7 m (12 ft) away from the test pile. The soil profile consists primarily of layers of poorly-graded sand and gravel mixtures, which is typical of "outwash" geologic regions in Indiana (as discussed in Chapter 2 of Volume II)—the gravel content is less than 20% up to a depth of 16 m (52.5 ft), except in a thin layer at a depth of 9 m (29.5 ft) where the gravel content is about 50%. From 16–35 m (52.5–115 ft) depth, the gravel content is typically greater than 30% and as high as 50%–60% at certain depths. When the cone could not be pushed through layers with high gravel content, a drill-and-push scheme was adopted by Han et al. (2020)—this scheme consisted of pushing the cone through a hollow stem auger that was used to drill through the hard layer. The groundwater table was located at a depth of 3.05 m (10 ft) from the ground surface. Table 3.9 summarizes the gradation and morphological parameters of each soil layer at the site.

The open-ended pipe (OEP) pile was composed of two segments, a bottom segment and a top segment, each of length equal to 18.3 m (60 ft). The bottom segment is a double-wall system consisting of an outer pipe with an outer diameter B of 660.4 mm (26 in.) and an inner pipe with an outer diameter of 584.2 mm (23 in.)—both pipes have the same wall thickness of 12.7 mm (0.5 in.), as shown in Figure 3.6. The gap between the outer pipe and the cutting shoe (welded to the bottom of the inner pipe) was filled with silicone, resulting in a final wall thickness or annulus thickness of 50.8 mm (2 in.). The top segment of the pile has the same outer diameter as that of the bottom segment but a wall thickness of 19.1 mm (0.75 in.). The centerline average surface roughness R_a ranges from 14–18 μm (0.55–0.71 mils) for the

TABLE 3.8
Comparison between predicted capacities of H-pile and drilled shaft in Jasper County, Indiana

Pile Type	Design Method	Shaft Capacity (kips)	Base Capacity (kips)	Total Capacity[4] (kips)
H-pile	ICPDM (Case 1)[1]	272	195	467
	ICPDM (Case 2)[2]	218	195	413
Drilled shaft[3]	PPDM (Case 1)[1]	249	117	366
	PPDM (Case 2)[2]	255	117	372

[1]Using CPT results with N_k = 14.4 to obtain the properties of the "clay" layers.
[2]Using laboratory test results to determine the properties of the "clay" layers.
[3]Assuming K_0 = 0.45 for the "sand" layers and $\phi_{r,\min}$ = 15° for the "clay" layers.
[4]Ultimate load Q_{ult} corresponding to a pile head settlement of 0.1B.

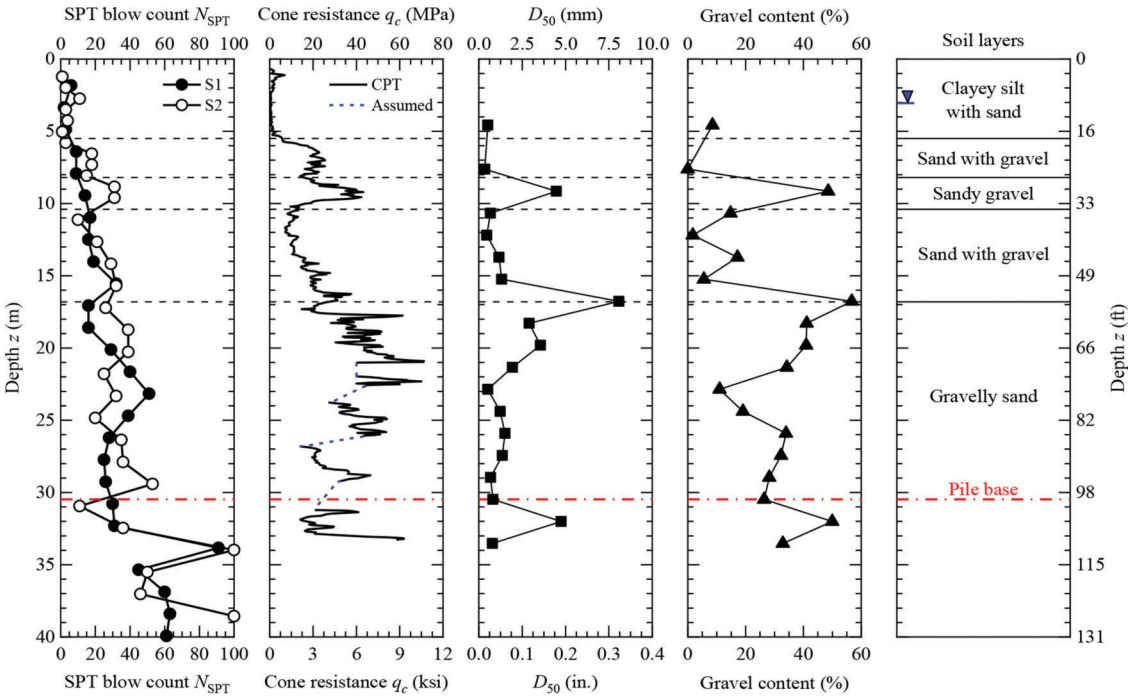

Figure 3.5 Profiles of N_{SPT}, q_c, D_{50}, gravel content and soil layers at OEP pile test site in Lafayette, Indiana (after Han et al., 2020).

TABLE 3.9
Properties of soil layers at OEP pile test site in Lafayette, Indiana (Han et al., 2019a, 2020)

Layer	z (ft)	Soil type	γ_m (pcf)	D_{50} (in.)	Gravel Content (%)	C_U	C_C	R	S	ϕ_c (°)
1	0.0–18.0	Clayey silt with sand	124.1	—	0	3.0	0.8	—	—	30
2	18.0–26.9	Sand with gravel	127.3	0.016	4	2.6	0.9	0.41	0.82	32
3	26.9–34.1	Sandy gravel	136.9	0.177	49	34.6	0.7	0.44	0.82	35
4	34.1–55.1	Sand with gravel	127.3	0.035	10	4.8	0.7	0.50	0.84	32
5	55.1–74.1	Gravelly sand	136.9	0.161	43	16.6	0.6	0.46	0.81	34
6	74.1–107.0	Gravelly sand	136.9	0.043	28	8.3	0.8	0.44	0.82	33

Note: z = depth from the ground surface, γ_m = unit weight (assumed based on soil type (Salgado, 2008)), D_{50} = mean particle size, C_U = coefficient of uniformity (= D_{60}/D_{10}), C_C = coefficient of curvature (= $(D_{30})^2/(D_{10} \times D_{60})$), R = roundness = the ratio of the average radius of curvature of the corners of a 2D projection of the particle to the radius of the largest inscribed circle for the same projection (Wadell, 1932), S = sphericity = the ratio of the diameter of a circle having the same area as the projected 2D area of the particle to the diameter of the smallest circle circumscribed about the 2D projection of the particle (Wadell, 1933), and ϕ_c = critical-state friction angle.

outer surfaces of the top and bottom pile segments and 4–8 μm (0.16–0.31 mils) for the inner surface of the inner pipe of the bottom segment.

A steel casing with a diameter of 0.91 m (35.8 in.) was installed from the ground surface up to a depth of 8.53 m (28 ft). The soil inside the casing was excavated prior to driving the two segments of the test pile; thus, pile driving started from a depth of 8.53 m (28 ft) and not from the ground surface. This operation was executed, according to Han et al. (2020), because the heads of the production piles for the Sagamore Parkway Bridge were to be located at a depth of 8.53 m (28 ft) below the ground surface to avoid problems related to potential scour/erosion at the site. The bottom segment of the pile, with the inner and outer pipes connected, was first lowered into the 0.91-m-(35.8-in.)-diameter borehole, centered, and driven into the ground up to a depth of 16.8 m (55 ft) with the help of a single-acting diesel hammer (ram weight = 68.7 kN (15.4 kips) and maximum stroke height = 3.43 m (11.25 ft)). Three days later, the top segment was welded to the bottom segment and driven into the ground until the pile base reached a final depth of 30.48 m (100 ft) from the ground surface. Figure 3.7 shows the profiles of the incremental filling ratio (IFR) and the soil plug length obtained during pile driving. The value of IFR decreased from 92% at the start of driving to 70% at the end of driving. The value of PLR at the end of driving was 77.7%. After pile driving, the gap between the casing and the pile was backfilled with loose pea gravel.

A slow, maintained static load test was performed on the OEP pile 8 days after pile driving. The ultimate load Q_{ult} corresponding to a pile head settlement of 66 mm (2.6 in.) (= 0.1B) was 4,782 kN (1,075 kips), whereas the load Q_L and pile head settlement required for the pile to start plunging into the ground were 6,228 kN (1,400 kips) and 149 mm (5.9 in.) (= 0.225B), respectively. The following steps show how to estimate the limit shaft capacity Q_{sL}, the ultimate base capacity $Q_{b,ult}$, and the ultimate load capacity Q_{ult} of the pile using CPT results.

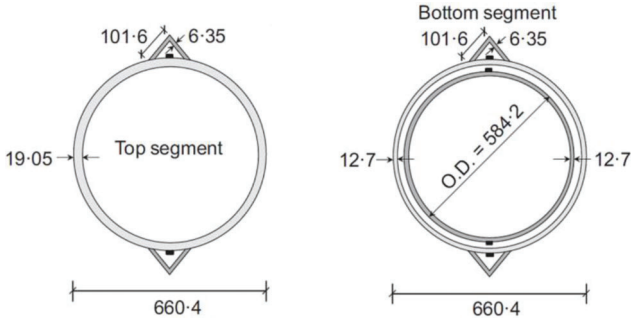

Figure 3.6 Dimensions (in mm) of top and bottom segments of OEP pile in Lafayette, Indiana (Han et al., 2020).

3.4.1 Estimation of Limit Shaft Capacity

Step 1: Obtain the site stratigraphy, the groundwater table depth, and the unit weight of the soil in each layer of the profile.

a. Figure 3.5 shows the soil profile obtained from SPT boring logs and laboratory test results.
b. Depth z_w of groundwater table = 10 ft. Han et al. (2020) determined the elevation of the water table by sending a measuring tape through the open-ended reaction piles during the load test.
c. Table 3.9 summarizes the unit weights of the soil layers.

Step 2: Select the pile type and decide the pile length.
Pile type = open-ended pipe (OEP) pile.
Outer diameter B of the pile = 26 in.
Embedded length L of the pile = 100 ft.
Bearing layer for placement of the pile base = gravelly sand.

Step 3: Classify the soil layers for pile design.
For this site, all the soil layers are classified as "sand" for the purpose of pile capacity analysis. The top 18-ft-thick clayey silt with sand layer (layer 1 in Table 3.9) is classified as "sand" because the fines are nonplastic.

Step 4: Correct the q_c data for pore pressure.
The pore pressure correction to the q_c data was ignored because the site consists primarily of saturated sand and gravel layers with relatively high q_c values compared to the measured pore pressure u_2 values.

Step 5: Divide the soil profile into sublayers.

Since the site consists of layers of poorly-graded sand and gravel mixtures with high gravel content, the lower bound of the q_c profile, drawn approximately through the valleys of the actual q_c profile (Figure 3.8), was considered in the analysis. Figure 3.9 shows the discretization of the lower bound q_c profile into 12 sublayers up to a depth equal to the embedded length of the pile (= 100 ft). The grey vertical bars indicate the representative (average) q_c values within each sublayer.

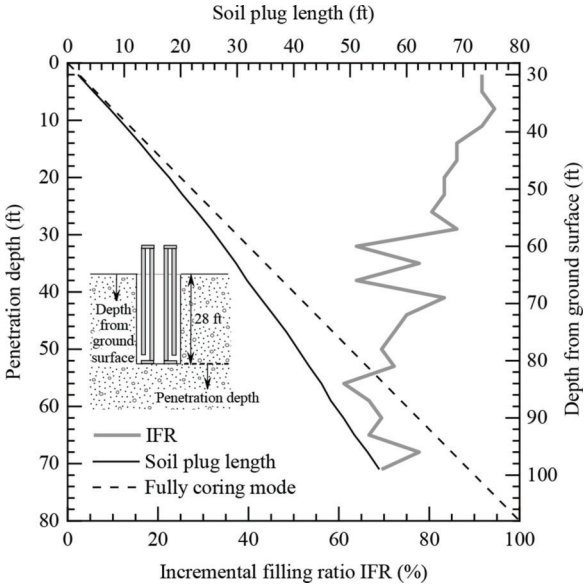

Figure 3.7 Profiles of IFR and soil plug length measured during driving of OEP pile in Lafayette, Indiana (after Han et al., 2020).

Step 6: Calculate vertical effective stresses.

Table 3.10 summarizes the *in situ* vertical effective stress at the middle of each sublayer.

Step 7: Calculate the limit unit shaft resistance of pile segments in contact with "sand" sublayers.

Table 3.10 summarizes the results obtained for all the sublayers using the Purdue pile design method (PPDM). An example calculation for sublayer 4, which is a "sand" sublayer, is shown in the following.

a. Depths from the ground surface to the top and bottom of the sublayer:

$$z_{top} = 34.12 \text{ ft and } z_{bottom} = 44.32 \text{ ft}$$

Depth from the ground surface to the middle of the sublayer:

$$z_{middle} = \frac{z_{top} + z_{bottom}}{2} = \frac{34.12 + 44.32}{2} = 39.22 \text{ ft}$$

Thickness of the sublayer $\Delta z = z_{bottom} - z_{top} = 44.32 - 34.12 = 10.2$ ft.
Representative cone resistance of the sublayer q_c = 1,239.4 psi (Figure 3.9).
In situ vertical total stress at the middle of the sublayer:

$\sigma_{v0} = 124.1(18.0) + 127.3(26.9 - 18.0) + 136.9(34.1 - 26.9) + 127.3(39.22 - 34.1) = 5{,}004.23$ psf (or 34.75 psi)

Hydrostatic pore water pressure at the middle of the sublayer:

$u_0 = \gamma_w(z_{middle} - z_w) = 62.45 \times (39.22 - 10.0) = 1{,}824.79$ psf (or 12.67 psi)

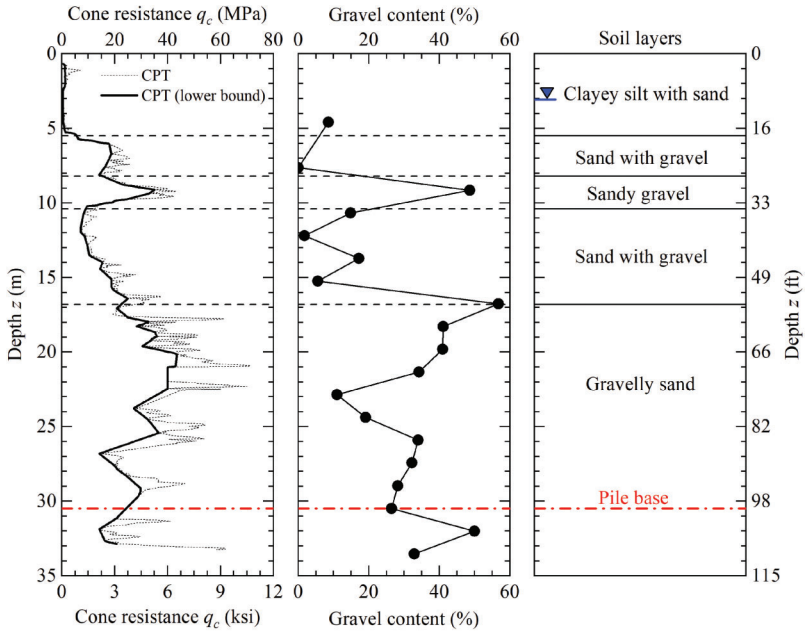

Figure 3.8 Lower bound of q_c profile, gravel content, and soil layers at OEP pile test site in Lafayette, Indiana (Han et al., 2020).

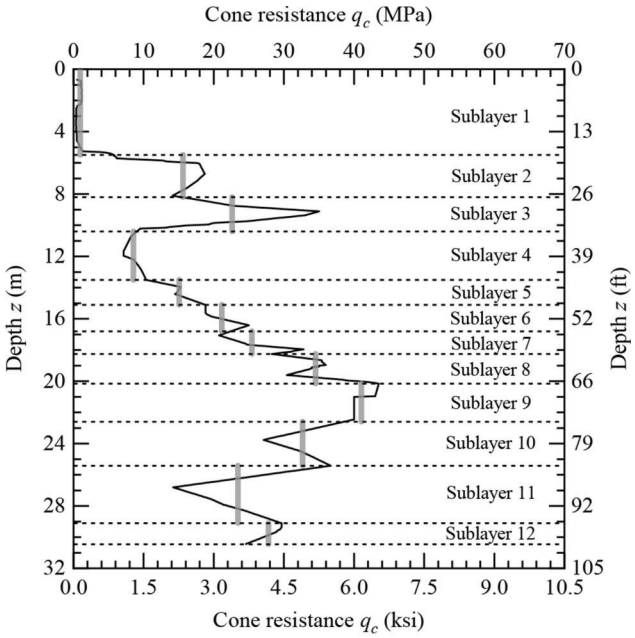

Figure 3.9 Discretization of lower bound q_c profile into 12 sublayers at OEP pile test site in Lafayette, Indiana.

In situ vertical effective stress at the middle of the sublayer (using Eq. 4.2 from Volume II):

$$\sigma'_{v0} = \sigma_{v0} - u_0 = 34.75 - 12.67 = 22.08 \text{ psi}$$

The coefficient of lateral earth pressure at-rest K_0 was taken as 0.45 for all the "sand" layers.
In situ horizontal effective stress at the middle of the sublayer:

$$\sigma'_{h0} = K_0\sigma'_{v0} = 0.45 \times 22.08 = 9.94 \text{ psi}$$

b. Critical-state friction angle ϕ_c of the sublayer = 32° (Table 3.9).
c. Mean particle size D_{50} of the sublayer = 0.9 mm (or 0.035 in.).
Coefficient of uniformity C_U of the sublayer = 4.8.
For D_{50} = 0.9 mm, C_U = 4.8, and rusted steel, the critical-state interface friction angle δ_c of the sublayer is $0.76\phi_c$ (= 0.76 × 32° = 24.3°) from Figure 4.2 of Volume II.
d. Ignore this substep as the pile is not an H-pile.
e. Vertical distance from the middle of the sublayer to the pile base:

$$h = L - z_{\text{middle}} = 100 - 39.22 = 60.78 \text{ ft}$$

Coefficient of lateral earth pressure (using Eq. 4.9 from Volume II):

$$K = 0.2 + \left[\frac{0.01\left(\frac{q_c}{p_A}\right)}{\sqrt{\frac{\sigma'_{h0}}{p_A}}} - 0.2\right]\exp\left(\frac{-0.14h}{L_R}\right)$$

$$= 0.2 + \left[\frac{0.01 \times \left(\frac{1{,}239.4}{14.5}\right)}{\sqrt{\frac{9.94}{14.5}}} - 0.2\right]\exp\left(\frac{-0.14 \times 60.78}{3.28}\right)$$

$$= 0.26$$

Soil plug length L_p = 10.37 ft (from Figure 3.7 corresponding to z_{middle} = 39.22 ft).
Pile penetration length L = 39.22 – 28.0 = 11.22 ft (because pile driving started from a depth of 28 ft below the ground surface).
Plug length ratio (PLR) of the sublayer $= \frac{L_p}{L} = \frac{10.37}{11.22} = 0.924$.

Limit unit shaft resistance of the pile segment in contact with sublayer 4 (using Eq. 4.8 from Volume II):

$$q_{sLi} = K(1 - 0.66\text{PLR})\sigma'_{v0}\tan\delta_c$$
$$= 0.26 \times [1 - (0.66 \times 0.924)] \times 22.08 \times \tan 24.3^\circ = 1.01 \text{ psi}$$

Pile shaft area interfacing with sublayer 4 (from Table 4.1 of Volume II):

$A_{si} = \pi B\Delta z_i = \pi \times 26 \times (10.2 \times 12) = 9{,}997.8$ in.^{2} (or 69.43 ft^2)

Limit shaft capacity of the pile segment in contact with sublayer 4:

$$Q_{sLi} = q_{sLi}A_{si} = 1.01 \times 9{,}997.8 = 10.1 \text{ kips}$$

As an example, if plug length measurements were not available for this site, the PLR can be approximated by Eq. 4.29 from Volume II:

$$\text{PLR} = \min\left[1; \left(\frac{B_i}{1.5L_R}\right)^{0.2}\right]$$
$$= \min\left[1; \left(\frac{22}{1.5 \times 39.4}\right)^{0.2}\right] = 0.821$$

where B_i = inner diameter of the OEP pile = inner diameter of the inner pipe in the bottom segment [= 23 – 2(0.5) = 22 in.]

$$q_{sLi} = K(1 - 0.66\text{PLR})\sigma'_{v0}\tan\delta_c$$
$$= 0.26 \times [1 - (0.66 \times 0.821)] \times 22.08 \times \tan 24.3^\circ = 1.19 \text{ psi}$$
$$Q_{sLi} = q_{sLi}A_{si} = 1.19 \times 9{,}997.8 = 11.9 \text{ kips}$$

Step 8: Calculate the limit unit shaft resistance of pile segments in contact with "clay" sublayers.

Ignore this step as there are no "clay" sublayers at the site.

TABLE 3.10
Calculation of limit shaft capacity of OEP pile in Lafayette, Indiana

Sublayer i	Soil Type	z_{top} (ft)	z_{bottom} (ft)	Δz (ft)	z_{middle} (ft)	q_c (psi)	σ_{v0} (psi)	σ'_{v0} (psi)	σ'_{h0} (psi)	h (ft)	K	PLR	δ_c (°)	q_{sLi} (psi)	A_{si} (ft^2)	Q_{sLi} (kips)
1	Sand	0.0	18.0	18.0	9.0	138	7.8	7.8	3.5	91.0	0.20	1.000	24.6	0.2	122.8	4.3
2	Sand	18.0	26.9	8.9	22.5	2,266	19.5	14.1	6.3	77.5	0.28	1.000	26.2	0.7	60.3	5.7
3	Sand	26.9	34.1	7.2	30.5	3,283	26.8	17.9	8.1	69.5	0.35	0.919	23.1	1.0	49.1	7.4
4	Sand	34.1	44.3	10.2	39.2	1,239	34.8	22.1	9.9	60.8	0.26	0.924	24.3	1.0	69.4	10.2
5	Sand	44.3	49.6	5.3	46.9	2,187	41.6	25.6	11.5	53.1	0.36	0.901	24.3	1.7	35.7	8.6
6	Sand	49.6	55.1	5.5	52.3	3,067	46.4	28.0	12.6	47.7	0.47	0.884	24.3	2.5	37.8	13.5
7	Sand	55.1	59.9	4.8	57.5	3,692	51.1	30.5	13.7	42.5	0.59	0.871	23.1	3.3	32.6	15.4
8	Sand	59.9	66.1	6.2	63.0	5,007	56.3	33.3	15.0	37.0	0.86	0.852	23.1	5.4	42.4	32.7
9	Sand	66.1	74.1	8.0	70.1	5,954	63.1	37.0	16.7	29.9	1.22	0.830	23.1	8.7	54.5	68.2
10	Sand	74.1	83.4	9.3	78.8	4,739	71.3	41.5	18.7	21.2	1.28	0.813	25.1	11.5	63.0	104.7
11	Sand	83.4	95.5	12.1	89.4	3,402	81.4	47.0	21.1	10.6	1.31	0.788	25.1	13.8	82.4	164.2
12	Sand	95.5	100.0	4.5	97.8	4,036	89.3	51.3	23.1	2.3	2.02	0.778	25.1	23.6	30.6	104.1

Note: z_{top}, z_{bottom}, and z_{middle} = depth measured from the ground surface to the top, bottom and middle of the sublayer, respectively, Δz = thickness of the sublayer, q_c = representative cone resistance of the sublayer, σ_{v0} and σ'_{v0} = *in situ* vertical total and effective stresses, respectively, at the middle of the sublayer, σ'_{h0} = *in situ* horizontal effective stress at the middle of the sublayer, h = vertical distance from the middle of the sublayer to the pile base, K = coefficient of lateral earth pressure, PLR = plug length ratio, δ_c = critical-state interface friction angle, q_{sLi} = limit unit shaft resistance of pile segment in contact with sublayer i, A_{si} = pile shaft area interfacing with sublayer i, and Q_{sLi} = limit shaft capacity of pile segment in contact with sublayer i.

Step 9: Repeat steps 7 and 8 for all sublayers in contact with the pile shaft.

Table 3.10 summarizes the results obtained for all the sublayers in contact with the pile shaft.

Step 10: Compute the limit shaft capacity Q_{sL} of the pile.

Limit shaft capacity of the pile (using Eq. 4.23 from Volume II):

$$Q_{sL} = \sum_{i=1}^{12} Q_{sLi} = \sum_{i=1}^{12} q_{sLi} A_{si} = 539 \text{ kips}$$

(obtained by summing the last column of Table 3.10).

3.4.2 Estimation of Ultimate Base Capacity

Step 1: Estimate the average cone resistance q_{cb} at the pile base.

a. Depth corresponding to $L - B = 100 - 2.17 = 97.83$ ft.
Depth corresponding to $L + 2B = 100 + 2(2.17) = 104.34$ ft.
Depth corresponding to $L + (B/2) = 50.6 + (1.17/2) = 101.08$ ft.

   i. Following the Purdue pile design method (PPDM), the representative cone resistance q_{cb} for use in pile base capacity calculation is obtained by averaging the lower-bound q_c values between $1B$ above and $2B$ below the pile base, corresponding to a 97.83–104.34 ft depth range. This yields $q_{cb} = 3{,}219$ psi.

Step 2: Calculate the ultimate unit base resistance $q_{b,ult}$ of the pile.

a. Based on the plug length measurements shown in Figure 3.7, the incremental filling ratio (IFR) averaged over the last $3B$ (= 6.5 ft) of pile driving is equal to 0.704.
Ultimate unit base resistance of the pile (using Eq. 4.28 from Volume II):

$$\begin{aligned} q_{b,ult} &= \min\left[0.21(\text{IFR})^{-1.2} q_{cb};\ 0.6 q_{cb}\right] \\ &= \min\left[0.21(0.704)^{-1.2} \times 3{,}219;\ 0.6 \times 3{,}219\right] \\ &= 1{,}030 \text{ psi} \end{aligned}$$

Step 3: Compute the ultimate base capacity $Q_{b,ult}$ of the pile.

Cross-sectional area of the pile base (from Table 4.2 of Volume II):

$$A_b = \frac{\pi B^2}{4} = \frac{\pi \times 26^2}{4} = 530.93 \text{ in.}^2$$

Ultimate base capacity of the pile (using Eq. 4.34 from Volume II):

$$Q_{b,ult} = q_{b,ult} A_b = 1{,}030 \times 530.93 = 547 \text{ kips}$$

Step 4: Compute the ultimate load capacity Q_{ult} of the pile.

Ultimate load capacity of the pile (using Eq. 4.35 from Volume II):

$$Q_{ult} = Q_{sL} + Q_{b,ult} = 539 + 547 = 1{,}086 \text{ kips}$$

3.4.3 Comparison Between Predicted and Measured Pile Capacities

Table 3.11 compares the shaft, base and total capacities of the OEP pile obtained from the static load test (after correction for residual loads) with those predicted using the Purdue pile design method (PPDM) and the Unified pile design method (UPDM) (Table 4.19 of Volume II). The base capacity of an OEP pile has two components: (1) plug capacity, and (2) annulus capacity, both of which were measured by Han et al. (2020) at the end of the static load test. The ultimate load capacity Q_{ult} of the pile predicted using the PPDM (= 1,086 kips) is in good agreement with that obtained from the static load test (= 1,075 kips) for the prediction using the measured PLR and IFR values obtained from plug length measurements. In the absence of plug length measurements, the ultimate load capacity Q_{ult} of the pile predicted using the PPDM is less than that obtained from the static load test by about 8%. In contrast, the UPDM overestimates the ultimate load capacity Q_{ult} of the pile by about 50% regardless of the availability of plug length measurements.

3.5 Closed-Ended Pipe Pile in Gravelly Sand (Tippecanoe County, IN, USA)

Ganju et al. (2020) reported the results of a static axial load test performed on an instrumented, driven, closed-ended steel pipe pile at the Sagamore Parkway bridge construction site described in Section 3.4. The closed-ended pipe (CEP) pile was installed at a horizontal distance of 7.31 m (24 ft) from the location of the open-ended test pile. The outer diameter and wall thickness of the CEP pile are 610 mm (24 in.) and 13 mm (0.5 in.), respectively. The pile was driven using a single-acting diesel hammer down to a depth of 17.37 m (57 ft) from the ground surface. The final embedment depth of the pile, however, was 17.68 m (58 ft) due to the addition of 0.3 m (1 ft) of sandy backfill material in order to raise the ground surface. The pile base was embedded in the gravelly sand layer (i.e., layer 5 in Table 3.9), which has a gravel content of 43%.

A slow, maintained static load test was performed on the CEP pile 13 days after pile driving. The ultimate load Q_{ult} corresponding to a pile head settlement of 61 mm (2.4 in.) (= $0.1B$) was 4,559 kN (1,025 kips), whereas the load Q_L and pile head settlement required for the pile to start plunging into the ground were 5,449 kN (1,225 kips) and 129 mm (5.1 in.) (= $0.21B$), respectively. The following steps show how to estimate the limit shaft capacity Q_{sL}, the ultimate base capacity $Q_{b,ult}$, and the ultimate load capacity Q_{ult} of the pile using CPT results.

TABLE 3.11
Comparison between predicted and measured capacities of OEP pile in Lafayette, Indiana

Source of Capacity	Test/Design Method	Shaft Capacity (kips)	Plug Capacity (kips)	Annulus Capacity (kips)	Base Capacity (kips)	Total Capacity (kips)
Measurement (static load test)	Ultimate load at pile head settlement of $0.1B$[1]	509	70	496	566	1,075
Prediction	PPDM[2]	539	—	—	547	1,086
	UPDM[2]	1,042	—	—	579	1,621
	PPDM[3]	537	—	—	455	992
	UPDM[3]	1,064	—	—	536	1,600

[1]After correction for residual loads (Han et al., 2020).
[2]Using the measured PLR and IFR values obtained from plug length measurements.
[3]Using the estimated PLR and IFR values in the absence of plug length measurements.

3.5.1 Estimation of Limit Shaft Capacity

Steps 1–4 are the same as those detailed in Section 3.4.1, except that the pile is a closed-ended pipe pile with L = 17.68 m (58 ft) and B = 610 mm (24 in.). Calculations from step 5 onward are shown as follows.

Step 5: Divide the soil profile into sublayers.

Figure 3.10 shows the discretization of the lower bound q_c profile into 7 sublayers up to a depth equal to the embedded length of the pile (= 58 ft). The grey vertical bars indicate the representative (average) q_c values within each sublayer.

Step 6: Calculate vertical effective stresses.

Table 3.12 summarizes the *in situ* vertical effective stress at the middle of each sublayer.

Step 7: Calculate the limit unit shaft resistance of pile segments in contact with "sand" sublayers.

Table 3.12 summarizes the results obtained for all the sublayers using the Purdue pile design method (PPDM). An example calculation for sublayer 4, which is a "sand" sublayer, is shown as follows.

a. Recall from step 7 of Section 3.4.1 that z_{top} = 34.12 ft, z_{bottom} = 44.32 ft, z_{middle} = 39.22 ft, Δz = 10.2 ft, q_c = 1,239.4 psi, σ'_{v0} = 22.08 psi, and σ'_{h0} = 9.94 psi.
b. Critical-state friction angle ϕ_c of the sublayer = 32° (Table 3.9).
c. Critical-state interface friction angle δ_c of the sublayer = $0.76\phi_c$ = 0.76 × 32° = 24.3° (from Figure 4.2 of Volume II).
d. Ignore this substep as the pile is not an H-pile.
e. Vertical distance from the middle of the sublayer to the pile base:

$$h = L - z_{middle} = 58 - 39.22 = 18.78 \text{ ft}$$

Coefficient of lateral earth pressure (using Eq. 4.9 from Volume II):

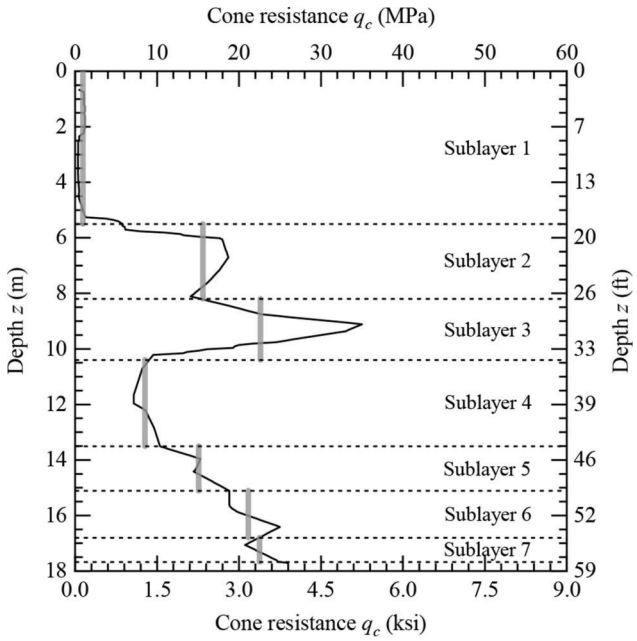

Figure 3.10 Discretization of lower bound q_c profile into 7 sublayers at CEP pile test site in Lafayette, Indiana.

$$K = 0.2 + \left[\frac{0.01\left(\frac{q_c}{p_A}\right)}{\sqrt{\frac{\sigma'_{h0}}{p_A}}} - 0.2\right] \exp\left(\frac{-0.14h}{L_R}\right)$$

$$= 0.2 + \left[\frac{0.01 \times \left(\frac{1{,}239.4}{14.5}\right)}{\sqrt{\frac{9.94}{14.5}}} - 0.2\right] \exp\left(\frac{-0.14 \times 18.78}{3.28}\right)$$

$$= 0.57$$

Limit unit shaft resistance of the pile segment in contact with sublayer 4 (using Eq. 4.8 from Volume II):

$$q_{sLi} = F_{\text{load}} K \sigma'_{v0} \tan \delta_c$$
$$= 1 \times 0.57 \times 22.08 \times \tan 24.3^{\circ} = 5.68 \text{ psi}$$

Pile shaft area interfacing with sublayer 4 (from Table 4.1 of Volume II):

$A_{si} = \pi B \Delta z_i = \pi \times 24 \times (10.2 \times 12) = 9{,}228.7$ in.^{2} (or 64.1 ft^2)

Limit shaft capacity of the pile segment in contact with sublayer 4:

$$Q_{sLi} = q_{sLi} A_{si} = 5.68 \times 9{,}228.7 = 52.4 \text{ kips}$$

Step 8: Calculate the limit unit shaft resistance of pile segments in contact with "clay" sublayers.

Ignore this step as there are no "clay" sublayers at the site.

Step 9: Repeat steps 7 and 8 for all sublayers in contact with the pile shaft.

Table 3.12 summarizes the results obtained for all the sublayers in contact with the pile shaft.

Step 10: Compute the limit shaft capacity Q_{sL} of the pile.

Limit shaft capacity of the pile (using Eq. 4.23 from Volume II):

$$Q_{sL} = \sum_{i=1}^{7} Q_{sLi} = \sum_{i=1}^{7} q_{sLi} A_{si} = 408 \text{ kips}$$

(obtained by summing the last column of Table 3.12).

3.5.2 Estimation of Ultimate Base Capacity

Step 1: Estimate the average cone resistance q_{cb} at the pile base.

a. Depth corresponding to $L - B = 58 - 2 = 56$ ft.
Depth corresponding to $L + 2B = 58 + 2(2) = 62$ ft.
Depth corresponding to $L + (B/2) = 58 + (2/2) = 59$ ft.

   i. Following the Purdue pile design method (PPDM), the representative cone resistance q_{cb} for use in pile base capacity calculation is obtained by averaging the lower-bound q_c values between $1B$ above and $2B$ below the pile base, corresponding to a 56–62 ft depth range. This yields $q_{cb} = 4{,}168$ psi.

Step 2: Calculate the ultimate unit base resistance $q_{b,ult}$ of the pile.

a. *In situ* vertical total stress at the depth corresponding to $L + (B/2)$:

$\sigma_{v0} = 124.1(18.0) + 127.3(26.9 - 18.0) + 136.9(34.1 - 26.9) + 127.3(55.1 - 34.1) + 136.9(59 - 55.1) = 7{,}559.7$ psf (or 52.5 psi)

Hydrostatic pore water pressure at the depth corresponding to $L + (B/2)$:

TABLE 3.12
Calculation of limit shaft capacity of CEP pile in Lafayette, Indiana

Sublayer i	Soil Type	z_{top} (ft)	z_{bottom} (ft)	Δz (ft)	z_{middle} (ft)	q_c (psi)	σ_{v0} (psi)	σ'_{v0} (psi)	σ'_{h0} (psi)	h (ft)	K	δ_c (°)	q_{sLi} (psi)	A_{si} (ft^2)	Q_{sLi} (kips)
1	Sand	0.0	18.0	18.0	9.0	138	7.8	7.8	3.5	49.0	0.20	24.6	0.7	113.5	11.6
2	Sand	18.0	26.9	8.9	22.5	2,266	19.5	14.1	6.3	35.5	0.68	26.2	4.7	55.7	37.5
3	Sand	26.9	34.1	7.2	30.5	3,283	26.8	17.9	8.1	27.5	1.08	23.1	8.2	45.4	53.8
4	Sand	34.1	44.3	10.2	39.2	1,239	34.8	22.1	9.9	18.8	0.57	24.3	5.7	64.1	52.9
5	Sand	44.3	49.6	5.3	46.9	2,187	41.6	25.6	11.5	11.1	1.13	24.3	13.1	33.0	62.1
6	Sand	49.6	55.1	5.5	52.3	3,067	46.4	28.0	12.6	5.7	1.83	24.3	23.1	34.9	116.0
7	Sand	55.1	58.0	2.9	56.6	3,267	50.2	30.0	13.5	1.4	2.21	23.1	28.3	18.2	73.9

Note: z_{top}, z_{bottom}, and z_{middle} = depth measured from the ground surface to the top; bottom and middle of the sublayer, respectively; Δz = thickness of the sublayer; q_c = representative cone resistance of the sublayer; σ_{v0} and σ'_{v0} = *in situ* vertical total and effective stresses, respectively, at the middle of the sublayer; σ'_{h0} = *in situ* horizontal effective stress at the middle of the sublayer; h = vertical distance from the middle of the sublayer to the pile base; K = coefficient of lateral earth pressure; δ_c = critical-state interface friction angle; q_{sLi} = limit unit shaft resistance of pile segment in contact with sublayer i; A_{si} = pile shaft area interfacing with sublayer i; and Q_{sLi} = limit shaft capacity of pile segment in contact with sublayer i.

$u_0 = \gamma_w(z - z_w) = 62.45 \times (59 - 10) = 3{,}060.05$ psf (or 21.25 psi)

In situ vertical effective stress at the depth corresponding to $L + (B/2)$:

$$\sigma'_{v0} = \sigma_{v0} - u_0 = 52.5 - 21.25 = 31.25 \text{ psi}$$

In situ horizontal effective stress at the depth corresponding to $L + (B/2)$:

$$\sigma'_{h0} = K_0\sigma'_{v0} = 0.45 \times 31.25 = 14.06 \text{ psi}$$

Critical-state friction angle $\phi_c = 34^\circ$ (Table 3.9).
Relative density (using Eq. 4.30 from Volume II):

$$D_R = \frac{\ln\left(\frac{q_{cb}}{p_A}\right) - 0.4947 - 0.1041\phi_c - 0.841\ln\left(\frac{\sigma'_{h0}}{p_A}\right)}{0.0264 - 0.0002\phi_c - 0.0047\ln\left(\frac{\sigma'_{h0}}{p_A}\right)}$$

$$= \frac{\ln\left(\frac{4{,}168}{14.5}\right) - 0.4947 - 0.1041(34) - 0.841\ln\left(\frac{14.06}{14.5}\right)}{0.0264 - 0.0002(34) - 0.0047\ln\left(\frac{14.06}{14.5}\right)}$$

$$= 83.7\%$$

Ultimate unit base resistance of the pile (using Eq. 4.28 from Volume II):

$$q_{b,ult} = (1 - 0.0058D_R)q_{cb}$$
$$= [1 - 0.0058(83.7)] \times 4{,}168 = 2{,}144.6 \text{ psi}$$

Step 3: Compute the ultimate base capacity $Q_{b,ult}$ of the pile.

Cross-sectional area of the pile base (from Table 4.2 of Volume II):

$$A_b = \frac{\pi B^2}{4} = \frac{\pi \times 24^2}{4} = 452.4 \text{ in.}^2$$

Ultimate base capacity of the pile (using Eq. 4.34 from Volume II):

$$Q_{b,ult} = q_{b,ult}A_b = 2{,}144.6 \times 452.4 = 970 \text{ kips}$$

Step 4: Compute the ultimate load capacity Q_{ult} of the pile.

Ultimate load capacity of the pile (using Eq. 4.35 from Volume II):

$$Q_{ult} = Q_{sL} + Q_{b,ult} = 408 + 970 = 1{,}378 \text{ kips}$$

3.5.3 Comparison Between Predicted and Measured Pile Capacities

Table 3.13 compares the shaft, base and total capacities of the CEP pile obtained from the static load test (after correction for residual loads) with those predicted using the Purdue pile design method (PPDM), the Unified pile design method (UPDM)

TABLE 3.13
Comparison between predicted and measured capacities of CEP pile in Lafayette, Indiana

Source of Capacity	Test/Design Method/Program	Shaft Capacity (kips)	Base Capacity (kips)	Total Capacity (kips)
Measurement (static load test)	Ultimate load at pile head settlement of $0.1B$[1]	485	540	1,025
Prediction	PPDM	408	970 (585)	1,378 (993)[2]
	UPDM	494	869	1,363[3]
	DrivenPiles program	640	262	902

[1]After correction for residual loads (Ganju et al., 2020).
[2]Ultimate load Q_{ult} corresponding to a pile head settlement of $0.1B$ (= 2.4 in). The values in the parenthesis were obtained by considering $q_{cb} = q_{bL}$ [$= Q_{bL}/A_b = (Q_L - Q_{sL})/A_b$] = [(1,225–485) × 1,000]/452.4 = 1,636 psi, where q_{bL} = limit unit base resistance of the pile (obtained from the static load test). This was done due to the high gravel content of the bearing layer in which the pile base was embedded. The value of q_{cb} (4,168 psi) calculated in step 1 of Section 3.5.2 is unrealistically high because of particle scale effects on cone resistance.
[3]Ultimate load corresponding to a pile base settlement of $0.1B$. The representative cone resistance q_{cb} for base capacity calculation was obtained by averaging the lower-bound q_c values over a vertical distance of $1.5B$ above to $1.5B$ below the pile base.

(Table 4.19 of Volume II), and the DrivenPiles program. The ultimate load capacity Q_{ult} of the pile predicted using the PPDM and the UPDM is greater than that obtained from the static load test by about 33%; this is mainly due to the significant overprediction of the base capacity, which is attributed to the high gravel content of the bearing layer in which the pile base was embedded. Further research is needed to investigate the response of piles in gravelly soils and to develop a CPT-based pile design method for such soils (Ganju et al., 2020, 2021).

The SPT blow counts obtained from boring S2 were entered into the DrivenPiles program and the option "correct the N values for the influence of the effective overburden pressure" was selected to then obtain the corresponding values of ϕ for each of the soil layers listed in Table 3.9. The ϕ values obtained for each layer are 28.6° for layer 1, 31.4° for layer 2, 36.4° (limited to 36°) for layer 3, 33.0° for layer 4, and 34.3° for layer 5. The DrivenPiles program predicts a nominal pile capacity of 902 kips.

3.6 Load and Resistance Factor Design of Pile Group

This example problem shows how to design a pile group using LRFD. The pile group consists of driven, closed-ended pipe (CEP) piles with outer diameter, wall thickness, and embedment length of 356 mm (14 in.), 9.53 mm (0.375 in.), and 15.42 m (50.6 ft), respectively. The soil profile at the site is the same as that described in Section 3.1, and the span length of the bridge is 45.7 m (150 ft).

Step 1: Obtain the nominal dead and live loads on the foundation.

Nominal dead load DL^n=2,611 kips (assumed).

Bridge span length L_b = 45.7 m (150 ft).

Dynamic load allowance IM = 0.33 (AASHTO, 2020).

Ratio of nominal live load to nominal dead load (Han et al., 2015; Hansell & Viest, 1971):

$$\frac{LL^n}{DL^n} = \frac{1}{0.0433(1+IM)\dfrac{L_b}{L_R}}$$

$$= \frac{1}{0.0433(1+0.33)\left(\dfrac{150}{3.28}\right)} = 0.38$$

where L_R = reference length (= 1 m or 3.28 ft).

Nominal live load LL^n=$0.38DL^n$=$0.38 \times 2{,}611$=992 kips.

Step 2: Set the load factors.

Load factor for dead load LF_{DL} = 1.25 and load factor for live load LF_{LL} = 1.75 (AASHTO, 2020).

Step 3: Obtain the nominal limit shaft and ultimate base capacities of a single pile in the group.

The following refer to the results tabulated in Table 3.3 for the Purdue pile design method (PPDM).

Nominal limit shaft capacity Q^n_{sL} of a single CEP pile = 433 kips.

Nominal ultimate base capacity $Q^n_{b,ult}$ of a single CEP pile = 280 kips.

Step 4: Set the pile spacing and group configuration.

Outer diameter B of the pile = 14 in.

Pile center-to-center spacing $s_{cc} = 2B = 2 \times 14 = 28$ in. (assumed).

Pile group configuration = 4×4 (i.e., 4 center piles, 8 side piles, and 4 corner piles—refer to Figure 4.3 of Volume II).

Step 5: LRFD of pile groups in "sand."

Table 3.1 shows that the soil profile at the site consists predominantly of "sand."

a. Using Eq. 4.10 from Volume II, the average relative density D_R of the "sand" layers crossed by the pile group is about 80%. Furthermore, the relative density of the "sand" layer at the base of the pile group is also approximately equal to 80% (see Section 3.1.2).
b. Pile head settlement $w = 0.1B = 0.1 \times 14 = 1.4$ in.
For a 4×4 pile group with $s_{cc} = 2B$, $D_R = 80\%$, and w = 1.4 in., the values of the shaft and base efficiencies, $\eta_{s,i}$ and $\eta_{b,i}$, respectively, for the center, side and corner piles are obtained from Table 4.7 of Volume II.
Center piles: $\eta_{s,i}$ = 1.01 and $\eta_{b,i}$ = 0.99.
Side piles: $\eta_{s,i}$ = 1.32 and $\eta_{b,i}$ = 0.80.
Corner piles: $\eta_{s,i}$ = 1.02 and $\eta_{b,i}$ = 0.75.
c. For a target probability of failure of 10^{-4}, the resistance factors, RF_s and RF_b, for the shaft and base resistances, respectively, of CEP piles in sand based on the PPDM are: RF_s = 0.60 and RF_b = 0.30 (Table 4.3 of Volume II).
d. Number of piles in the group n_p = 16.
Nominal limit shaft resistance of the pile group:

$$\sum_{i=1}^{16} \eta_{s,i} Q^n_{sL,i} = Q^n_{sL} \sum_{i=1}^{16} \eta_{s,i}$$

$$= 433 \times [4(1.01) + 8(1.32) + 4(1.02)] = 8{,}088 \text{ kips}$$

Nominal ultimate base resistance of the pile group:

$$\sum_{i=1}^{16} \eta_{b,i} Q^n_{b,ult,i} = Q^n_{b,ult} \sum_{i=1}^{16} \eta_{b,i}$$

$$= 280 \times [4(0.99) + 8(0.80) + 4(0.75)] = 3{,}741 \text{ kips}$$

Factored resistance of the pile group:

$$RF_s \left[\sum_{i=1}^{n_p} \eta_{s,i} Q_{sL,i}\right] + RF_b \left[\sum_{i=1}^{n_p} \eta_{b,i} Q_{b,ult,i}\right]$$

$$= 0.60[8{,}088] + 0.30[3{,}741] = 5{,}975 \text{ kips}$$

Factored load on the pile group:

$$LF_{DL} DL^n + LF_{LL} LL^n$$

$$= 1.25(2{,}611) + 1.75(992) = 5{,}000 \text{ kips}$$

As the factored resistance of the pile group is greater than the factored load applied on the pile group, the LRFD inequality (Eq. 4.38 from Volume II) is satisfied, and thus the pile group design is satisfactory for a target probability of failure of 10^{-4}. Because LRFD is a more rational and evolved design method than

Working Stress Design (WSD), there is no need to further calculate safety factors. However, as an example, the factor of safety (FS) obtained using Eq. 4.39 from Volume II is:

$$\mathrm{FS} = \frac{\sum_{i=1}^{n_p} \eta_{s,i} Q^n_{sL,i} + \sum_{i=1}^{n_p} \eta_{b,i} Q^n_{b,ult,i}}{DL^n + LL^n} = \frac{8{,}088 + 3{,}741}{2{,}611 + 992} = 3.3$$

REFERENCES

AASHTO. (2020). *AASHTO LRFD bridge design specifications* (9th ed.). American Association of State Highway and Transportation Officials.

Briaud, J.-L., & Gibbens, R. (1997). *Large-scale load tests and data base of spread footings on sand* (Report No. FHWA-RD-97-068). Federal Highway Administration.

Briaud, J.-L., & Gibbens, R. (1999). Behavior of five large spread footings in sand. *Journal of Geotechnical and Geoenvironmental Engineering*, *125*(9), 787–796. American Society of Civil Engineers.

Foye, K. C., Basu, P., & Prezzi, M. (2008). Immediate settlement of shallow foundations bearing on clay. *International Journal of Geomechanics*, *8*(5), 300–310.

Ganju, E., Han, F., Prezzi, M., & Salgado, R. (2020). Static capacity of closed-ended pipe pile driven in gravelly sand. *Journal of Geotechnical and Geoenvironmental Engineering*, *146*(4), 04020008.

Ganju, E., Han, F., Prezzi, M., & Salgado, R. (2021). The axial capacity of closed-ended pipe piles driven in gravelly sands. In C. El Mohtar, S. Kulesza, T. Baser, & M. D. Venezia (Eds.), *IFCEE 2021: Installation, Testing, and Analysis of Deep Foundations, GSP 323*, 377–387. American Society of Civil Engineers.

Han, F., Ganju, E., Prezzi, M., Salgado, R., & Zaheer, M. (2020). Axial resistance of open-ended pipe pile driven in gravelly sand. *Géotechnique*, *70*(2), 138–152.

Han, F., Ganju, E., Salgado, R., & Prezzi, M. (2019a). Comparison of the load response of closed-ended and open-ended pipe piles driven in gravelly sand. *Acta Geotechnica*, *14*(6), 1785–1803.

Han, F., Ganju, E., Salgado, R., Prezzi, M., & Zaheer, M. (2019b). *Experimental study of the load response of large diameter closed-ended and open-ended pipe piles installed in alluvial soil* (Joint Transportation Research Program Publication No. FHWA/IN/JTRP-2019/03) West Lafayette, IN: Purdue University, https://doi.org/10.5703/1288284316880

Han, F., Lim, J., Salgado, R., Prezzi, M., & Zaheer, M. (2015). *Load and resistance factor design of bridge foundations accounting for pile group–soil interaction* (Joint Transportation Research Program Publication No. FHWA/IN/JTRP-2015/24). West Lafayette, IN: Purdue University. http://dx.doi.org/10.5703/1288284316009

Han, F., Prezzi, M., Salgado, R., & Zaheer, M. (2017). Axial resistance of closed-ended steel-pipe piles driven in multi-layered soil. *Journal of Geotechnical and Geoenvironmental Engineering*, *143*(3), 04016102.

Hansell, W. C., & Viest, I. M. (1971). Load factor design for steel highway bridges. *Engineering Journal*, *8*(4), 113–123. American Institute of Steel Construction.

IN.gov. (2019). *INDOT geotechnical design manual*. Indiana Department of Transportation. https://www.in.gov/indot/2804.htm

Lee, J., & Salgado, R. (2002). Estimation of footing settlement in sand. *International Journal of Geomechanics*, *2*(1), 1–28.

Lee, J., Salgado, R., & Carraro, J. A. H. (2004). Stiffness degradation and shear strength of silty sands. *Canadian Geotechnical Journal*, *41*(5), 831–843.

Lehane, B. M., Doherty, J. P., & Schneider, J. A. (2008). Settlement prediction for footings on sand. In S. E. M. Burns, P. W. Mayne, & J. C. Santamarina (Eds.), *Proceedings of 4th International Symposium on Deformation Characteristics of Geomaterials*, *1*, 133–150. IOS Press.

Lehane, B. M., Ismail, M. A., & Fahey, M. (2004). Seasonal dependence of in situ test parameters in sand above the water table. *Géotechnique*, *54*(3), 215–218.

MDSC, Inc. (2018, September 3). *DrivenPiles–user manual*. Multidimensional Software Creations.

Nordlund, R. L. (1963). Bearing capacity of piles in cohesionless soils. *Journal of the Soil Mechanics and Foundations Division*, *89*(3), 1–36.

Nordlund, R. L. (1979). Point bearing and shaft friction of piles in sand. *Proceedings of the 5th Annual Short Course on the Fundamentals of Deep Foundation Design*.

Peck, R. B., Hanson, W. E., & Thornburn, T. H. (1974). *Foundation engineering* (2nd ed.). John Wiley & Sons.

Robertson, P. K., Campanella, R. G., & Wightman, A. (1983). SPT-CPT correlations. *Journal of Geotechnical Engineering*, *109*(11), 1449–1459.

Robertson, P. K., & Campanella, R. G. (1989). *Guidelines for geotechnical design using the cone penetrometer test and CPT with pore pressure measurement* (4th ed.). Hogentogler & Co.

Salgado, R. (2008). *The engineering of foundations* (1st ed.). McGraw-Hill.

Salgado, R., Bandini, P., & Karim, A. (2000). Shear strength and stiffness of silty sand. *Journal of Geotechnical and Geoenvironmental Engineering*, *126*(5), 451–462.

Schmertmann, J. H., Hartmann, J. P., & Brown, P. R. (1978). Improved strain influence factor diagrams. *Journal of the Geotechnical Engineering Division*, *104*(8), 1131–1135. American Society of Civil Engineers.

Schnaid, F., Wood, W. R., Smith, A. K. C., & Jubb, P. (1993). An investigation of bearing capacity and settlements of soft clay deposits at Shellhaven. In G. T. Houlsby & A. N. Schofield (Eds.), *Predictive Soil Mechanics: Proceedings of the Wroth Memorial Symposium* (pp. 609–627). Thomas Telford Limited.

Schneider, J. A. (2007). *Analysis of piezocone data for displacement pile design* [Doctoral thesis, The University of Western Australia].

Seo, H., Yildirim, I. Z., & Prezzi, M. (2009). Assessment of the axial load response of an H pile driven in multilayered soil. *Journal of Geotechnical and Geoenvironmental Engineering*, *135*(12), 1789–1804.

Tomlinson, M. J. (1980). *Foundation design and construction* (4th ed.). Pitman Advanced Publishing.

Tomlinson, M. J. (1986). *Foundation design and construction* (5th ed.). Longman Scientific & Technical.

Wadell, H. (1932, August). Volume, shape, and roundness of rock particles. *The Journal of Geology*, *40*(5), 443–451.

Wadell, H. (1933). Sphericity and roundness of rock particles. *The Journal of Geology*, *41*(3), 310–331.

Xu, X., & Lehane, B. M. (2008). Pile and penetrometer end bearing resistance in two-layered soil profiles. *Géotechnique*, *58*(3), 187–197.

About the Joint Transportation Research Program (JTRP)

On March 11, 1937, the Indiana Legislature passed an act which authorized the Indiana State Highway Commission to cooperate with and assist Purdue University in developing the best methods of improving and maintaining the highways of the state and the respective counties thereof. That collaborative effort was called the Joint Highway Research Project (JHRP). In 1997 the collaborative venture was renamed as the Joint Transportation Research Program (JTRP) to reflect the state and national efforts to integrate the management and operation of various transportation modes.

The first studies of JHRP were concerned with Test Road No. 1—evaluation of the weathering characteristics of stabilized materials. After World War II, the JHRP program grew substantially and was regularly producing technical reports. Over 1,600 technical reports are now available, published as part of the JHRP and subsequently JTRP collaborative venture between Purdue University and what is now the Indiana Department of Transportation.

Free online access to all reports is provided through a unique collaboration between JTRP and Purdue Libraries. These are available at http://docs.lib.purdue.edu/jtrp.

Further information about JTRP and its current research program is available at http://www.purdue.edu/jtrp.

About This Report

An open access version of this publication is available online. See the URL in the citation below.

Sakleshpur, V. A., Prezzi, M., Salgado, R., & Zaheer, M. (2021). *CPT-based geotechnical design manual, Volume 3: CPT-based design of foundations—Example problems* (Joint Transportation Research Program Publication No. FHWA/IN/JTRP-2021/24). West Lafayette, IN: Purdue University. https://doi.org/10.5703/1288284317348